A Physics-based, Dynamic Model of a Pressurized Water Reactor Plant with Programmable Logic Controllers for Cybersecurity Applications

Mohamed S. El-Genk, Timothy Schriener, Andrew Hahn, Ragai Altamimi
Institute for Space and Nuclear Power Studies and Nuclear Engineering Department, University of New Mexico, Albuquerque, NM, USA

Technical Work Scope: *Nuclear Energy–Cybersecurity Research Topics and Metrics Analysis (NE-1).* DOE-NEUP Project 18-15055. DOE Contract No. Nu-18-NM-UNM-050101-01 to University of New Mexico (UNM)

Period of Performance: 07-01-2018 to 06-30-2021

Report No. UNM-ISNPS-02-2020
Institute for Space and Nuclear Power Studies, The University of New Mexico
Albuquerque, NM, USA

July 2020

Executive Summary

Digital instrumentation and control (I&C) systems in commercial nuclear power plants raise cybersecurity concerns and emphasize the need to develop tools and capabilities to perform high fidelity cybersecurity analyses of I&C architectures within these plants. To address this need, the University of New Mexico's Institute for Space and Nuclear Power Studies (UNM-ISNPS) in collaboration with Sandia National Laboratories (SNL) are developing the Nuclear Instrumentation & Control Simulation (NICSim) platform. This platform would couple emulation and simulation models of digital I&C system components to a physics-based, dynamic model of a Pressurized Water Reactor (PWR) plant to enable cybersecurity investigations.

The developed physics based dynamic PWR plant model is the subject of this report. This model comprises physics-based models of the major components. These includes the reactor, primary coolant loop, primary water pump, pressurizer, and steam generator. The developed plant model within the Matlab Simulink platform couples the dynamic models of various plant's components and could easily be customized to different plant designs. The components models include those of: (a) the reactor with coupled point-kinetics and thermal-hydraulics, (b) a 3-region Pressurizer, (c) a Steam Generator, and (d) primary coolant Pump. These models are integrated into the Primary Loop Model which solves the overall mass, momentum, and energy balance equations.

The reactor 6-point kinetics equations are solved using a robust and efficient exponential matrix technique developed by UNM-ISNPS for determining the reactor thermal power as functions of the external and feedback reactivities in the reactor core. These equations together with those of the reactor thermal-hydraulics model of the primary loop calculate the coolant mass flow rate and inlet and exit temperatures in the reactor core. The point-kinetics solution approximates the exponential matrix a 7th order accurate Padé(3,3) function to ensure stability and accuracy irrespective of the time step size. The reactor thermal-hydraulic submodel uses a lumped model of the core with an average fuel rod cooled by forced convection and solves the mass, energy, and momentum balance equations in the primary loop. The primary loop model is coupled to those of the pressurizer and the steam generator as well as that of the primary coolant pumps.

The three region non-equilibrium transient pressurizer model accounts for all physical processes taken place such as flash evaporation, rainout and wall condensation, liquid droplets spray, and heat addition by the proportional and backup heaters. It calculates the changes in system pressure and water level in the pressurizer during operation transients resulting in over-pressurization or under-pressurization in the primary loop. The recirculating U-tube steam generator model calculates the heat removal rate from the primary loop water flow on the tube side to the secondary water flow on the shell side, and calculates to exit steam quality and the water level in the steam generator.

The developed PWR Plant physics-based dynamic model functions with the programable logical controllers (PLCs) in the I&C systems. These are the safety PLCs for the protection and safety monitoring I&C system, the PLCs in the plant operation I&C system, and the designed Core Protection Calculator (CPC) PLC for performing the reactor trip function and the Engineered Safety Features Actuation System (ESFAS) PLC for autonomously actuating the plants engineered safety features are developed and coupled to. The plant's operation I&C System includes a reactor regulation PLC, the pressurizer pressure and water level PLCs, the steam generator feedwater control PLC, and a reactor coolant pump PLC. These PLCs

continuously receive state variables from the primary loop model and return control signals to adjust the plant's operation to stay within programed setpoints.

The developed PWR plant's components models are validated using reported design values or experimental results from scaled test facilities. Results show adequate agreement with reported values. The integrated PWR model is also used to investigate transient operation of the representative PWR plant design to be used for testing and demonstrating the NICSim platform. Investigated transient are those of startup from hot zero power condition to 100% nominal operation power and following a 5% increase in the load demand of the plant. Results demonstrated that the I&C system PLCs maintain smooth operation of the plant without large spikes in the state variables.

List of Contents

List of Figures

List of Tables

Nomenclature and Abbreviations List

A_{cs}: Cross sectional area (m^2)
C_p: Specific heat capacity (J/kg.K)
C*: Combined control parameter for PLCs
D_e: Equivalent diameter (m)
f: Darcy friction factor
f_{rec}: Recoverable fission energy fraction
g: Gravitational constant (m/s^2)
h: Specific enthalpy (J/kg), non-dimensional pump head
h_{fg}: Heat of vaporization (J/kg)
H: Pump head (m), height (m)
H_R: Rated pump head (m)
H_o: Non-boiling height in steam generator (m)
K: Hydraulic resistance coefficient
L: Length (m), water level (m)
L_d: Desired water level (m)
M: Mass (kg)
M_{cl}: Cold leg coolant mass (kg/s)
M_{hl}: Hot leg coolant mass (kg/s)
M_{pu}: Pump coolant mass (kg/s)
M_{Rx}: Reactor mass (kg/s)
M_{sg}: Steam generator coolant mass (kg/s)
M_{tot}: Total coolant mass (kg/s)
$\dot{m}$: Mass flow rate (kg/s)
$\dot{m}_{ch}$: Charging rate into primary loop (kg/s)
$\dot{m}_{fw}$: Feedwater flow rate (kg/s)
$\dot{m}_{ld}$: Letdown rate from primary loop (kg/s)
$\dot{m}_p$: Flow in steam generator U-tubes (kg/s)
$\dot{m}_{rv}$: Pressurizer relief valve flow rate (kg/s)
$\dot{m}_s$: Steam flow rate (kg/s)
$\dot{m}_{sg}$: Steam generator flow rate (kg/s)
$\dot{m}_{sp}$: Spray rate (kg/s)
$\dot{m}_{su}$: Pressurizer surge rate (kg/s)
p: Pressure (Pa)
p_{ref}: Reference pressure (Pa)
p_{sys}: System pressure (Pa)
P: Reactor fission power (W)
P_c: Rate of heat transfer from convection from the cladding to the coolant (W)
P_{cool}: Rate of change of energy due to the inflow and outflow of coolant (W)
P_{diss}: Rate of energy dissipation in the coolant
P_f: Power deposited in fuel (W)
P_g: Rate of heat transfer from the fuel to the cladding across the gap (W)
P_{loss}: Heat losses (W)
P_m: Power deposited in moderator (W)
P_{Rx}: Reactor thermal power (W)
Re: Reynolds number

q":	Heat flux (W/m^2)
Q:	Volumetric flow rate (m^3/s)
Q_R:	Rated volumetric flow rate (m^3/s)
Qsg:	Rate of thermal energy transferred to the secondary shell side of the steam generator
R_c:	Radius of curvature (m)
S:	Soluble boron concentration (ppm)
S_0:	Source power (W)
SG:	Steam Generator
t:	Time (s)
T_b:	Bulk coolant temperature (K)
T_c:	Cladding temperature (K)
$T_{c,i}$:	Cladding inner surface temperature (K)
$T_{c,o}$:	Cladding outer surface temperature (K)
T_{ex}:	Exit temperature (K)
T_{in}:	Inlet temperature (K)
T_f:	Fuel temperature (K)
T_{ref}:	Reference temperature (K)
v:	Fluid velocity (m/s)
W_T:	Work of turbine (W)
X_{db}:	Deadband filter size
Xe:	Exit steam quality
Y:	Fission power from delayed neutron precursors

Greeks

α:	Reactivity feedback coefficient, non-dimensional pump speed
β:	Delayed neutron fraction, non-dimensional torque
Δp_c:	Curvature pressure loss (Pa)
Δp_{cl}:	Cold leg pressure loss (Pa)
Δp_{con}:	Contraction pressure loss (Pa)
Δp_{exp}:	Expansion pressure loss (Pa)
$\Delta p_{exp-con}$:	Sum of expansion and contraction pressure losses (Pa)
Δp_f:	Friction pressure losses (Pa)
Δp_{hl}:	Hot leg pressure loss (Pa)
Δp_{in}:	Reactor vessel inlet pressure loss (Pa)
Δp_{loss}:	Pressure losses (Pa)
Δp_{out}:	Reactor vessel outlet pressure loss (Pa)
Δp_{pump}:	Pump pressure head (Pa)
η_T:	Turbine efficiency
θ:	Angle (rad)
λ:	Delayed neutron lifetime (units)
Λ:	Neutron lifetime (units)
ρ:	Reactivity, density (kg/m^3)
ρ_b:	Soluble boron reactivity ($)
$\rho_{c(T)}$:	Cladding temperature reactivity feedback ($)
ρ_{ex}:	External reactivity ($)

$\rho_{f(T)}$: Fuel temperature reactivity feedback ($s)
ρ_{fb}: Feedback reactivity ($)
$\rho_{m(p)}$: Moderator pressure reactivity feedback ($)
$\rho_{m(T)}$: Moderator temperature reactivity feedback ($)
$\rho_{s(T)}$: Structure temperature reactivity feedback ($)
ρ_{tot}: Total reactivity($)
τ: Pump torque (N.m)
τ_R: Pump rated torque (N.m)
υ: Non-dimensional volumetric flow rate
ω: Pump shaft rotational speed (rads/s)
ω_R: Rated shaft rotational speed (rads/s)

Abbreviations

BOL: Beginning of Life
CEA: Control Element Assembly
CEDM: Control Element Drive Mechanism
CHF: Critical Heat Flux
CHFR: Critical Heat Flux Ratio
CPC: Core Protection Calculator
DOE: Department of Energy
EOL: End of Life
ESF: Engineered Safety Features
ESFAS: Engineered Safety Features Actuation System
IAPWS: International Association for the Properties of Water and Steam
I&C: Instrumentation and Control
ICS: Industrial Control System
IT: Internet Technology
LOCA: Loss-Of-Coolant Accident
LOFT: Loss-of-Fluid Test
MOI: Moment of Inertia
N: Number
NEUP: Nuclear Engineering University Program
NICSim: Nuclear Instrumentation and Control Simulation
NRC: Nuclear Regulatory Commission
PI: Proportional-Integral
PID: Proportional-Integral-Differential
PLC: Programmable Logic Controller
PMS: Plant Protection and Safety Monitoring System
PWR: Pressurized Water Reactor
RCP: Reactor Coolant Pump
TCP/IP: Transmission Control Protocol over Internet Protocol
UNM-ISNPS: University of New Mexico's Institute for Space and Nuclear Power Studies

1. Introduction

Digital Industrial Control Systems (ICSs) are being used in many fields including energy generation and transmission infrastructure. Examples are smart grids; aerospace and aviation; defense systems; oil and gas processing and refining; and manufacturing. Multiple cyber-attack campaigns have been executed in recent years against control systems worldwide. Notable examples are the Crashoverride and Blackenergy campaigns against the electrical transmission infrastructure in Ukraine, and the Stuxnet campaign against the Iranian uranium enrichment program (Dragos Inc., 2017; Karnouskos, 2011). The Stuxnet campaign targeted the specialized digital Programmable Logic Controller (PLC) computers. Unlike enterprise IT networks, ICSs frequently do not have the same levels of safeguards and defensive technologies against potential cyberattacks.

Replacing the analog systems with digital Instrumentation and Control (I&C) in existing commercial nuclear power plants in the USA and abroad, has enhanced safety and reliability, and increased availability or load factor by minimizing down time. In addition, it supported power uprates, increased electricity generating capacity, and improved economics. Generation III and III+ reactor plant designs would use digital I&C systems for autonomous control and the activation of safety and protection systems (Korsah, et al., 2008).

Unlike analog systems, digital ICS are vulnerable to potential cyberattacks. Therefore, it is imperative to assess and evaluate potential cyber-vulnerabilities of current and planned nuclear I&C architectures in nuclear power plants (US Department of Homeland Security, 2015; Nuclear Energy Institute, 2010; National Research Council, 1997). Nuclear power plants typically employ separate I&C systems for autonomous plant control and for plant safety and protection by initiating a reactor trip and/or actuating the Engineered Safety Features (ESF) (Korsah, K., et al., 2008). These systems operate mostly independent of the reactor operators' actions. Therefore, a cyber-compromise of the safety PLCs could potentially provide access to a hostile actor, significantly impacting the plant's operation and safety.

Therefore, it is desirable to develop an I&C system platform that could effectively be used to investigate cyber vulnerabilities of nuclear plants' ICSs. Developing functional models of PLCs or communication buses within the plant and of simulation models of various components would be useful for investigating responses of I&C system architectures. However, high-fidelity computer emulation models would be required to investigate cyber-vulnerabilities of software and firmware on various devices. A platform with emulytics capabilities is therefore needed, which would allow researchers to investigate cybersecurity vulnerabilities in nuclear plants I&C systems and understand plants' response to successful cyber-compromise.

To address these needs, the University of New Mexico's Institute for Space and Nuclear Power Studies (UNM-ISNPS) in collaboration with Sandia National Laboratories (SNL) are developing a Nuclear Instrumentation and Control Simulation (NICSim) platform, which when coupled to the SCEPTRE emulytics framework at SNL could investigate cybersecurity of ICSs (Sandia National Laboratories, 2016). Figure 1.1 shows the elements of the NICSim platform and the coupling to the SCEPTRE framework at SNL. The emulated I&C system components are coupled to a fast running, physics-based models of the integrated PWR plant and of various components for direct feedback on the behavior of the integrated I&C systems.

These physics-based dynamic models are developed and run on the versatile Matlab Simulink platform (The MathWorks, Inc., 2018). The integrated PWR plant model is fast-running to support real-time simulation of various transients when linked with the PLCs. In addition, this model could be configured to different PWR plant designs and integrated to

different I&C system architectures. The developed Matlab Simulink models are compatible with the Simulink C/C++ coder and cab be compiled into stand-alone executable for easy deployment. The SCEPTRE framework would emulate (*via precise firmware and software execution within virtual machine environments*) and simulate (*via computational models*) the plant's I&C system components. It would handle intercommunication between devices across a virtual computer network using real ICS communication protocols and can embed physical hardware components into its virtual network.

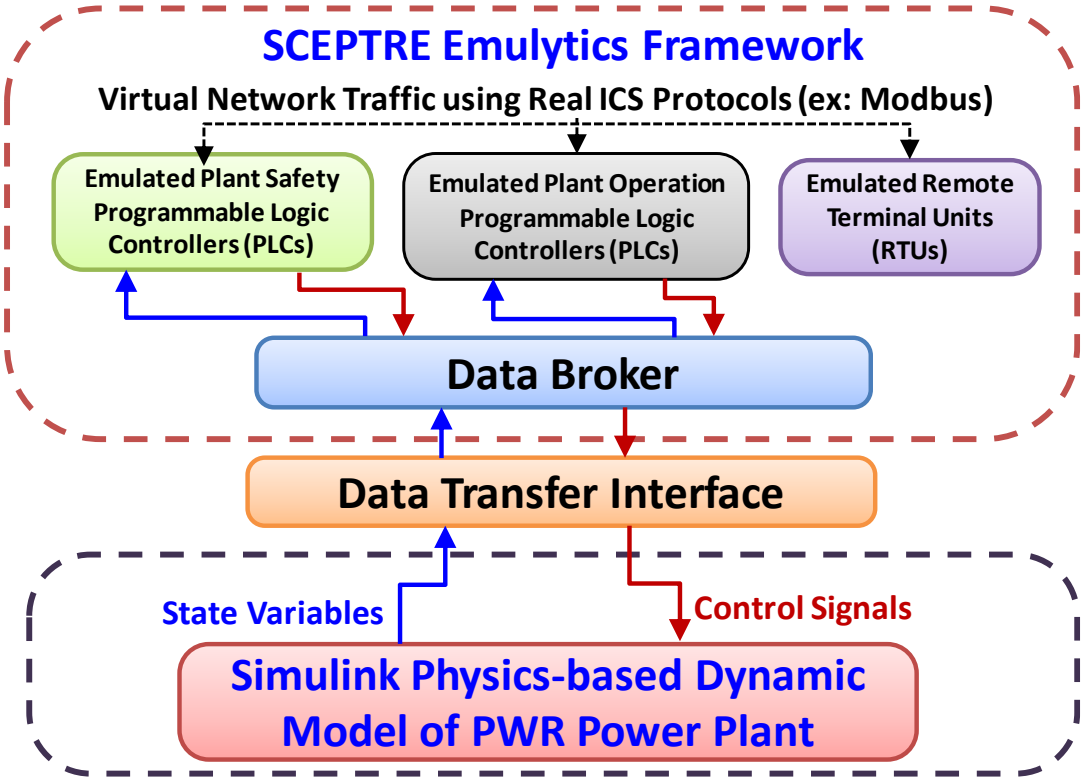

Fig. 1.1: Elements of NICSim platform for investigating cybersecurity of PWR plant I&C systems.

The coupling of an emulytics model of the plant's I&C system to a dynamic model of the integrated nuclear power plant within NICSim platform makes it possible to examine the effects of postulated cyber-attacks on the I&C system, the nuclear reactor operation, and plant safety within a repeatable, sandboxed virtual testing environment (Fig. 1.1). The physics-based dynamic model of a PWR plant in NICSim would be linked to the emulated, simulated, and/or physical PLCs and other I&C system components by a data transfer interface program (Fig. 1.2), which communicates with a data broker program within SCEPTRE (Sandia National Laboratories, 2016).

The developed Data Transfer Interface is shown in Fig. 1.2. A specialized Simulink S-function written in the C programming language is developed to communicate the simulation state variables to an external interface program written in the python programming language using synchronized shared memory inter-process communication (Hahn, Schriener and El-Genk, 2020). The calculated state variables by the physics-based nuclear power plant model are communicated to the external python interface using shared memory inter-process communication. These variables are written and read from a shared memory location named

'Publish' (Fig. 1.2). The control signals determined by the I&C system's emulated PLCs are passed back to the Simulink model through a second shared memory location named 'Update'. Inter-process communication semaphores are used to ensure that only one side of the interface can access a given shared memory location at a time. The data transfer interface program also includes a time synchronization routine to ensure that the NICSim nuclear power plant model running in Matlab Simulink runs in the same time scale as the emulated PLCs' control programming. For controllers using real-time clocks, this will ensure that the response timing of the nuclear plant model is in tune with that expected by the controllers' software.

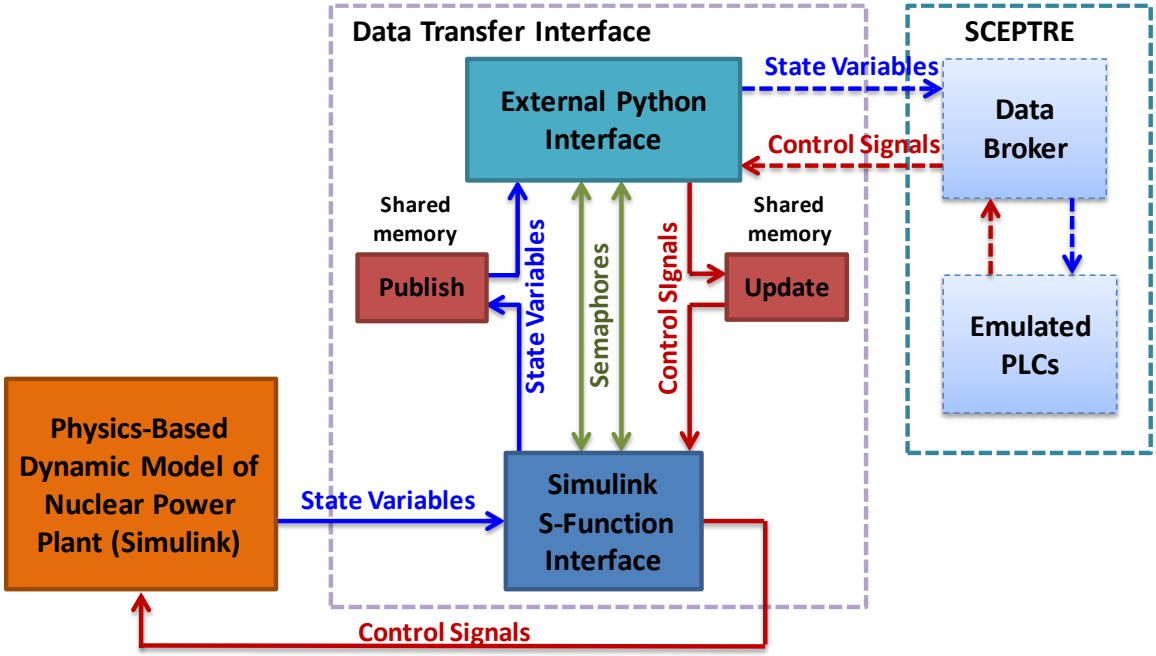

Fig. 1.2: Block diagram of developed NICSim data transfer interface program.

The focus of the work described in this report is on the development of a physics-based dynamic model of a representative PWR plant design, which can be used to simulate the transient behavior of the plant. The plant model couples functional models of major components within the primary loop. The developed PWR plant model, which uses the Matlab Simulink platform (The Mathworks 2019), must be fast-running to support real-time simulation of plant transients. The developed models of major plant components are connected to emulated PLCs within the representative PWR plant I&C systems to provide autonomous control during operation. The modeling employs a representative PWR design to support the development and demonstration of the NICSim platform.

In this report, *Section 2 - Physics-based, Dynamic Model of a PWR Plant*, describes the developed models of key components within the PWR primary loop. These are the reactor model, which couples the PWR point kinetics and thermal-hydraulics models, the pressurizer model, the steam generator model, and the primary coolant pump model. This section also describes the primary loop model which integrates key components models and solves the overall mass, momentum, and energy balance equations for a PWR primary coolant loop. *Section 3 - Programmable Logic Controllers in I&C Systems of a Representative PWR Plant*, describes the PLCs which make up the protection and operation I&C systems of a representative PWR

plant. The testing and development of these PLCs is the subject of a companion report (El-Genk et al., 2020b *in progress*). *Section 4 - PWR Plant Model Results and Model Validation,* presents results of comparing the predictions of the developed PWR plant component models to rereported experimental results. This section also presents the results of using the integrated PWR plant model to simulate operational transients. These include reactor startup to nominal full power operation and the plant response to a change in load demand. *Section 5 - Summary and Conclusions***,** summarizes the results described in this report and explains how the results presented in this progress report will be applied to future tasks in this DOE NEUP project.

2. Physics-based, Dynamic Model of a PWR Plant

The NICsim platform includes a physics-based, dynamic model of a PWR primary loop, which is integrated with the emulated operation and plant safety monitoring and protection PLCs for cybersecurity and control systems investigations. Fig. 2.1 is a layout of a representative PWR plant modeled in the NICSim platform. The representative PWR layout in Fig. 2.1 is a two-loop design (Fig. 2.2). The representative PWR plant has two hot legs exiting the reactor to two steam generators. The return flow from each steam generator splits between two reactor coolant pumps, one for each cold leg. The hot legs and steam generators are labeled 1 and 2, the cold legs and reactor coolant pumps are labeled 1a, 1b, 2a, and 2b. The pressurizer is connected to hot leg 1.

The developed PWR plant model includes charging and letdown lines for inject and removing coolant from the primary loop to/from the reactor coolant management and chemistry control system. During nominal operation, coolant is continuously injected and removed from the primary loop to adjust the soluble boron concentration and the water chemistry to limit corrosion. The charging line is connected to cold leg 2a, and the letdown line is connected to cold leg 2b. The steam generators 1 and 2 couple the primary loops to the secondary loops, which include the energy conversion systems. The secondary loops are not modeled in detail, but assumptions are made of the operation parameters for the steam generator model.

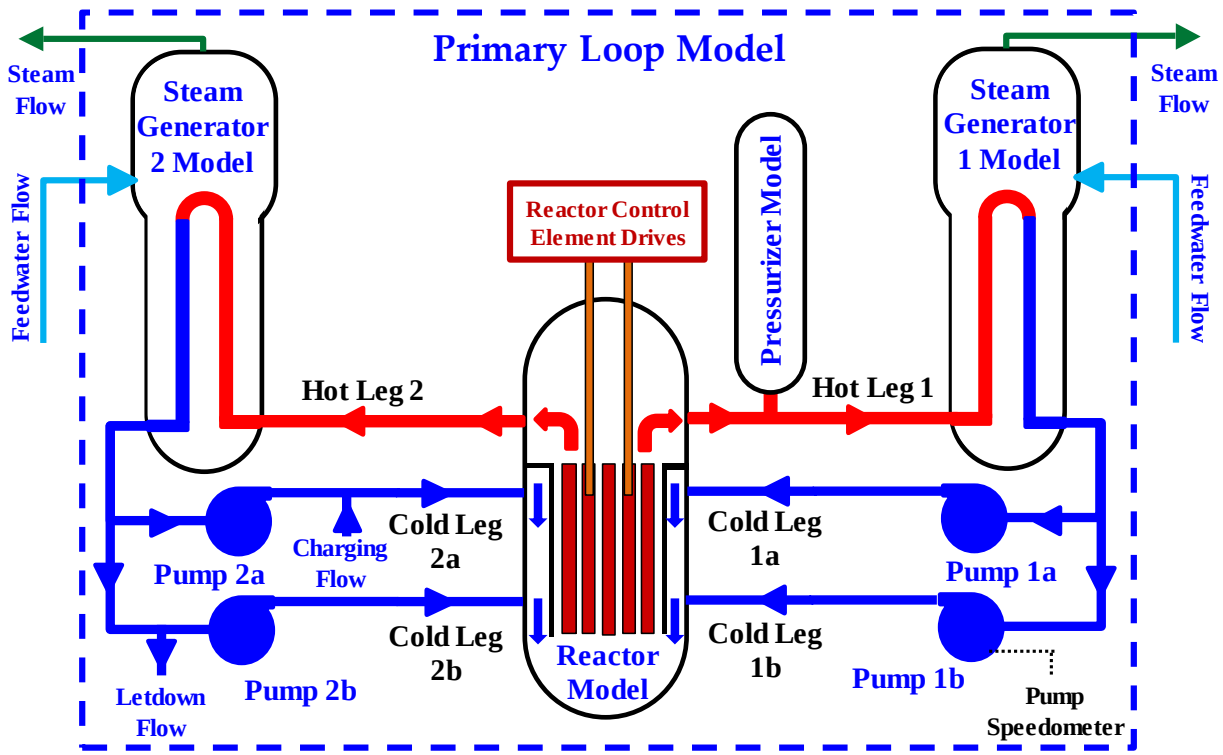

Fig. 2.1: Developed physics-based components models in a representative PWR primary loop.

The developed PWR plant model could be configured to represent different reactor and components designs. The user can change the components' dimensions, materials properties, the reactor reactivity feedback coefficients, the primary coolant pump characteristics, among others. The present PWR plant model is developed within the versatile Matlab Simulink platform (The Mathworks 2018), which is constructed using discrete-time blocks to facilitate compilation into

an executable by the Matlab Simulink Coder and to support parallel processing. Simulink simultaneously solves the coupled governing equations in various models of the plant components using a fixed timestep discrete solver. The selected timestep size ensures numerical stability and convergence of results within a short running time. The selected modeling approach and efficient use of the Matlab Simulink support running synchronous with real time for integration with the emulated PLCs in the NICSim platform.

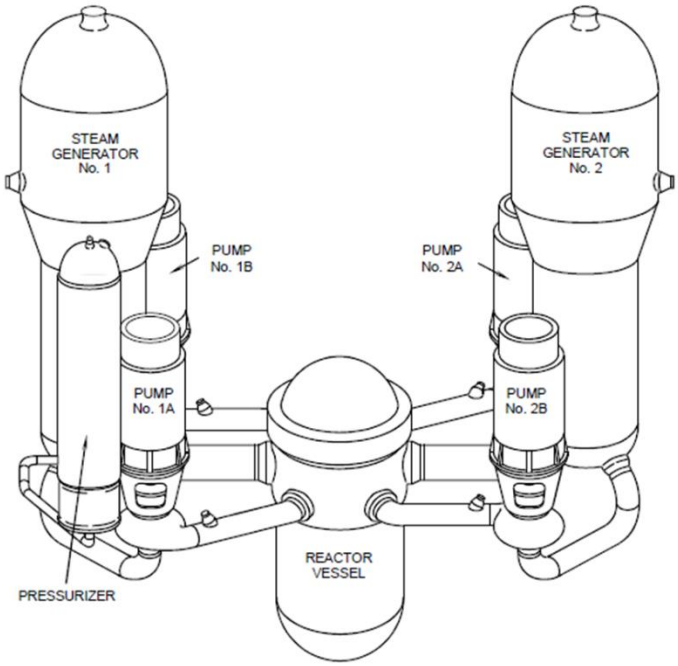

Fig. 2.2: A layout Combustion Engineering two-loop PWR (US Nuclear Regulatory Commission, 2007).

The temperature and pressure dependent thermophysical properties of water in the primary loop are calculated using the International Association for the Properties of Water and Steam (IAPWS), Industrial Formulation 1997 standard (International Association for the Properties of Water and Steam, 2007). These properties are integrated into Simulink using C++ S-functions, derived from the open source CoolProp/IF97 C++ code (Bell et al., 2015). The following five sub-sections describe the developed physics-based models of the components in the primary loop of the PWR plant. These are the reactor model, the pressurizer model, the steam generator model, the reactor primary coolant pump model, and the primary loop model.

2.1 Reactor Model

A fast-running reactor model is developed to simulate the neutronics and thermal-hydraulics behavior of a PWR core during transient and steady state operation (Fig 2.3). The primary coolant enters from the cold legs through inlet nozzles into the reactor vessel. It flows down through the annular downcomer to the lower plenum at the bottom of the reactor vessel before. From there the primary coolant flow up through the lower core support plate and support structure before entering the reactor core. The hot water exiting the fuel rod assemblies in the reactor core mixes in the upper plenum and exits the reactor vessel through the outlet nozzles to the hot legs. The Control Element Assemblies (CEAs) enter the reactor core through the top and are connected to drive mechanisms mounted onto the top of the reactor vessel head (Fig. 2.3).

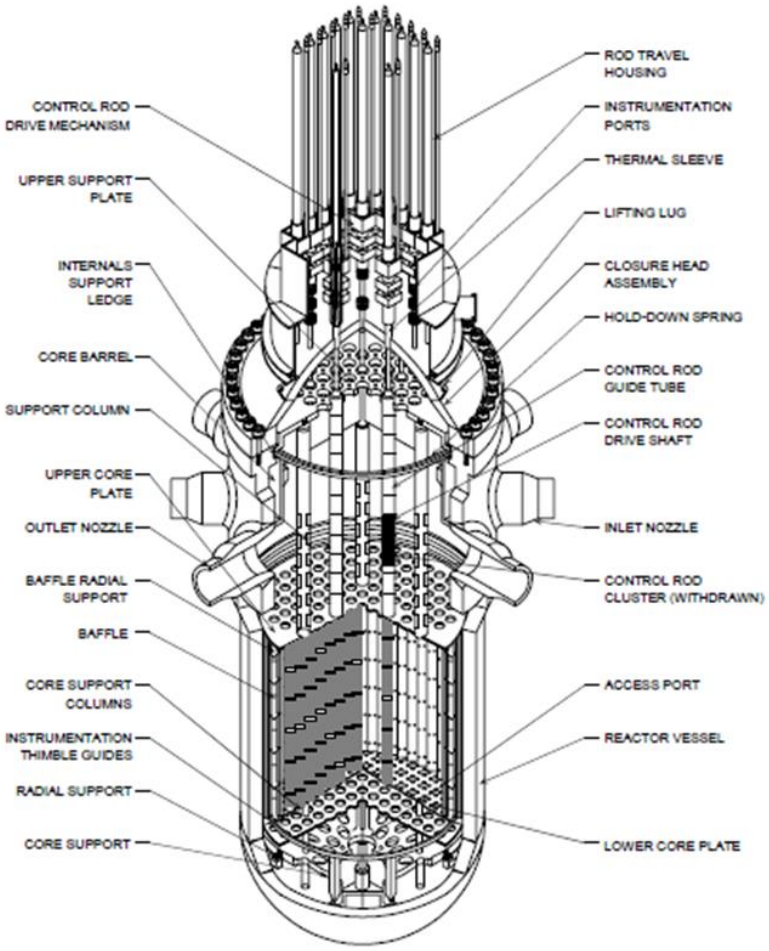

Fig. 2.3: Cutaway view of PWR reactor vessel (US Nuclear Regulatory Commission, 2007)

The building blocks of the developed PWR reactor model are the point kinetics and reactor thermal-hydraulic submodels (Fig. 2.4). The point kinetics submodel calculates the change in the reactor power, P_{Rx}, in response to changes in the total reactivity, ρ_{tot}. This submodel solves the coupled energy balance equations to calculate the change in the temperatures for the fuel, cladding, and moderator as well as the core exit temperature.

The core inlet temperature and primary coolant flow rate are calculated using the primary coolant loop model. The core temperature, coolant pressure, and the specified soluble boron concentration are used to calculate the feedback reactivity values for the point-kinetics submodel (Fig. 2.4). The reactor thermal-hydraulic submodel also calculates the pressure losses, Δp_{Rx}, within the reactor for the overall momentum balance equation in the primary loop submodel.

The point kinetics solve seven coupled equations for the reactor fission power, P, and six groups of delayed-neutron precursors, Y_i. These equations are written as:

$$\frac{dP}{dt} = \frac{\rho_{tot} - \bar{\beta}}{\Lambda} \times P + \sum_{i=1}^{6} \lambda_i Y_i + S_0, \text{ and} \quad (2.1)$$

$$\frac{dY_i}{dt} = \frac{\beta_i}{\Lambda} \times Q_{fis} - \lambda_i Y_i , \quad i = 1 \text{ to } 6 \quad (2.2)$$

In these equations, Y_i and S_0 are the fission powers generated by the delayed neutron precursors and the initial startup source. These reactor point kinetics equations are solved using a robust and efficient exponential method, which approximates the exponential matrix using 7th order accurate Padé(3,3) function (El-Genk and Tournier 2016). This method is highly stable and independent of the time step size. It is capable of accurately calculating the change in the reactor power associated with a rapid reactivity insertion using large timestep sizes on the order of seconds. This method has been integrated within the MELCOR accident analysis code for modeling high temperature gas-cooled reactors (El-Genk and Tournier 2016). The present point kinetics model (Fig. 2.4) supports a range of different reported reactivity feedback effects for a given reactor type and design.

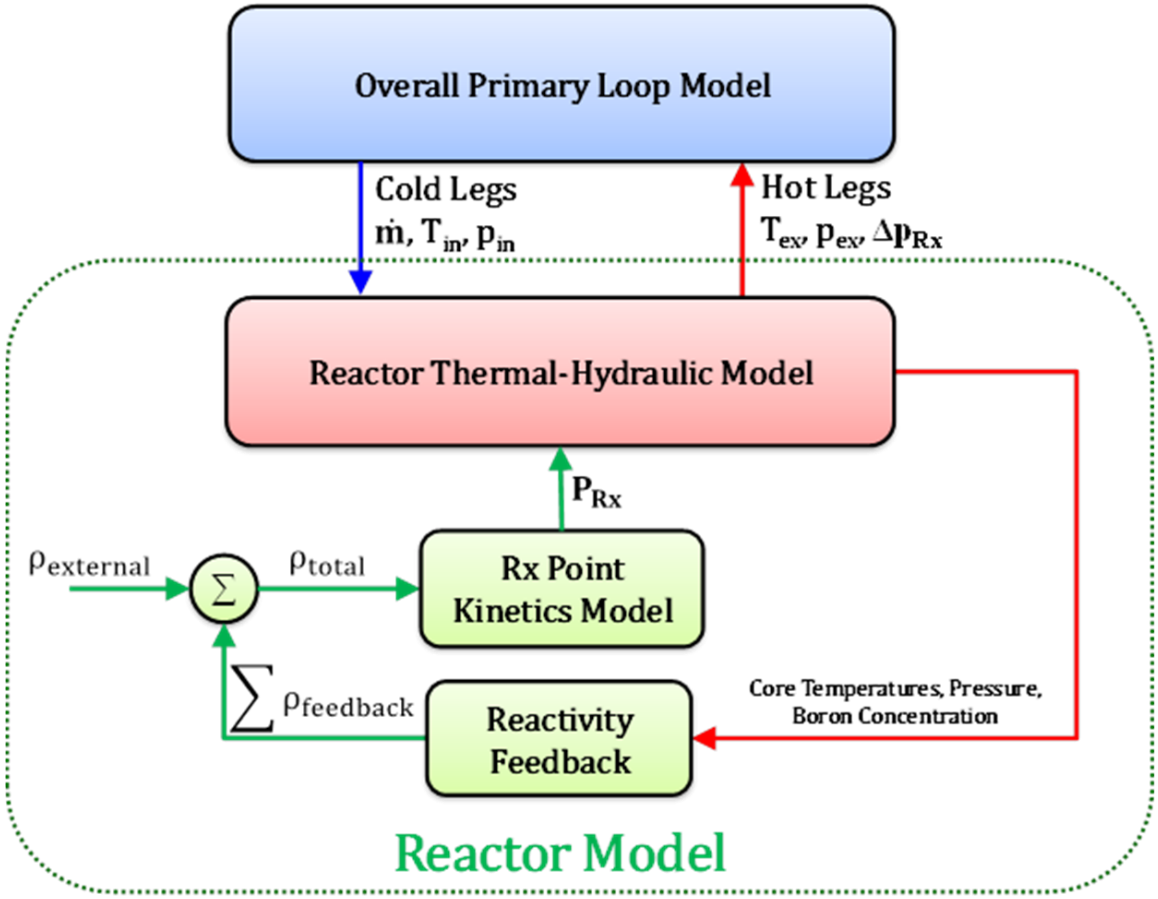

Fig. 2.4: Block diagram of PWR Model with point kinetics and thermal-hydraulic models.

The total reactivity in Fig. 2.4 is the sum of the external reactivity insertion by the movement of the reactivity control assemblies, ρ_{ex} and soluble boron, ρ_b, and the reactivity feedbacks in the core materials and structure, $\Sigma\rho_{fb}$ (Fig. 2.4), as:

$$\sum \rho_{fb} = \rho_{f(T)} + \rho_{m(T)} + \rho_{m(p)} + \rho_{c(T)} + \rho_{s(T)} \quad (2.3)$$

In this equation, $\rho_{f(T)}$ is the fuel temperature reactivity feedback due to thermal expansion and Doppler broadening of the neutron cross sections, $\rho_{m(T)}$ is the moderator temperature reactivity feedback effect, $\rho_{m(p)}$ is the moderator density reactivity feedback as a function of pressure, $\rho_{c(T)}$ is the cladding temperature reactivity feedback due to thermal expansion and Doppler

broadening, and $\rho_{s(T)}$ is the temperature reactivity feedback of the steel core barrel and support plate. In addition to being a function of temperature, $\rho_{m(T)}$ accounts for the effects of the soluble boron concentration on the moderator temperature reactivity feedback. Each reactivity feedback is introduced in the point kinetics model as 4th order polynomial functions in temperature and calculated using a reference temperature, T_{ref}, and pressure, p_{ref}, defined by the user. For the moderator temperature reactivity feedback, each polynomial coefficient in the temperature function is expressed as a 4th order polynomial function of the boron concentration in ppm.

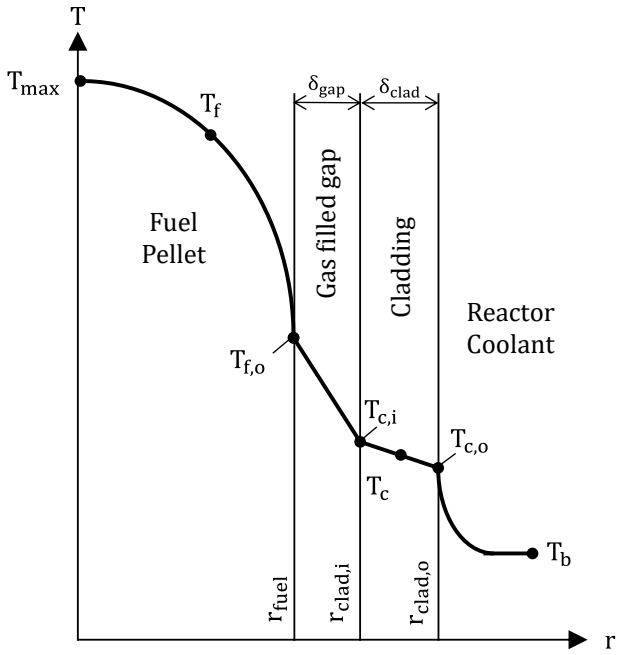

Fig. 2.5: Single average fuel rod thermal model with calculated temperature

The calculated value of P_{Rx} by the reactor point kinetics is provided to the reactor's thermal-hydraulic. The thermal power of the reactor, P_{Rx}, which is removed by the primary coolant flow through the reactor core, equals the fission power multiplied by the recoverable energy fraction, f_{rec}, which could vary from 0.85 - 0.90, depending on the reactor design, as:

$$P_{Rx} = f_{rec}\, P \tag{2.4}$$

The thermal-hydraulic model of the reactor is a simplified lumped model of the core that uses an average fuel rod to represent all fuel rods in the reactor core, and assumes thermal equilibrium of the coolant with the steel structure of the reactor vessel and core internals. The thermal-hydraulic model discretizes the average fuel rod into axial segments, n, and accounts for the user specified axial fission power distribution in the reactor core, N(n). The recoverable thermal power is the sum of the fission powers deposited in the fuel, P_f, and in the coolant, P_m, according to the reported fraction of reactor power deposited in the fuel, f_f:

$$P_f(n) = N(n)\,(P_{Rx}\, f_f) \tag{2.5}$$

$$P_m(n) = N(n)\,(P_{Rx} - P_f) \tag{2.6}$$

The mean fuel rod model calculates the average temperatures of the fuel, cladding, and water coolant in different axial segments of the reactor core (Fig. 2.5). The energy balance equations for solving for these in the n^{th} axial segment are written, respectively, as:

$$\frac{M_f}{n} C_p \frac{dT_f(n)}{dt} = P_f(n) - P_g(n) \tag{2.7}$$

$$\frac{M_c}{n} C_p \frac{dT_c(n)}{dt} = P_g(n) - P_c(n) \tag{2.8}$$

$$\left[M_m(n)C_p + \frac{\sum M_s C_p}{n}\right] \frac{dT_b(n)}{dt} = P_c(n) + P_m(n) - P_{cool}(n) - \frac{1}{n} P_{loss} \tag{2.9}$$

In Eq. (2.7), M_{fuel} is the total mass of fuel in the reactor core, $T_f(n)$ the mean fuel temperature in the n^{th} axial segment, $P_f(n)$ is from Eq. (2.5), and P_g is the rate of heat transfer from the fuel to the cladding across the radial gas gap in the fuel rod, which could be either open or closed. In Eq. (2.8), M_c is the total mass of the cladding in the reactor core, $T_c(n)$ the mean cladding temperature in the n^{th} axial segment, and P_c is the rate of heat transfer by convection from the cladding to the coolant flow. In Eq. (2.9), $M_m(n)$ is the coolant/moderator volume in the n^{th} axial segment, $T_b(n)$ the bulk coolant temperature in the core, $\Sigma M_s C_p$ is the sum thermal inertia in the reactor vessel and core internal structures, $P_{cool}(n)$ the rate heat removal by the flowing coolant in the n^{th} axial segment, and P_{loss} through the thermal insulation to the ambient. This rate of heat losses is a user specified fraction, f_{loss}, of P_{Rx}.

Eq. (2.7-2.9) accounts for the radial heat conduction through the fuel pellet with volumetric heat generation, heat transfer by conduction and radiation across the radial gas gap, heat conduction across cladding, and convective heat transfer from the outer cladding surface to the flowing coolant (Fig. 2.5). The thermal conductivity in the gas in radial the gap of the fuel rod, k_{mix}, is calculated as that of a mixture of Helium, Krypton, and Xenon (Mason and Saxena,1958), as:

$$k_{mix} = \sum_{a=1}^{3} \frac{x_a k_a}{\sum_{b=1}^{3} x_b \varphi_{ab}}, \text{ for } 1 = He,\ 2 = Kr,\ 3 = Xe \tag{2.10a}$$

$$\varphi_{ab} = \frac{1}{\sqrt{8}} \left(1 + \frac{MW_a}{MW_b}\right)^{-0.5} \left[1 + \left(\frac{MW_a}{MW_b}\right)^{0.5} \left(\frac{MW_a}{MW_b}\right)^{0.25}\right]^2 \tag{2.10b}$$

In this expression, x is the mole fraction, MW is molecular weight, and k is the thermal conductivity of the gas species of interest. The term φ_{ab} is calculated for each pair of gas species.

The rate of heat transfer removal from the outer surface of the cladding to the reactor coolant flow is calculated using Nusselt number, Nu, correlations of Su and El-Genk (1993). These correlations are for laminar, Nu_{FL}, and turbulent, Nu_{FT}, forced convection in rod bundles with a square lattice. For these conditions, Nu is expressed as a function of the bundle Reynolds number, R_b, and coolant Prandtl number, Pr, as:

(a) For Forced Laminar Convection: $$Nu_{FL} = A\, {Re_b}^{B} Pr^{0.33} \tag{2.11a}$$

(b) For Forced Turbulnet Convection: $$Nu_{FT} = C\, {Re_b}^{0.8} Pr^{0.33} \tag{2.11b}$$

In these correlations, the coefficients "A" and "C" and the exponent "B" are given (Su and El-Genk, 1993) as:

$$A = 2.34 - 3.0\left(1 - \frac{\pi}{4(P/D)^2}\right) \tag{2.11c}$$

$$B = 0.89\left(1 - \frac{\pi}{4(P/D)^2}\right) - 0.044 \tag{2.11d}$$

$$C = 5.5 \times 10^{-3}\left[\frac{4.47}{\left(\frac{\pi}{4(P/D)^2}\right)^{0.5}} - 1\right] \tag{2.11e}$$

Reynolds number at the transition between forced laminar and forced turbulent convection, Re_T for rod bundles with square lattice, which is a sole function of P/D, is expressed (Su and El-Genk, 1993) as:

$$Re_T = 1.33 \times 10^4 (P/D - 1) \tag{2.12}$$

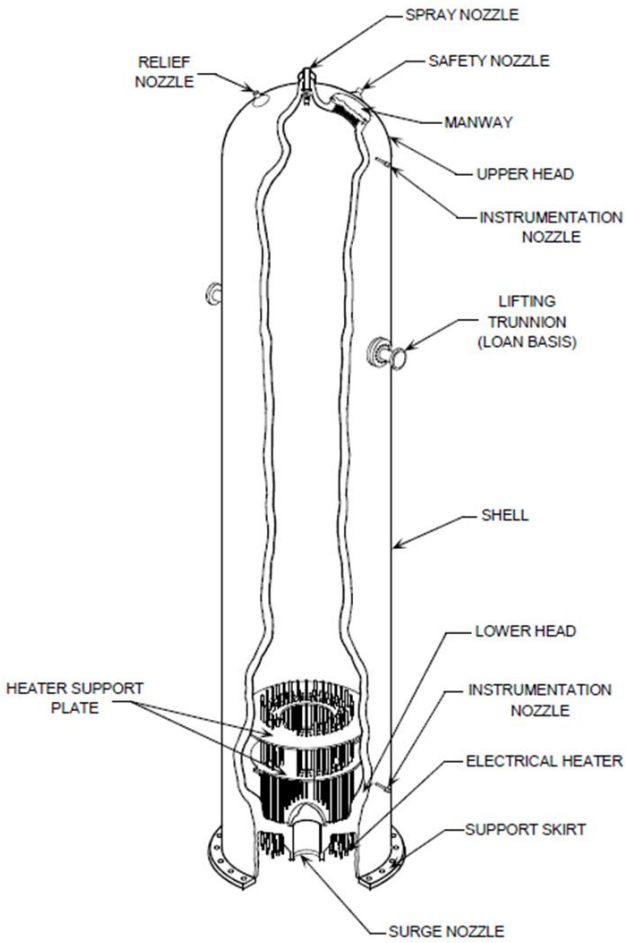

Fig. 2.6: A cutaway view of a PWR pressurizer (US Nuclear Regulatory Commission, 2007)

2.2 Pressurizer Model

The physics-based, three regions non-equilibrium transient model of the pressurizer accounts for all physical processes taken place (Figs. 2.6, 2.7) during transient operation of a PWR plant. These processes are flash evaporation, rainout and wall condensation, liquid droplets spray, and heat addition by proportional and backup heaters. It calculates the changes in system pressure and water level in the pressurizer during operation transients resulting in over-pressurization or under-pressurization in the primary loop. Fig. 2.7 presents a sketch of a PWR pressurizer that indicates the different physical process associated with the functionality and operation of the pressurizer during operation transients resulting in a surge in or surge out of the coolant from and to the hot leg, as a result of an over and under pressurization, respectively. This fast-running and transient model divides the pressurizer volume intro three regions; a saturated vapor region at the top, a saturated liquid region in the middle, and a subcooled liquid region at the bottom (Fig. 2.7). The later exists following a surge-in of the coolant from the hot leg. The model assumes the same pressure in the three regions of the pressurizer and solves the coupled mass and energy conservation equations in these regions to calculate the system pressure and the water level in the pressurizer during steady state and operation transients. It accounts for the changes of the fluid properties in all three regions of the pressurizer as function of pressure and temperature.

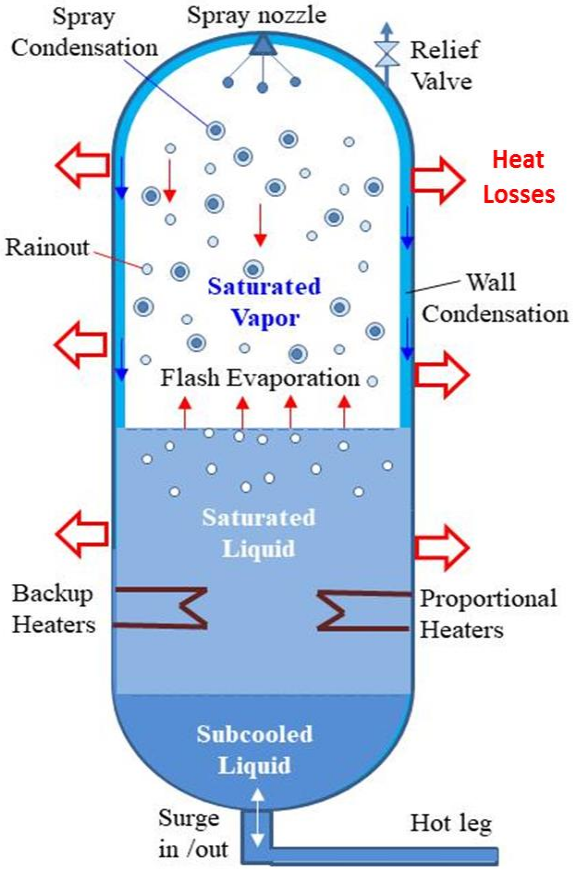

Fig. 2.7: Sketch of PWR pressurizer with physical processes incorporated in the developed physics-based model (Altamimi et al. 2020)

In the vapor region, the pressurizer model accounts for the condensation on the inner surface of the wall, flash evaporation at the interface with the middle region of saturated water, rain out condensation and spray condensation. The calculated rate of rainout condensation assumes that latent heat of condensation is supplied by the vapor region in order to maintain saturation conditions. The produced condensate flows from the vapor region to the saturated liquid region (Fig. 2.7). The model activates the subcooled water spray system when the system pressure increases above a defined set point. The released latent heat from the condensing vapor on the spray droplets increase the temperature of the spray water droplets (Fig. 2.7). Owing to the small average diameter of the droplets, they are assumed to reach saturation temperature during flight and before entering the saturated liquid region.

In the saturated liquid region, the pressurizer model accounts for flash evaporation into the saturated vapor region (Fig. 2.7). The rate of flash evaporation assumes that the latent heat is supplied by the saturation liquid region, with submerged proportional and backup heaters. The proportional heaters are on all the time to compensate for the heat losses from the surface of the pressurizer wall. The pressure controller maintains the heater's power inversely proportional to the system pressure during normal operation. The backup heaters play a critical role in preventing the system pressure from decreasing below the set point during operation transients by evaporating liquid from the saturated water region into the vapor region to increase the system pressure. The backup heaters are either on or off, depending on the setpoints of the system pressure.

The subcooled liquid region at the bottom of the pressurizer accommodates the surge water from the primary loop during an under or over pressure transient resulting in a surge in of the hot leg water into the pressurizer or a surge out of water from the pressurizer to the hot leg (Figs. 2.1 and 2.7). The rate of surge in or surge out is calculated by the primary loop model. If the surge in water reaches the submerged electric heaters, the pressurizer model allows the surge in water that reaches saturation to transfer to the saturated water region.

The pressurizer model accounts for the mass loss from the saturated vapor region through the relief valve or nozzle (Fig. 2.6), which opens when the pressure exceeds the safety setpoint. It also accounts for the added liquid mass from the spray nozzle (Fig. 2.6) and the water surge from the connected primary loop hot leg. The spray water from the cold leg model is at the calculated temperature and pressure at that location using the primary loop model. The pressurizer model accounts for the surge out of water from the pressurizer into the primary loop as the system pressure approaches its nominal value and the water level approaches the controllers' setpoints.

The pressurizer pressure PLC maintains or restores the system pressure to a preset target value during steady-state and following an operation transient. The pressure control is accomplished by sending signals to change the power of the submerged electric heaters in the liquid regions, and by adjusting the liquid spray and the steam relief nozzles in the saturated vapor region (Figs. 2.6, 2.7). The water PLC regulates the water level in pressurizer by sending signals to adjust the charging and letdown rates of the coolant for the primary loop (Fig. 2.1). These controllers are discussed in more details in a companion report (El-Genk et al., *2020b in progress*).

2.3 Steam Generator Model

A simplified, fast-running transient model is developed of a PWR recirculating steam generator. High pressure primary coolant from the hot legs flows through bundles of U-shaped tubes (Fig. 2.8). The coolant from the secondary loop is injected through the feedwater ring into a narrow annular downcomer before flowing upward on the sell side of the bundles of the U-

tubes. The secondary coolant flow is heated by the hot primary coolant flow in the steam generator U-tubes and generates steam by nucleate boiling on the shell side of the U-tubes. The moisture separators and steam dryers in the upper section of the steam generator (Fig. 2.8) ensures that saturated dry steam exits the steam generator to the power turbines for energy conversion in the secondary loops. The separated liquid is recirculated to mix in the downcomer with the colder feedwater flow back from the secondary loops. Therefore. the steam generator model thermally couples the PWR primary and secondary loops.

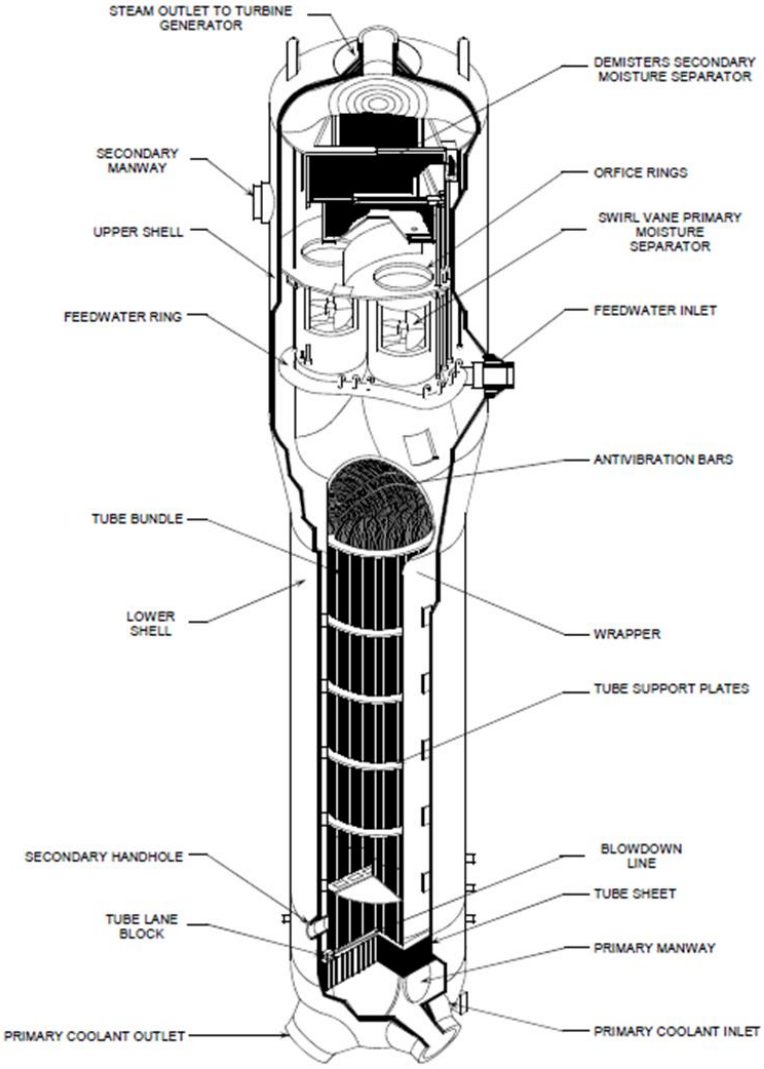

Fig. 2.8: Cutaway view of recirculating steam generator (US Nuclear Regulatory Commission, 2007).

Unlike the primary loops in the current PWR plant model, the secondary loop components are not modeled in detail, but the control of discharge rate of the feedwater pumps to the steam generators is accounted for in the steam generator model. Fig. 2.9 presents a schematic diagram of coupling the steam generator models and the secondary loop. The primary loop coolant enters the steam generator to flow on the tube side of the bundles of U-tubes, where thermal energy transfers to the secondary liquid and steam flow on the "shell" side of the U-tubes. The lower

enthalpy primary water exiting the U-tubes is circulated by the primary coolant pumps to the cold leg of the primary coolant loop before returning to the reactor.

The developed steam generator model is coupled to that of the primary loop which solves the overall mass, energy, and momentum balance equations for the primary coolant flow on the tube side in the steam generator. The steam generator-primary loop models calculate the total pressure losses, and the mass flow rate and the inlet and exit enthalpies for the primary coolant flow through the steam generator U-tube bundle. For the secondary coolant on the shell side, the steam generator model solves only the mass and energy balance equations for calculating the circulation rate and the exit steam quality as a function of the inlet temperature of the secondary water flow. The secondary feedwater mixes with the recirculated saturated water in the downcomer of the steam generator, before flowing upward on the shell side of the U-tubes bundles. On the tube side, the steam generator model calculates the non-boiling and boiling heights, the steam exit quality and flow rate to the turbine in the secondary loop. It also determines the water level in the annular downcomer from equating the weight of the water column in the downcomer to that of the water and steam win the central section of the steam generator. The model does not account, however, for the thermal inertia in the energy balance for the secondary side coolant, but includes the changes in the thermal inertia of the primary coolant flow in the U-tubes and lower plenum of the steam generator.

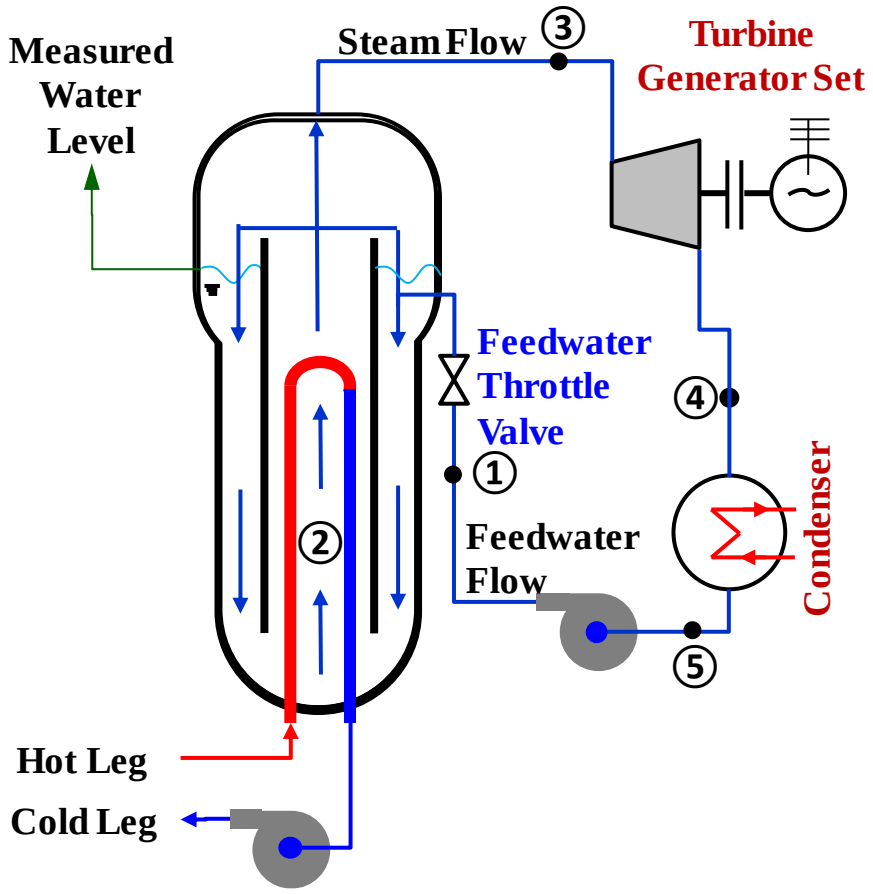

Fig. 2.9: A schematic of coupling steam generator model and secondary loop in a PWR plant.

The thermodynamic state points (1-5 in Fig. 2.9) along the secondary loop are specified by the user in the input to the steam generator model. Point 1 is of the state of the liquid entering

through the feedwater throttle valve to the feedwater injection ring, point 2 is where the heated liquid reaches saturation at the end of the non-boiling height of the steam generator, and point 3 is of the dry steam exiting the steam generator and entering the turbine. Point 4 is the thermodynamic state at the secondary coolant exiting the turbine to the condenser and point 5 is the thermodynamic state at the secondary coolant exiting the condenser to the feedwater pump.

The present steam generator keeps the exit pressure (3) constant at the specified pressure, which would be controlled using the turbine controller system. The condenser exit pressure (5) is also assumed constant. The steam generator model also assumes constant turbine and feedwater pump efficiencies to be specified by the user and a constant pressure head of the feedwater pump but allows the shaft speed to change commensurate with the desired feedwater flow rate.

The transient change in the steam flow rate, $\dot{m}_s$, in terms of that the turbine work demand, W_T, is calculated in terms of the turbine efficiency, η_T, and specified thermodynamic states as:

$$\frac{d\dot{m}_s}{dt} = \frac{dW_T/dt}{\eta_T(h_3 - h_{4s})} \tag{2.13}$$

The determined steam flow rate is used to calculate the exit quality, X_e, of the 2-phase mixture entering the steam separators and dryers and the total flow rate of secondary water flows on the shell side of the U-tube bundles in the steam generator, $\dot{m}_{sg}$. This is the sum of flow rates of the secondary feedwater, $\dot{m}_{fw}$, and that of the water separated from the exiting wet steam the steam separators (Fig. 2.8). These quantities are calculated using the following transient equations, as:

$$\frac{dX_e}{dt} = \frac{1}{\dot{m}_{sg}}\left(\frac{d\dot{m}_s}{dt} - X_e\frac{d\dot{m}_{sg}}{dt}\right) \tag{2.14a}$$

$$\frac{d\dot{m}_{sg}}{dt} = \frac{d\dot{m}_s}{dt} + \left(\frac{d\dot{m}_{fw}}{dt} - X_e\frac{d\dot{m}_s}{dt} - \dot{m}_s\frac{dX_e}{dt}\right) \tag{2.14b}$$

The steam generator feedwater controller adjusts the feedwater flow rate, $\dot{m}_{fw}$, by changing the throttle valve position (Fig. 2.9). The change in the rate of thermal energy transfer to the secondary coolant flow on shell side of the steam generator, Q_{sg}, is determined in terms of those of the changes in the feedwater exiting steam flow rates and exit quality in steam generator, as:

$$\frac{dQ_{sq}}{dt} = \left(h_2 + h_{fg}\right)\left[X_e\frac{d\dot{m}_{sg}}{dt} + \dot{m}_{sg}\frac{dX_e}{dt}\right] - h_1\frac{d\dot{m}_{fw}}{dt} \tag{2.15}$$

The thermal energy transferred to the secondary coolant decreases the temperature of the primary water flow on the tube side in the steam generator. The energy balance of the primary water flow is used to calculate the rate of change of the its bulk temperature, $T_{b,sg}$, as:

$$M_{sg}C_p\frac{dT_{b,sg}}{dt} = -Q_{sg} - \dot{m}_p(h_{ex} - h_{in}) \tag{2.16a}$$

The temperature of primary water flow exiting the steam generator U-tubes, $T_{ex,sg}$, is given as:

$$T_{ex,sg} = 2T_{b,sg} - T_{in,sg} \tag{2.16b}$$

The water level in the downcomer of the steam generator is calculated from equating the static head of the liquid in the downcomer to that the liquid and vapor mixture in the steam generator. The density of the saturated in the downcomer of the steam generator is calculated from the enthalpy, $h_{sg\text{-}dc}$, of the mixture of colder feedwater with the recirculated saturated water, as:

$$\frac{dh_{sg-dc}}{dt} = h_1 \dot{m}_{sg} \frac{d\dot{m}_{fw}}{dt} - h_2 \frac{dX_e}{dt} \tag{2.17}$$

The calculated non-boiling height, H_0, on the shell side in the steam generator determines the weight of the static column in the inner section of the steam generator. The non-boiling height is calculated using the following equations:

$$\frac{dH_0}{dt} = \left\{\left(0.5\, L_{tubes}\, h_{fg}\left(Q_{sg}\frac{d\dot{m}_s}{dt} - \dot{m}_s\frac{dQ_{sq}}{dt}\right)\right)/{Q_{sg}}^2\right\} \tag{2.18}$$

The water level in the downcomer in the Steam Generator is monitored by Feedwater Controller to make required adjustment to maintain the water level within programed setpoints.

2.4 Pump Model

A transient model is developed for the primary Reactor Coolant Pumps (RCPs), which circulate the water coolant in the primary loop. Fig. 2.10 presents a cutaway view of a reactor coolant pump with its major components. The pump impeller is connected by a shaft to a high voltage electric motor that operates the pump. The pump shaft has a labyrinthine seal to restrict the leakage of hot, highly pressurized water from the primary loop along the shaft. The seal is actively cooled such that the colder, denser water in the seal reduces leakage. The rotational speed of the pump shaft is measured using variable reluctance speedometers installed around slotted disks mounted to the shaft. A voltage signal is applied as the poles on the slotted disk pass the sensors, with the amplitude and frequency of the pulses depend on the pump speed.

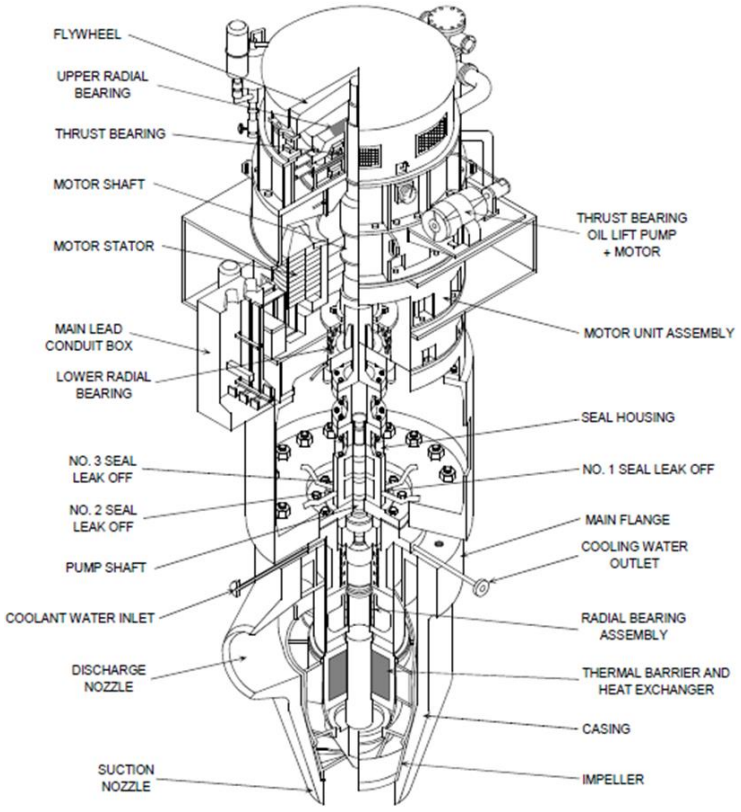

Fig. 2.10: Cutaway view of PWR reactor primary coolant pump (US Nuclear Regulatory Commission, 2007)

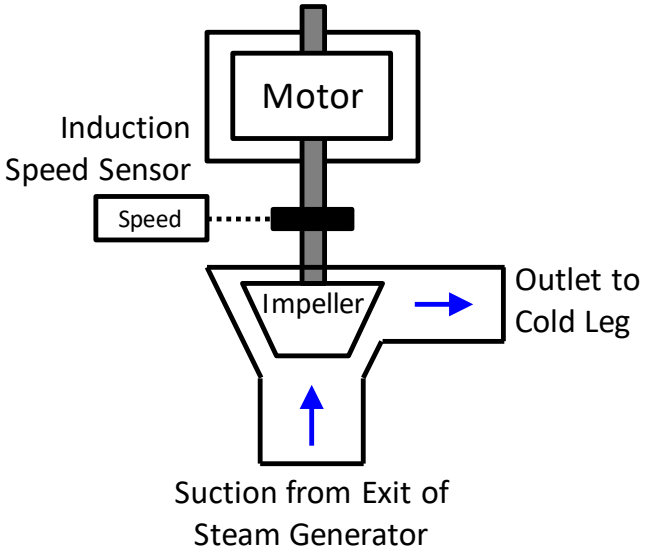

Fig. 2.11: Block diagram of reactor coolant pump model.

Figure 2.11 shows a block diagram of the developed reactor coolant pump model. The developed pump model calculates the pressure head generated by the rotating impeller for circulating the coolant in the primary loop. This pressure head is included the momentum balance of the primary loop and the energy dissipation by the pump to the coolant is included in the energy balance of the primary loop. The present pump model is based in part on the model implemented within the RELAP5 system analysis code (Nuclear Safety Analysis Division, 2001). In addition to being coupled to the PWR plant model, the pump model provides the supply curves of the pump head versus coolant mass flow rate, as functions of the rotation speed of the pump shaft. The pump model also includes a model of a pump speedometer which calculates a measured RPM value from specified sensor response characteristics (2.11). The calculated pump characteristics are also incorporated with digital controllers for monitoring the primary coolant flow rate and pump performance.

The pump model uses homologous pressure head and torque curves to define the performance characteristics. These homologous curves are a non-dimensional representation of the pump present performance relative to the rated performance specifications. These normalized curves allow the same homologous curves to represent different size pumps, which share similar performance characteristics. The specified rated pump performance values are used to un-normalize the non-dimensional pump performance parameters are those for the pump when operating peak efficiency. For a specific pump design, these unique performance parameters are specified by the user in the input to the pump model.

The homologous curves for the head and the torque are used in the input to the pump model and accessed using interpolating lookup tables. The homologous pump head and torque curves are expressed in terms of four non-dimensional parameters, namely: (a) the pump speed, α, defined as the ratio of the shaft rotational speed, ω, to the rated speed, ω_R, as: $\alpha = (\omega/\omega_R)$, (b) the pump head, h, defined as the ratio of the pump head, H, to its rated head, H_R, as: $h = (H/H_R)$, (c) the torque, β, defined as the ratio of the pump hydraulic torque, τ, to its rated torque, τ_R, as $\beta = (\tau/\tau_R)$, and (d) the volumetric flow rate, ν, defined as the ratio of the volumetric flow rate at the pump inlet, Q, to its rated flow rate, Q_R, as: $\upsilon = (Q/Q_R)$.

The pump homologous head and torque curves are divided into 8 segments, which represent the different regimes for the full range of normal and off-normal operation conditions. The eight segments of operating regime are defined using a three-letter naming convention. The first letter specifies whether the curve is for non-dimensional pump head ('H' for head) or non-dimensional torque ('B' for torque). The second letter specifies the term used in the denominator for the independent and dependent variables of the homologous curves. The independent variable for the pump curves is specified in terms of either α/ν or ν/α, while the dependent variable is plotted as either h/ν^2 or h/α^2 for head curve, or as β/ν^2 or β/α^2 for the torque curve.

The second letter in the naming convention is specified as 'A' if the denominator is α for the independent and α^2 for the dependent variable, and as 'V' if the denominator is ν for the independent and ν^2 for the dependent variable. The third letter specifies the pump operation regime, 'N' for normal operation with the rotational direction and the direction of flow are both positive with respect to the pump outlet; and 'D' for the pump operation in the energy dissipation mode of resisting the flow with that in the reversed direction while the rotation in the positive direction. The letter 'T' is for normal turbine operation when the directions of the flow and the rotation are both opposite from that for normal pump operation, and 'R' is for reversed pump operation when the rump rotation is reversed while the direction of flow remains in the positive direction.

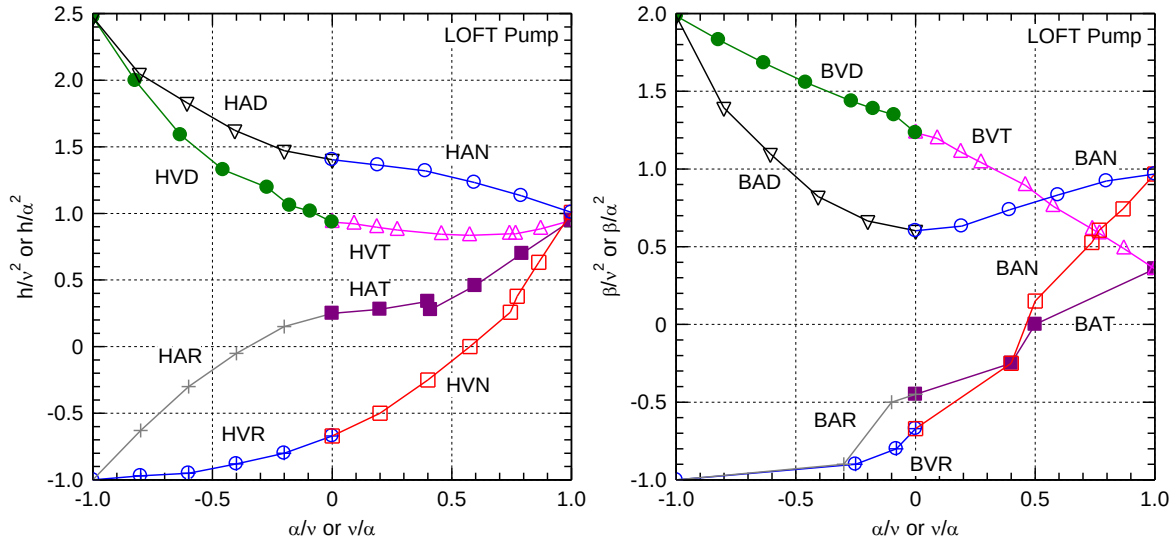

Fig. 2.12: Homologous curves for centrifugal coolant pumps in the Loss-of-Fluid Test (LOFT) facility (Reeder, 1978)

Figure 2.12 presents the homologous head and torque curves for the centrifugal coolant pumps used in the Loss-of-Fluid Test (LOFT) experimental facility constructed at Idaho National Engineering Laboratory to investigate loss-of-coolant accidents (LOCAs) in PWRs (Reeder 1978). These figures show the homologous curves transition seamlessly between operating regimes (HAN, HVN, HVR, HAR, HAT, HVT, HVD, HAD in Fig. 2.12a and BAN, BVN, BVR, BAR, BAT, BVT, BVD, BAD in Fig. 2.12b). The work performed by the coolant pump dissipates thermal energy that increases the temperature of the exiting fluid. Prior to reactor startup, the energy dissipation by the reactor coolant pumps is typically used to heat up the coolant within the primary loop. For liquid flows the rate of energy dissipation to the coolant is calculated, as:

$$P_{diss} = \tau_{tot}\omega - gH\,(\rho v)A_{cs} \tag{2.19}$$

In the event of a loss of power, a reactor coolant pump is designed to coast down slowly in order to maintain the primary coolant flow through the reactor core for as long as possible. The moment of inertia can be an input by the user either as a constant or as a function of the rotation speed, depending on the modeled pump design.

2.5 Primary Loop Model

The primary loop model couples the models of the various loop components and solves the overall mass, momentum, and energy conservation equations. The overall mass balance equation calculates the change in the coolant inventory in the primary loop as functions of in the charging and letdown flow rates (Fig. 2.1) and determines the rate of the surge in and surge out to the pressurizer from and to the primary loop. The overall momentum balance equation calculates the total pressure losses in the primary loop and compares it to supply curves for the primary pump to calculate mass flow rate in the hot and cold legs. The overall energy equation in primary loop equates the reactor thermal power to the sum of the total heat losses and the rate of energy transfer to the steam generator.

2.5.1 Overall Mass Balance Equation

During normal and transient operation, the pressurizer is the only primary loop component containing water steam. The remainder of the loop is filled solid with water. When this water thermally expands due to an increase in reactor power, it initiates a surge in of water from the primary loop into the pressurizer. Conversely when the volume of water in the primary loop decrease due to a decrease in the reactor power, water flows out of the pressurizer and enters the primary loop. The surge in and surge out rates of water from and to the primary loop, $\dot{m}_{su}$, is calculated as:

$$\dot{m}_{su} = \dot{m}_{ch} - \dot{m}_{ld} - \dot{m}_{sp} - \left(\frac{dM_{Rx}}{dt} + \frac{dM_{hl}}{dt} + \frac{dM_{sg}}{dt} + \frac{dM_{cl}}{dt} + \frac{dM_{pu}}{dt}\right) \tag{2.20}$$

In this equation, $\dot{m}_{ch}$ is the primary loop charging flow rate and $\dot{m}_{ld}$ is the letdown flow rate. These rates are determined by the pressurizer's water level controller by adjusting the charging pumps and the opening the letdown valve. The subcooled water spray rate in the pressurizer, $\dot{m}_{sp}$, is determined by the pressure controller. During normal operation, the spray water comes from a line connected to the cold legs and appears as a mass loss term in the primary loop mass balance (Eq. 2.19) and a gain term in the pressurizer internal mass balance. The 4th term on the right hand side of equation(2.19): $\left(\frac{dM_{Rx}}{dt} + \frac{dM_{hl}}{dt} + \frac{dM_{sg}}{dt} + \frac{dM_{cl}}{dt} + \frac{dM_{pu}}{dt}\right)$ is the sum of the rates of change in primary coolant mass in the reactor, the hot leg, steam generator on tube side, the cold leg, and the reactor coolant pump, respectively. Since the internal volumes of these components are fixed, the changes in primary coolant mass in these components are calculated by multiplying the volumes by the time derivatives of the coolant density in the respective components. The volumes are either an input to the model by the user or calculated based on the specified components' geometry and dimensions.

The pressurizer model in the primary coolant loop communicates the water and steam masses in the pressurizer and the steam flow rate through the pressure relief valve, $\dot{m}_{rv}$, to the primary loop model to calculate the total water inventory in the loop. The rate of change in the total water inventory in the primary loop is calculated using the following expression, as:

$$\frac{dM_{tot}}{dt} = \dot{m}_{ch} - \dot{m}_{ld} - \dot{m}_{rv} \tag{2.21}$$

2.5.2 Overall Momentum Balance Equation

The overall momentum balance of the primary loop equates the total pressure losses in the loop to the pressure head calculated by the pump model to determine the coolant flow rate. The total pressure losses in the primary loop are the sum of those due friction in the reactor core and vessel, the hot legs, the primary side of the steam generator, and the cold legs of the primary loop. The internal pressure losses in the reactor coolant pumps are accounted for in determining the net pressure head by the pump model. The friction losses in the primary loop piping and various components are calculated using the following general expression, as:

$$\Delta p_f = \left(\frac{a}{2}\right)\left(\frac{L}{A_{cs}^{2-b}\, D_e^{1+b}}\right)\left(\frac{\mu^b}{\rho}\right)\dot{m}^{2-b} \tag{2.22}$$

In this equation, a = 64 and b= 1 for laminar flow (Re $\leq$ 2100) and for turbulent flow (Re > 3000) a = 0.3164 and b = 0.25 (Haskins and El-Genk, 2017). For transition flow (2100 < Re < 3000) the pressure losses are calculated by interpolation.

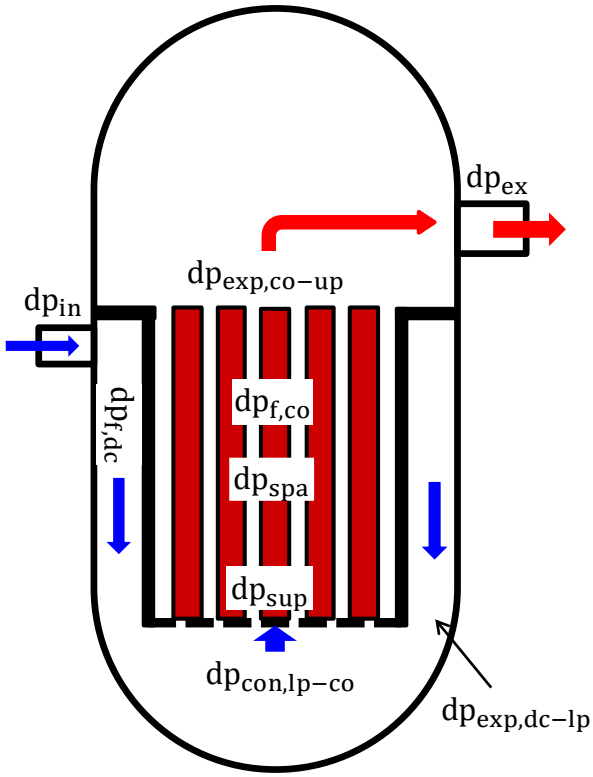

Fig. 2.13: Components of the reactor pressure losses.

2.5.2.1 Reactor Pressure Losses

Figure 2.13 shows the components the reactor total pressure losses. These are for the friction pressure losses in the core, $\Delta p_{f,co}$, the friction pressure losses in the downcomer, $\Delta p_{f,dc}$, the pressure losses due to the lower core support and orificing, Δp_{sup}, the pressure losses due to the spacer grids, Δp_{spa}, and the sum of the expansion and contraction pressure losses, $\Delta dp_{exp\text{-}con}$, Thus the total pressure losses in the PWR can be expressed as:

$$\Delta p_{Rx} = \Delta p_{f,co} + \Delta p_{f,dc} + \Delta p_{sup} + \Delta p_{spa} + \Delta p_{exp-con} \quad (2.23)$$

The pressures losses in the lower core support structure and due to the spacer grids in the fuel assemblies are expressed in terms of flow resistance coefficients, K_{sup} and K_{spa}, respectively. The pressure losses for the flow through the lower core support structure are calculated as:

$$\Delta p_{sup} = \frac{K_{sup}}{2} \frac{\dot{m}^2}{\rho(T_{in}){A_{cs}}^2} \quad (2.24)$$

In this expression, the value of the resistance coefficient K_{sup} depends on the size and geometry of the orifices and baffles in the lower core structures. For an orifice plate, the hydraulic resistance can be calculated using a relationship compiled by Idel'Chik (1960) for flow through a thick-edged plate with orifices (Appendix Fig. A.1).

The pressure losses due to the fuel assembly spacer grids are calculated as the sum of the pressure drops across the number of spacers, N_{spa}, arraigned along the length of the assembly:

$$\Delta p_{spa} = N_{spa} \frac{K_{spa}}{2} \frac{\dot{m}^2}{\rho(T_b){A_{cs}}^2} \quad (2.25)$$

The mass flow rate, $\dot{m}$, is that for the average assembly as in Eq. 2.22, with the thermophysical properties of the coolant evaluated at T_b. The resistance coefficient K_{spa} is calculated using a relationship compiled by Idel'Chik (1960) for rectangular grids (Appendix Fig. A.2-3).

The expansion and contraction pressure losses, $dp_{exp-con}$, which are the sum of the expansion gain from the downcomer to the lower plenum, the contraction losses from the lower plenum to the fuel assemblies in the core, and the expansion gain from the exit of the fuel assemblies to the upper plenum, are expressed as:

$$\Delta p_{exp-con} = dp_{exp,dc-lp} + dp_{con,lp-co} + dp_{exp,co-up} \quad (2.26)$$

In this expression:

$$\Delta p_{exp,dc-lp} = \frac{\dot{m}^2}{\rho(T_{in})} \left[\frac{1}{A_{dc}A_{lp}} - \frac{1}{{A_{lp}}^2} \right] \quad (2.27a)$$

$$\Delta p_{con,lp-co} = 0.7 \frac{\dot{m}^2}{\rho(T_{in})} \left[\frac{1}{{A_{lp}}^2} - \frac{1}{{A_{co}}^2} \right] \quad (2.27b)$$

$$\Delta p_{exp,co-up} = \frac{\dot{m}^2}{\rho(T_{ex})} \left[\frac{1}{A_{co}A_{up}} - \frac{1}{{A_{up}}^2} \right] \quad (2.27c)$$

In these equations, A_{dc}, A_{lp}, A_{co}, and A_{up} are the cross-sectional flow areas in the downcomer, lower plenum, the reactor core, and upper plenum, respectively.

The pressure losses for the flow entering the reactor vessel from the cold legs through inlet nozzles into the vertical downcomer and for the primary water flow exiting the reactor vessel through the hot legs are calculated, respectively, as:

$$\Delta p_{in} = \frac{K_{in}}{2} \frac{\dot{m}^2}{\rho(T_{in}){A_{cs}}^2} \quad (2.28a)$$

$$\Delta p_{out} = \frac{K_{out}}{2} \frac{\dot{m}^2}{\rho(T_{ex}){A_{cs}}^2} \quad (2.28b)$$

The resistance coefficients in these expressions, K_{in} and K_{out} are taken from the tables in Idel'Chik (1960) for a conical diffuser entering a volume with a vertical baffle (Appendix Fig. A.4) and for a conical nozzle with an end wall (Appendix Fig. A.5), respectively.

2.5.2.2 Hot and Cold Leg Pressure Losses

The pressure losses in the reactor hot and cold legs are equal the sum of the friction losses in the circular duct and those due to the ducts' curvature, Δp_c, as:

$$\Delta p_{hl} = \Delta p_{f,hl} + \Delta p_{c,cl} \tag{2.29a}$$

$$\Delta p_{cl} = \Delta p_{f,cl} + \Delta p_{c,cl} \tag{2.29b}$$

In these expressions, Δp_c is determined using a relationship described by Idel'chik (1960) for tubes with a constant bend radius (Appendix Fig. A.6-9) as a function of the angle of the bend in degrees, θ, and the mean radius of curvature R_c.

2.5.2.3 Steam Generator Pressure Losses

The pressure losses model for the two steam generators in the PWR plant simulated (Fig. 2.2) calculates the internal pressures losses for the primary coolant flowing through the lower plenums and in the U-tube bundles. The total pressure losses for the primary coolant flow through the steam generator is the sum of the friction and curvature losses in the tubes, $\Delta p_{f,tu}$ and $\Delta p_{c,tu}$, and those due to the expansion and contraction, $\Delta p_{exp,sg}$ and $\Delta p_{con,sg}$, as:

$$\Delta p_{sg} = \Delta p_{f.tu} + \Delta p_{c,tu} + \Delta p_{exp,sg} + \Delta p_{con,sg}, \tag{2.30}$$

The steam generator model pressure losses are those for an average U-tube, assuming that the primary coolant flow is uniformly distributed among all the U-tubes. The length of the average U- tube is calculated based on the total water volume in all U-tubes and their number and the tube cross sectional flow area. The curvature of the 180° turn section of the average steam generator U-tube is based on the average tube length after subtracted the lengths of the straight sections. The calculated pressure losses in the U-tubes are the sum of the friction losses in the average tube and those due to the 180° bend, calculated using the relationship described by Idel'chik (1960) for tubes with a constant bend radius (Appendix Fig. A.6-9).

The expansion and contraction pressure losses for the primary coolant flow in the steam generator are those of the flow through the inlet nozzle from the hot leg that enters the inlet portion of the tube-sheet and for the U-tubes exit flow through the two nozzles to the suction of the reactor coolant pumps (Fig. 2.2). These losses can be expressed as:

$$\Delta p_{exp,sg} = \frac{\dot{m}^2}{\rho(T_{ex})}\left[\frac{1}{A_{hl}A_{sh}} - \frac{1}{{A_{sh}}^2}\right] \tag{2.31a}$$

$$\Delta p_{con,sg} = 0.7\,\frac{(\dot{m}/2)^2}{\rho(T_{in})}\left[\frac{1}{(A_{sh}/2)^2} - \frac{1}{{A_{pu}}^2}\right] \tag{2.31b}$$

In these equations, A_{hl} is the cross sectional flow area of the Hot Leg duct, A_{sh} is the total inlet/outlet flow area for the U-tube bundles tube-sheet, and A_{pu} is the cross sectional flow area for the pump suction duct.

2.5.2.4 Mass Flow Rate Calculation

The change in the rate of the water flow in the primary loops and through the reactor core is determined in terms of total pressure losses and generated pressure head by the coolant pumps, as:

$$\frac{d\dot{m}}{dt} = \left(\Delta p_{pump} - \sum \Delta p_{loss}\right)\frac{A_{cs}}{L_{tot}} \tag{2.32}$$

The primary coolant flow rate decreases when the total pressure losses in the primary loops exceed the pumping head and vice versa. At steady state operation the change in the primary coolant flow rate is zero, as the total pressure losses equals the pressure head provided by the pumps in the cold legs of the primary coolant loop (Fig. 2.2).

2.6 Summary

This section described the developed PWR plant's physics based transient model for future implementation in the NICSim platform. The developed model comprises multitude of transient and physics based models and sub-models of the different components in the primary loop, namely: (a) a dynamic reactor model with coupled point kinetics and thermal-hydraulics submodels, (b) a 3-region, non-equilibrium pressurizer model, (c) a steam generator model, and (d) a reactor coolant pumps model.

These physics-based models are integrated into the primary loop model that thermally and hydrodynamically couples them. The primary loop model solves the overall mass, momentum, and energy balance equations and calculate the plant state variables such as the total flow rate of the primary coolant, the reactor inlet and exit temperatures, the system pressure, and water levels in the pressurizer and the steam generator, the exit quality of the secondary coolant in the steam generator, the total pressure and heat losses and the total heat supplied to the steam generator. The component models of the integrated PWR plant model are coupled to the PLCs in the emulated plant I&C systems. The PLCs which make up the reactor safety monitoring and protection I&C system and the plant operation I&C systems are the subject of the next section.

3. PLCs in I&C Systems of a Representative PWR Plant

The I&C system of a representative PWR plant for implementation into the NICSim platform includes a few emulated PLCs within the safety and protection and the plant operation I&C systems. The PLCs within the plant protection and safety monitoring I&C system initiate the reactor trip function and the Engineered Safety Features (ESF) actuation function. The PLCs in the plant operation I&C system autonomously regulate the reactor power, system pressure, the water levels in the pressurizer and the steam generator, and the secondary feedwater flow to the steam generators. The developed PWR nuclear plant in Section 2 is linked to emulation models of the digital components within the plant's I&C system (Fig. 1.1). The calculated values of the state variables by the physics-based models of the plant components and primary coolant loop would be provided in the input to the developed and implemented digital I&C system of these components within SCEPTRE framework. These state variables are analogous to the sensor instrument measurements received by the physical PLC's I/O modules in a real plant. The PLCs respond to the input values of the calculated state variable according to their programming and transmit control signal values back to the plant model to adjust its operation.

Emulated PLCs in a representative PWR plant I&C system are developed to support future cybersecurity investigations and analyses. These controllers emulate the PLCs' operating system kernel and control software and communicate using the same ICS communication protocols. Each PLC is emulated using a virtual machine that runs using the open-source OpenPLC software with its control logic program (Alves, et al. 2014). The OpenPLC software runs control programs written in IEC 61131-3 standard PLC programming languages. The virtual machines use the VMWare virtualization platform (VMware, 2019), which runs an image of the Raspian operating system with OpenPLC installed. The individual emulated PLCs are created by changing the control programming within the OpenPLC runtime.

The values of the state variable calculated by the PWR plant model are communicated by the Data Interface (Fig. 1.2) to the control program within the OpenPLC runtime over the network using the Modbus ICS communication protocol over TCP/IP. The control signals generated by the PLCs are then communicated back to the Data Interface Program (Fig. 1.2) using Modbus over TCP/IP to be transmitted back to the PWR plant model (El-Genk et al., 2020a). These emulated PLCs are developed using an emulation methodology developed by the NICSim project team. This methodology characterizes key physical and digital signatures of the PLCs and validates these signatures against those of emulated PLCs (Fasanao et al., 2020). Validation and testing of the PLC emulation methodology is conducted to determine the required settings to ensure that the emulated PLCs replicate the performance and network traffic behavior of the physical devices. The description and the validation and testing for this PLC emulation methodology is described in a previous report (El-Genk et al., 2019) and is updated in a companion report (El-Genk et al., 2020b *in progress*).

3.1 Plant Protection and Safety Monitoring System PLCs

The Plant Protection and Safety Monitoring System (PMS) employs a series of PLCs to provide the actuation protective functions for the reactor trip and the Engineered Safety Features (ESF). The Core Protection Calculator (CPC) PLCs perform the reactor trip voting function (Fig. 3.1). The four independent CPC PLCs each receive values of the state variables from the physics based PWR plant model. These include the reactor thermal power, positions of the control element assembly, the water temperatures in the hot and cold legs of the primary loops, and system pressure and the water level in the pressurizer. The PLC uses the provided values of the

state variables to independently determine the coolant flow rate in the primary loop. The first determination is based the shaft speed and supply curve of the coolant pumps and the demand curve primary for the reactor primary loop. The second determination is from the measured pressure differential across a section of the hot leg. The logic programming of the CPC uses the provided state variables to calculate safety parameters (Fig. 3.2), namely: (a) the Critical Heat Flux Ratio (CHFR) and its margin to a minimum set point, (b) the reactor coolant flow rate based on sensor readings and determine if adequate to remove the heat generated in the reactor core, and (c) the margin of the coolant core exit temperature relative to that of saturation at system pressure (Fig. 3.1).

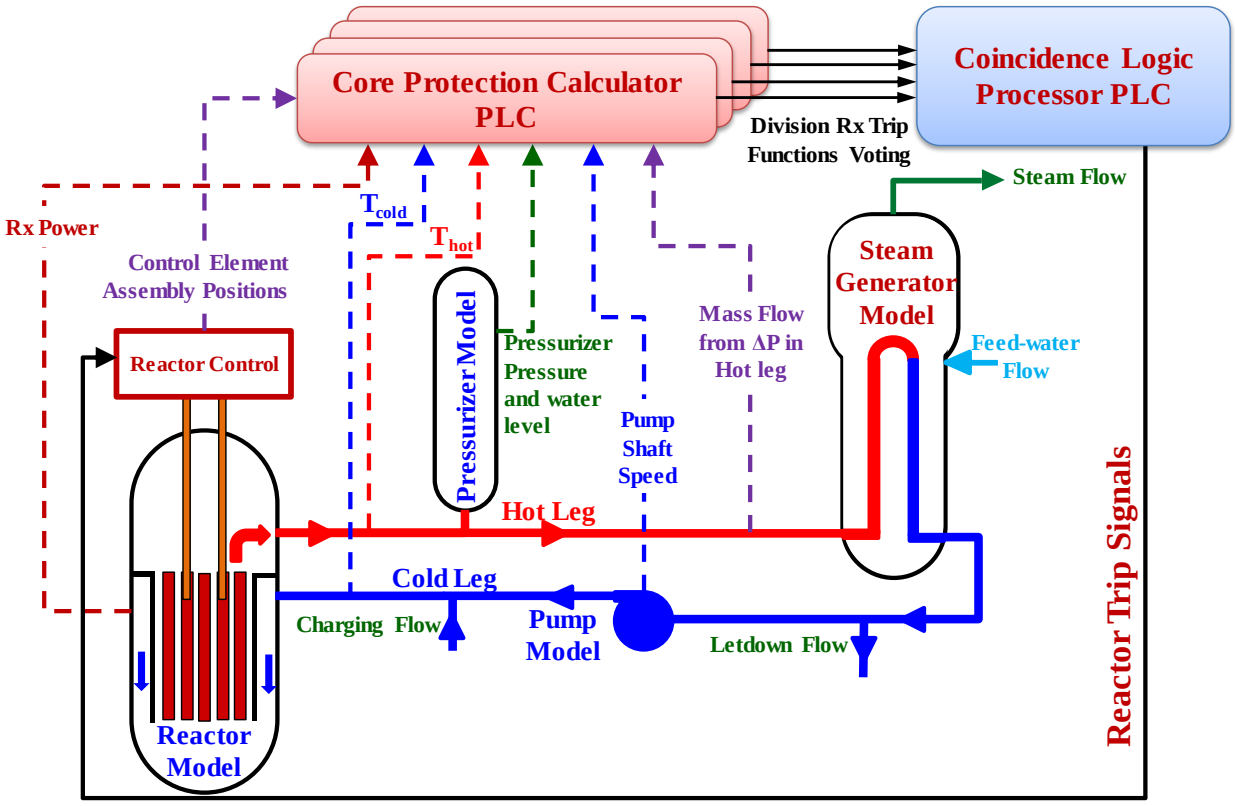

Fig. 3.1: A block diagram of a PWR digital reactor safety I&C system for trip function (El-Genk et al., 2020a).

The primary trip function of the CPC is to calculate the CHFR and compare it to the minimum allowable setpoint (Fig. 3.2). This setpoint is determined considering the response time of the PLC to trip the reactor before the CHFR drops below 1.0 and boiling ensues in the hot channel. The minimum CHFR setpoint, typically 1.5-2, provide sufficient margin to allow the CPC to respond before reactor conditions become unsafe. The Critical Heat Flux (CHF) is calculated using the ANL correlation (Jens and Lottes, 1951) in terms of the coolant mass flux and both the saturation temperature and the bulk temperature in the reactor core. The CPC calculates the surface heat flux axial distribution of at 10 discrete locations of the fuel rod in the hot channel and the axial distribution of the CHFR in the hot channel. It then compares the lowest CHFR to the specified minimum setpoint. If the calculated CHFR reaches or drops below the lowest set point the CPC sends a trip vote to a logic coincidence counter PLC (Fig. 3.2). The

calculated temperature margin of the reactor exit temperature to the saturation temperature, T_{sat}, is compared to the difference between the two setpoints (Fig. 3.2). If the margin decreases below the setpoint, the CPC sends a trip vote to the logic coincidence counter PLC. Additional trip functions can be easily added to CPC's programming.

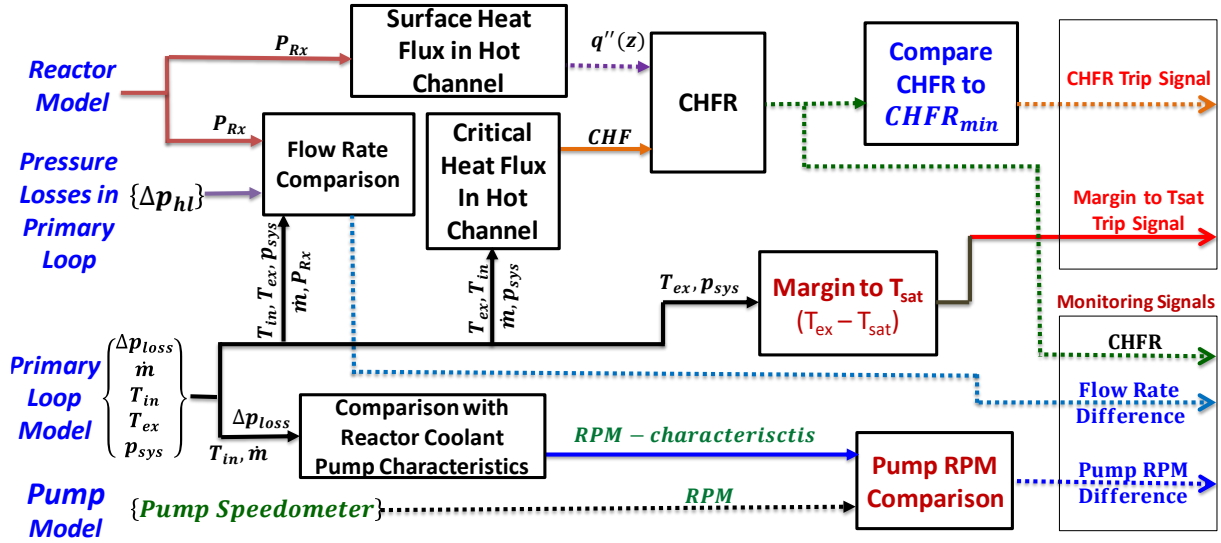

Fig. 3.2: CPC functional block diagram for determining and comparing CHFR and margin to saturation temperature for a PWR plant to set points for trip functions (Hahn, El-Genk, Schriener, 2020)

In addition to the trip protection function, the CPC also monitors the values of the different PWR state variables and sends a warning signal to the operators if these values exceed the programmed limits. Fig. 3.2 shows two monitoring functions added to the CPC. The first calculates the mass flow rate from the energy balance across the reactor using the calculated state variables, T_{in}, T_{ex}, p_{sys}, and P_{Rx}. This mass flow rate is compared to that determined from the measured different pressure drop across a segment of the hot leg, Δp_{hl}. If the difference is greater than the programed tolerance, the CPC sends a warning signal.

The second monitoring function shown in Fig. 3.2 compares the reported shaft rotation speed for the reactor coolant pumps from the pump model to the RPM estimated from the programed pump characteristics based on the calculated total flow rate and pressure losses in the primary loop, Δp_{loss}. The difference between the reported pump shaft RPM and that predicted from the pump characteristics, if more than the allowed tolerance, may indicate a malfunction in one of the reactor coolant pumps and the CPC sends a warning signal to the operator (Fig. 3.2). The CPC PLC's program communicates the signals for each of the separate trip functions to the coincidence logic processer PLC (Fig. 3.1). The coincidence logic processer PLC compares the separate voting signals of the four separate safety CPC PLCs and generates a reactor trip signal when 2/4 voting coincidence is satisfied. This signal is then communicated back to the PWR plant model to trip the reactor (Fig. 3.1).

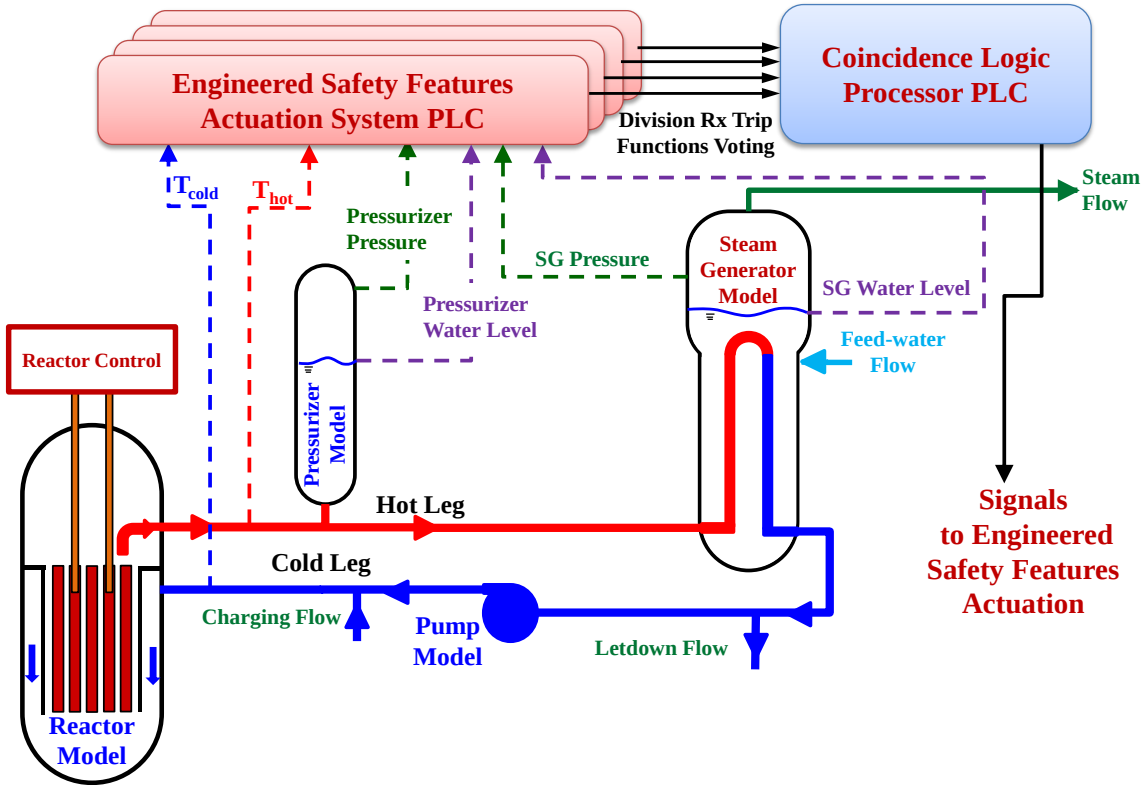

Fig. 3.3: Block diagram of the digital reactor safety I&C system for the engineered safety features actuation system (El-Genk et al., 2020a)

The PLC of the Engineered Safety Features Actuation System (ESFAS) performs the automatic actuation function for the plant's ESF. The four independent ESFAS PLCs receive values of the state variables from the models of the various components and of the primary loops of the PWR plant. These state variables are the hot and cold leg coolant temperatures, the system pressure, and the water levels in the pressurizer and the steam generators (Fig. 3.3). The values of these state variables are compared to setpoints programed within the PLCs for the different ESF systems of the plant. If the PLCs' programming determines that any of the state variables exceeds the safety setpoint for an ESF system, the PLC sends a voting signal to actuate that system. The Coincidence Logic Processor PLC receives the voting signals from the four ESFAS and sends an actuation signal to the various PWR plant components.

3.2 PWR Plant Operation PLCs

In addition to the PLCs of the plant protection and safety monitoring system, the representative I&C system architecture includes PLCs for the autonomous operation of plant components in the reactor primary loop. While the initial focus of the NICSim project is on the cybersecurity of the plant protection and safety monitoring I&C system, representations of the controllers in the plant operation I&C system are needed for the integrated PWR plant model to function properly. The plant operation I&C system in a nuclear plant is typically less isolated than the plant protection and safety monitoring I&C system. It has more network connections to other components, which may make its PLCs more vulnerable to cyber-attacks.

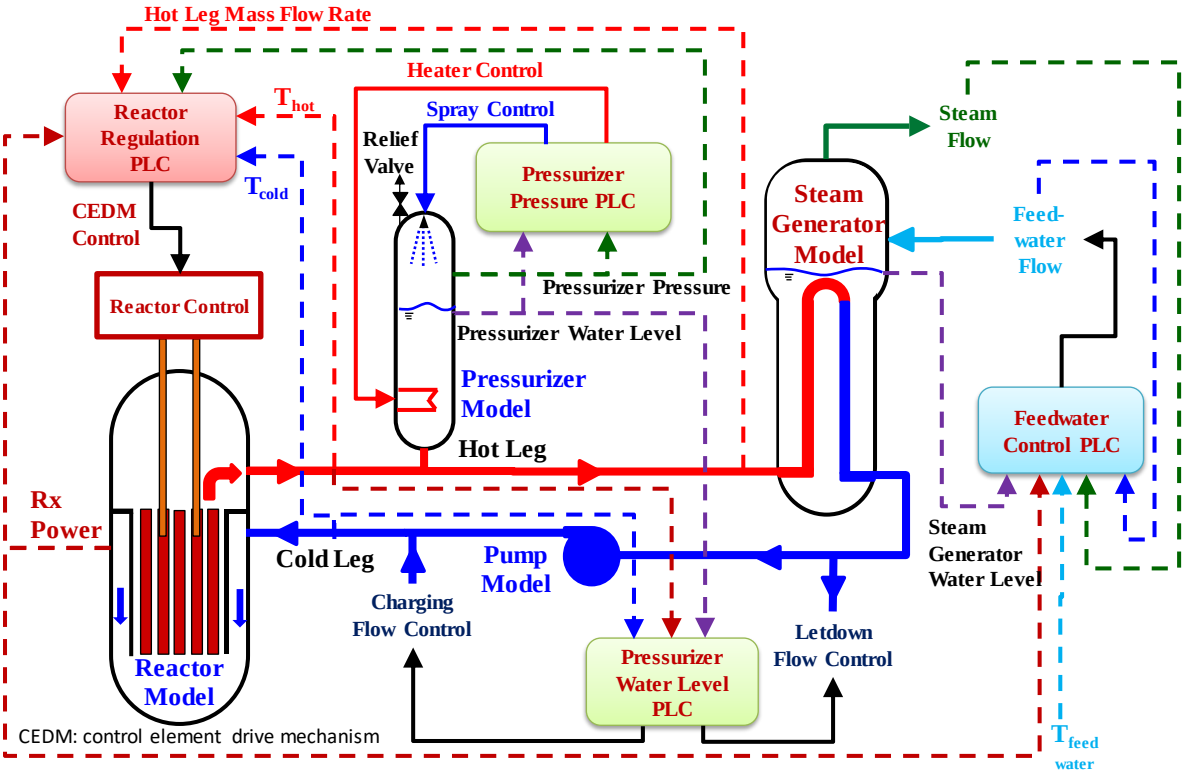

Fig. 3.4: Block diagram of operational I&C system programmable logic controllers for a PWR primary loops. (El-Genk et al., 2020a)

The representative PWR plant operation I&C system comprises five different PLCs. These are a reactor regulation PLC, a pressurizer pressure control PLC, a pressurizer water level control PLC, a steam generator feedwater control PLC, and a primary coolant pump control PLC (Fig. 3.4). These PLCs receive state variables from the physics-based plant model and send signals to the model for direct control feedback. Some of these PLCs function are mostly independent of the reactor operators using pre-programed setpoint values, while others allow for operators in the control room to change setpoints to adjust the state of the operating plant.

Each PLC in the plant operation I&C system is independently developed and tested. First, in connection with the a PWR plant model, and subsequently with the entire integrated plant model. Several of the plant operation I&C system PLCs use Proportional-Integral-Differential (PID) controllers that depend on the system time and require the controllers' integration and differentiation functions to be matched in time with the simulation. To support their use, the Data Transfer Interface program (Fig. 1.2) synchronizes the Simulink PWR plant model with a real-time clock to ensure that the emulated PLCs and plant model are running on same time scale.

3.2.1 Reactor Regulation PLC

The Reactor Regulation PLC provides autonomous control of the control rods to maintain the reactor thermal power at the level specified by the operator. Fig. 3.5 shows a functional diagram of the control programming of the reactor regulation PLC. It receives state variables from the PWR primary loop model that include the reactor inlet and exit temperatures, T_{in} and T_{ex}, the system pressure determined in the pressurizer model, p_{sys}, the total primary loop mass flow rate, $\dot{m}$, and the reactor thermal power, calculated by reactor model, P_{Rx}. The program for this PLC

has two functions. First, it compares P_{Rx} to the value $P_{th,}$ calculated from the overall energy balance in the primary loop, based on the temperature difference $\Delta T = T_{ex} - T_{in}$, the average specific heat capacity, C_p, of the primary coolant at its average temperature, T_{ave}, and p_{sys}. The difference between the two values of the reactor power is recorded and indicated to the operator. Such difference could indicate a malfunction in the nuclear instrumentation, or in the temperature and flow rate measurements used to calculate P_{th}.

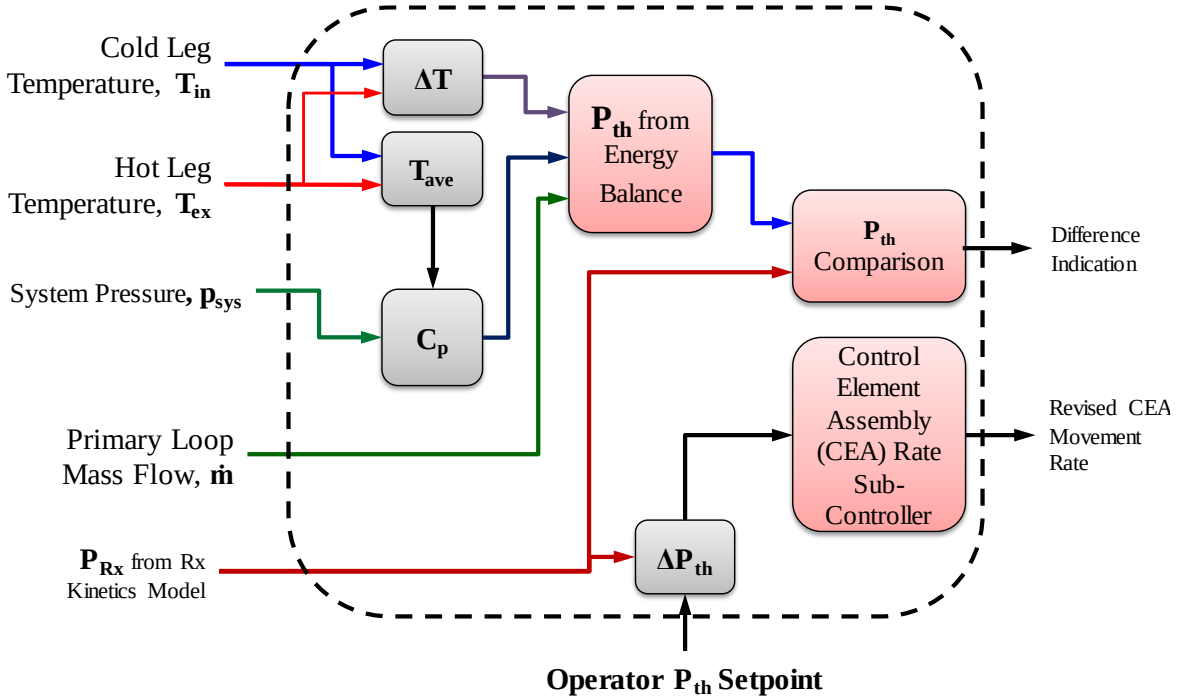

Fig. 3.5: Block diagram of the reactor regulation PLC.

The second function of the reactor regulation PLC is to regulate the reactor thermal power to match an operator specified setpoint by adjusting the position of the Control Element Assemblies (CEAs) in the reactor core (Fig. 3.5) It compares the P_{Rx} to an operator specified setpoint, P_{th}, and communicates the difference, $\Delta P_{th} = P_{Rx} - P_{th}$, to a sub-controller of the CEAs. The sub-controller calculates the needed rate of movement of the CEAs to adjust the external reactivity to maintain the specified steady reactor thermal power, P_{th}. If the reactor power is below the specified level the CEAs are withdrawn from the core to increase the power, and vice versa. The power regulation function is enabled during nominal operation and is not used during reactor startup, when the movement of the CEAs are controlled by the operator.

3.2.2 Pressurizer Pressure PLC

The two PLCs for the pressurizer control the pressure and the water level in the pressurizer within programed setpoints. The pressure PLC adjusts the system pressure by controlling the power generated by the proportional and backup electrical heaters and by opening or closing the water spray valve (Figs. 2.6 and 2.7). Fig. 3.6 presents a functional block diagram for the program of the pressurizer pressure PLC (Altamimi, El-Genk, Schriener, 2020). The system pressure, p_{sys}, is compared to the setpoints for three pressure control mechanisms. The PLC program has six pressure setpoints, which are pre-set prior to operation. These six setpoints mark the on and off points for the proportional and backup electrical heaters, and the spray nozzle.

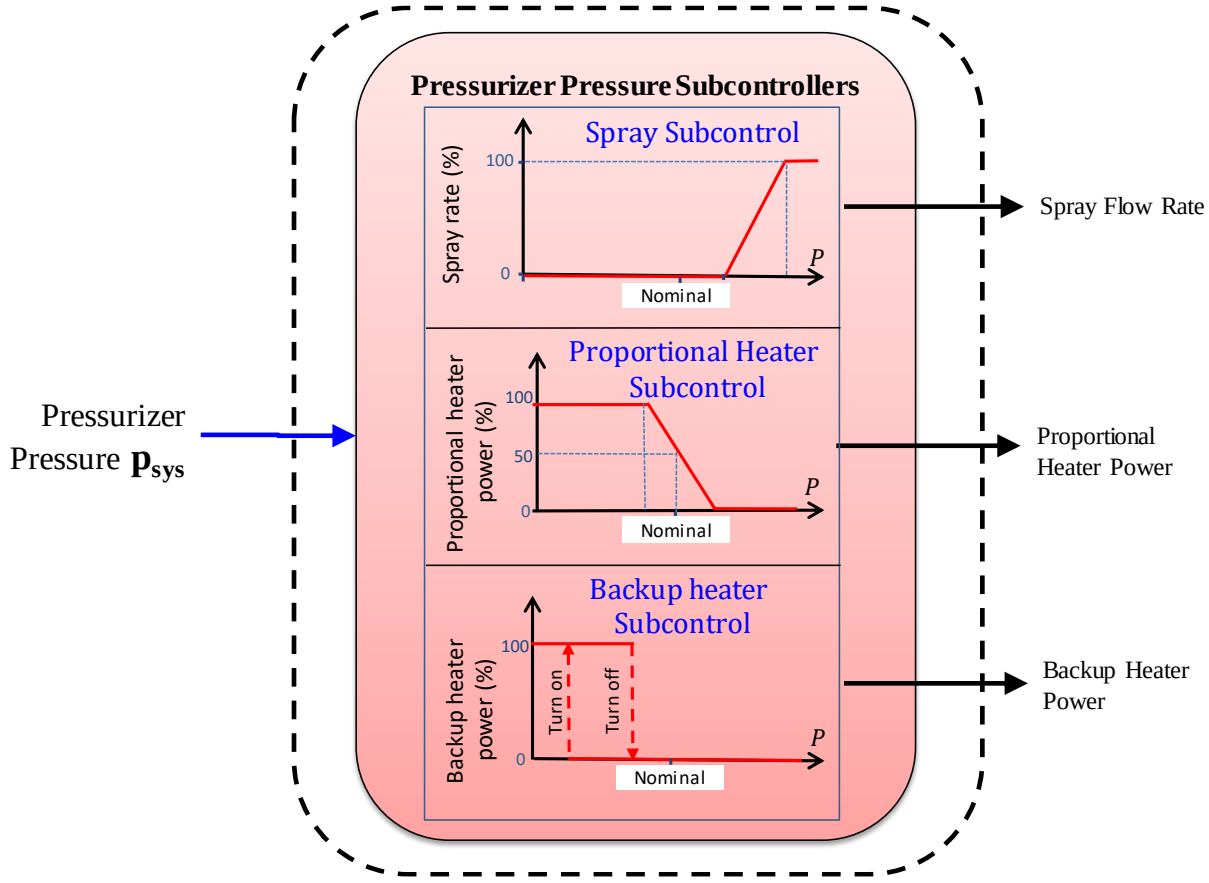

Fig. 3.6: Block diagram of pressurizer pressure PLC (Altamimi, El-Genk, Schriener, 2020)

A control routine regulates the power supplied to the proportional heaters bank (Fig. 3.6). During nominal operation. p_{sys} is midway between the off and on setpoints for the proportional heaters, with the heaters operating at 50% of full power to make up for heat losses through the pressurizer wall. The electrical power supplied to the proportional heaters changes proportional to the system pressure, and ranges from 100% power at the lower setpoint to 0% at the upper setpoint. The change in heater power increases or decreases the rate of flash evaporation in the pressurizer (Fig. 2.7) to adjust the system pressure to nominal level (Fig. 3.6). When the system pressure, p_{sys}, decreases below its lower setpoint, in addition to the proportional heaters, the backup heaters switch on to increase flash evaporation and raise the system pressure. Unlike the proportional heaters or the liquid spray value, the backup heaters are either off at 0% power or on at 100% power (Fig. 3.6). The backup heaters remain on until the system pressure reaches the upper setpoint to turn them off.

If the system pressure, p_{sys}, increases past the upper setpoint for the proportional heaters, the lower setpoint for the spray control will be exceeded and the control routine opens the spray nozzle (Figs. 2.7 and 3.6). Subcooled water injected through the swirl-vane nozzle breaks up into tiny droplets. These droplets provide a large surface area for condensing saturated vapor in the pressurizer and decreasing its vapor volume and thus the pressure. The spray valve controls the mass flow rate of the spray water proportional to the pressure. At the lower control setpoint, the spray valve closes, and the spray rate is zero. The spray rate increase with increased system pressure to 100% when the spray valve is fully open at the upper setpoint.

3.2.3 Pressurizer Water Level PLC

The pressurizer water level PLC regulates the water level in the pressurizer and hence the total water volume in the primary loops. It accommodates the changes in the water volume in the primary loops due to thermal expansion and contraction, following an increase or a decrease in the reactor thermal power. This PLC adjusts the water inventory in the primary loop and the pressurizer by controlling the rates of water inflow from the charging pumps and outflow through the letdown valves (Figs. 2.1 and 3.4).

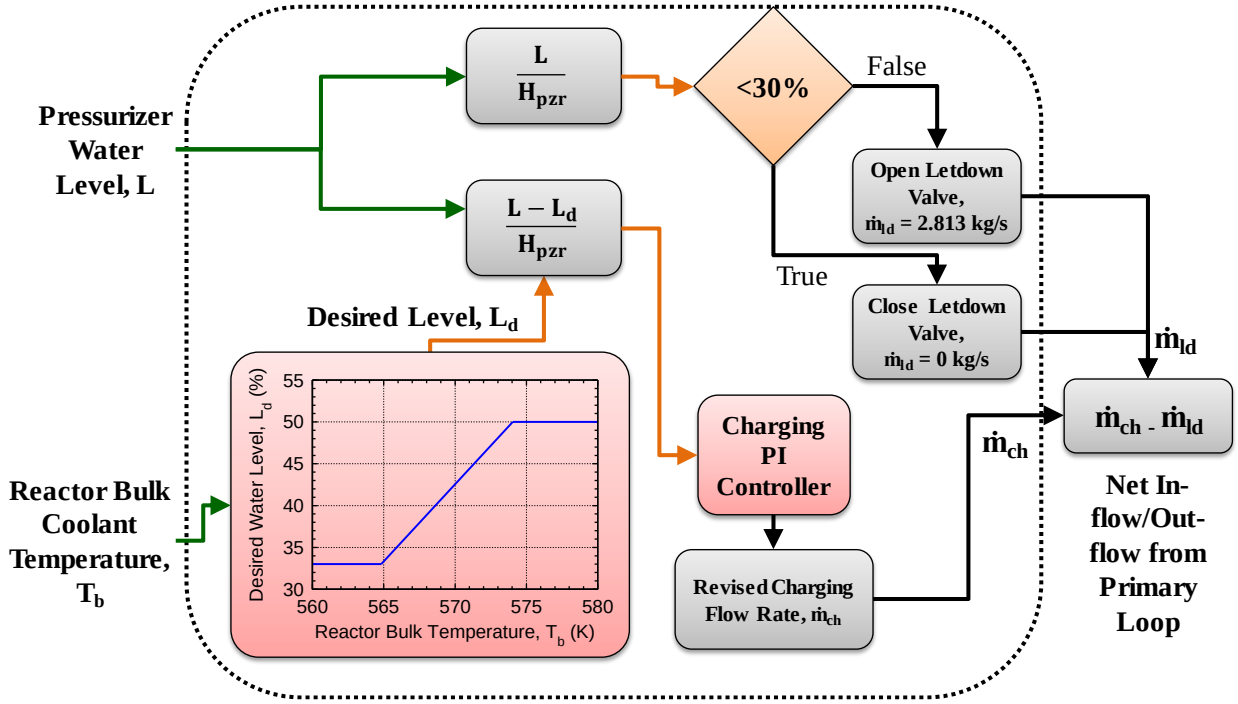

Fig. 3.7: Block diagram of the pressurizer water level PLC.

Fig. 3.7 presents a block diagram of the programming within the pressurizer water level PLC. This PLC compares the water level, L, from the pressurizer model to the desired water level, L_d, calculated by the PLC. The value of L_d varies with the bulk coolant temperature in the reactor to accommodate the thermal expansion of the primary coolant during startup. The difference between these water levels, normalized to the height of the pressurizer, $(L-L_d)/H_{pzr}$, is communicated to a Proportional-Integral (PI) controller, which adjust the flow rate for the charging pumps (Fig. 3.7). In addition, the water level normalized to the height of the pressurizer, L/H_{pzr}, is compared to a low setpoint of 30%. The letdown valve is nominally open and closes when the water level in the pressurizer is lower than the setpoint. The difference between the charging rate and the letdown rate determines the net inflow and outflow of coolant from the primary loop, assuming no leaks are present.

When the water level in the pressurizer drops below the desired level, the PLC's program adjusts the charging rate of the primary loops to increases the total coolant inventory in the primary loop. When the level is above the desired level, the charging rate decreases below the letdown rate to decrease the coolant inventory in the primary loops. The PI controller in the pressurizer water Level PLC adjust the level smoothly during reactor transients and avoids sharp changes in the water level.

3.2.4 Feedwater Control PLC

The steam generator feedwater control PLCs maintain the water inventory in the two steam generators such that the U-tube bundles are adequately covered with water. The PLCs monitor the water level measured in the downcomer of the steam generator and adjust the feedwater flow rate into the secondary side of the steam generator. The throttle valve between the main feedwater pumps and the feedwater injection ring in the steam generator adjusts the feedwater flow rate to the steam generator (Figs. 2.9 and 3.4). The feedwater control PLC adjusts the throttle valve position based on comparisons of two state variables (Fig. 3.8).

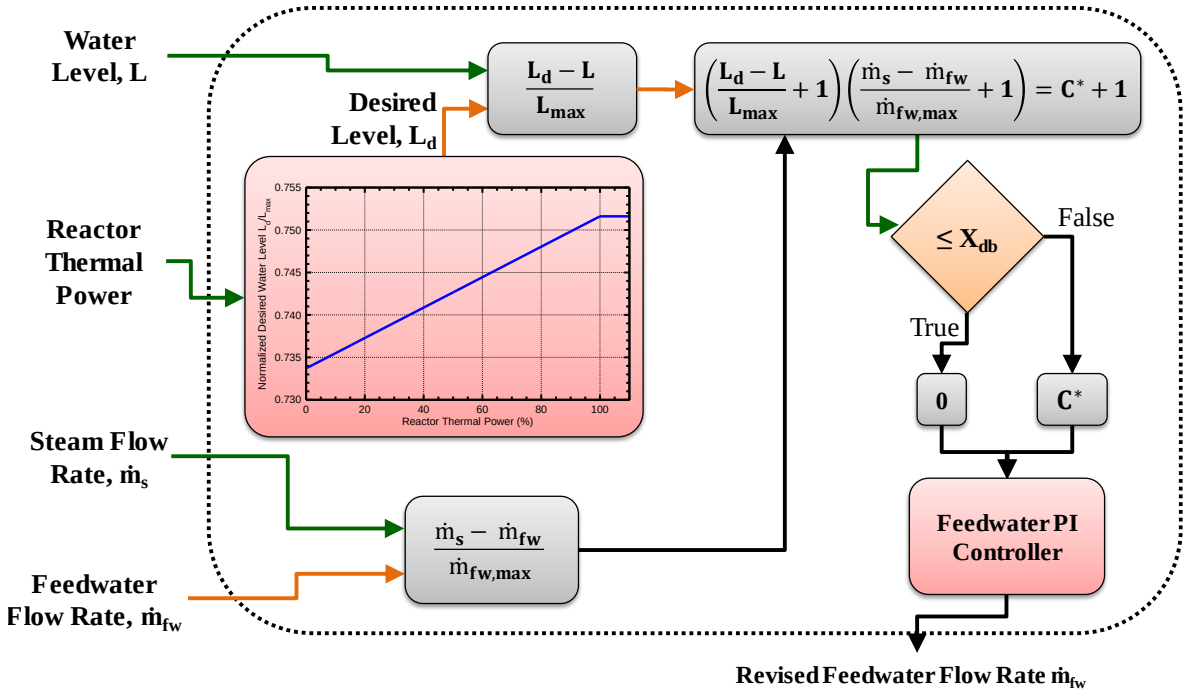

Fig. 3.8: Block diagram of steam generator feedwater control PLC

The PLC program compares the water level in the steam generator annular downcomer, L, to the desired level, L_d, calculated by the PLC as a function of the reactor thermal power, P_{Rx}. The PLC program also monitors the difference between the steam flow rate, $\dot{m}_s$, and the feedwater flow rate, $\dot{m}_{fw}$. The normalized difference between the water levels in the downcomer of the steam generator and the desired water level to the maximum water level in the steam generator, $(L_d - L)/L_{max}$, is determined. This calculated value is combined with the difference between the steam and feedwater flow rates, normalized to the maximum feedwater flow rate, $(\dot{m}_s - \dot{m}_{fw})/\dot{m}_{fw,max}$, into a control parameter C* (Fig. 3.8). The controller PLC works to minimize C*, considering both the water levels difference as well as the flow rates difference simultaneously. This minimizes sharp changes in the water level during operational transients and produces smooth changes in feedwater flow rate.

The combined control parameter C* is passed through a deadband filter, which zeros the value if it is within the programed deadband size, X_{db}. The deadband filter inhibits control action when the differences between the actual and desired water level, and between the steam and feedwater flow rates are small. This action limits the frequency of adjusting the throttle valve for the feedwater flow rate. The output from the deadband filter is communicated to a Proportional-Integral (PI) controller, which determines the new throttle valve position to adjust the feedwater

flow rate. The proportion and integral constants in the PI controller are tuned to ensure smooth response during operation transients.

3.2.5 Reactor Coolant Pump PLC

The reactor coolant pump (RCP) PLC controls the circulation of the coolant within the primary loop by adjusting the rotation speed of the pumps (Fig. 3.9). Each RCP in the developed PWR plant model has its own PLC. The PLC program receives the state variables of the cold leg and hot leg temperatures, T_{in} and T_{ex}, the system pressure, p_{sys}, and the reactor thermal power, P_{Rx}, and use them to to calculate the total mass flow rate through the reactor, $\dot{m}$, from the overall energy balance as: $\dot{m} = P_{Rx}/(C_p*(T_{ex} - T_{in})$. The primary coolant specific heat capacity, C_p, is calculated as functions of the state variable temperature and pressure (Fig. 3.9).

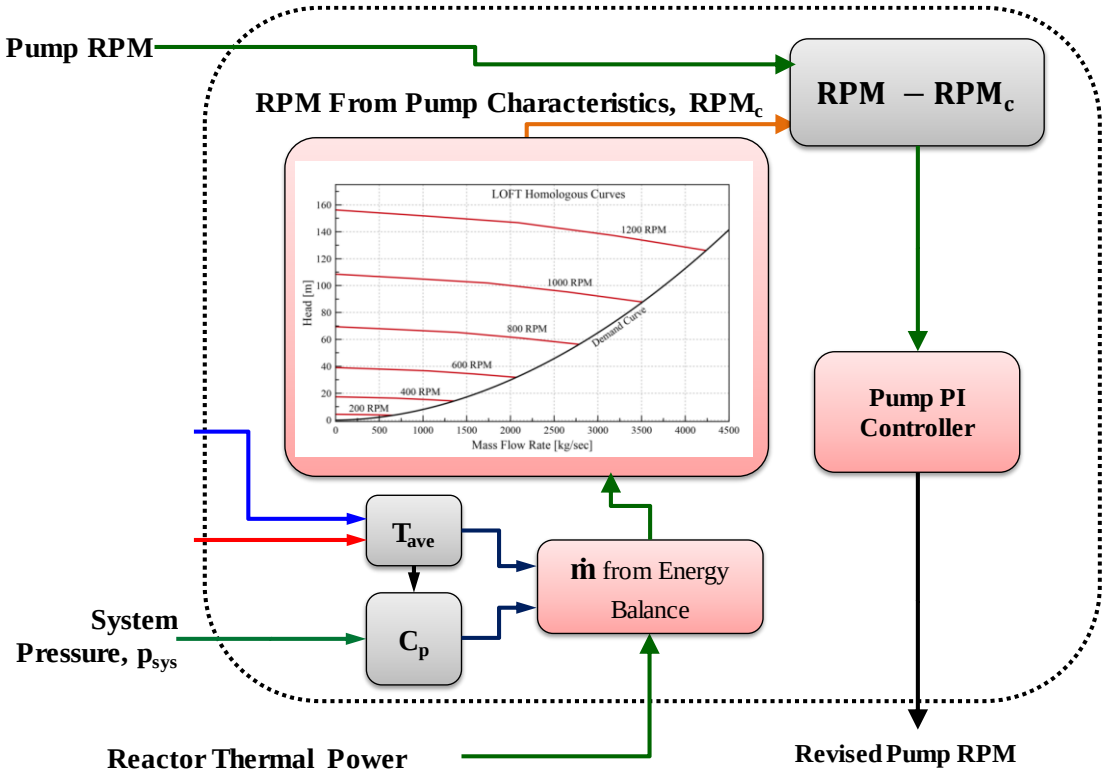

Fig. 3.9: Block diagram of reactor coolant pump (RCP) PLC.

The calculated mass flow rate is compared to the pre-programmed pump head demand curve to calculate the pump rotation speed RPM_c, from the pump characteristics. The PLC also receives the state variable value of the pump RPM from the corresponding RCP model, which represents the value which would be measured using speedometers on the RCPs in a PWR. The calculated RPM_c is compared to that reported by the RCP model and the difference is communicated to a PI controller. It controls the power supply to the pump to adjust its rotational speed to minimize the difference between the rotation speeds of the pump (RPM-RPM_c).

3.3 Summary

The developed integrated physics-based dynamic model of a representative PWR plant, like a real plant, does not function alone but is integrated with autonomous controllers in the plant's I&C systems. These include the safety PLCs in the plant protection and safety monitoring I&C

system, and the controller PLCs in the plant operation I&C system. Designs are developed for a CPC PLC that performs the reactor trip function and the ESFAS PLC that autonomously actuate the plant's engineered safety features. Within the plant operation I&C System, we developed a reactor power regulation PLC, a pressurizer pressure controller PLC, a pressurizer water level controller PLC, a steam generator feedwater control PLC, and a reactor coolant pump controller PLC.

These controllers continuously receive state variables from the PWR primary loop model and return control signals that adjusts the plant operation to keep state variable within the programed setpoints. More details on the development and testing of the PLCs can be found in a companion report (El-Genk et al., 2020b *in progress*). The next section presents results of validating the models of the various components in the PWR primary loop model, Results are also presented of the calculated state variables using the integrated PWR plant model to simulate operation transients of startup and following an increase in the load demand.

4. PWR Plant Model Results and Model Validation

This section presents results of the developed PWR plant model described in Section 2 to validate the component models in the primary loop by comparing predictions to reported design values for NRC-licensed PWR designs and to reported experimental results from scaled test facilities. Also presented and discusses are the results of the developed model of the integrated PWR plant for two operation transients of reactor startup and following an increase in the load demand. The dynamic response of the PWR plant dependent on those of the integrated physics-based models of the components in the primary loop and the connected PLCs.

4.1 PWR Plant Model Validation

For the validation effort the components models are investigated individually and not integrated within the primary loop model. The performed transient analyses directly incorporate the PLCs in the operation I&C system within the Matlab Simulink model of the PWR plant. The program logic for the controllers detailed in Section 3 are recreated using the Simulink model elements, with the calculated values of the state variables and control signal are communicated internally within Simulink between the PWR plant model and the controllers. A future technical task of the current NEUP project is to investigate integrating and testing the Simulink PWR plant model with emulated PLCs running inside virtual machines in the NICSim platform (Fig. 1.1).

To help validate the individual models the computed results are separately compared to experimental results or reported official design calculations for commercial PWRs and experimental facilities when available. The developed physics-based component models are tested against reported results to help validate their modeling approach and verify the implemented equations. Results are presented for validating portions of the reactor model, the pressurizer model, the primary pump model, and the pressure loss model in the primary loop. The results of this effort help validate the reactivity feedback effects within the reactor model are during the simulated operation transients.

4.1.1 Comparisons of Reactivity Feedback Effects

In order to examine the transient response of the components and the primary loop models for a PWR plant, expressions for the different temperature reactivity feedback effect are acquired and implemented in the reactor kinetic model. Theses expression are based on the reported data for the fuel temperature reactivity feedback, $\rho_{f(T)}$, and the total feedback reactivity, ρ_{fb}. The values of the temperature reactivity feedback effects depend on calculated temperatures as functions of the reactor power level. Because the boron concentrations were not reported, insufficient information was available in the report to compare the calculated total temperature feedback with the reported values. The values of the fuel temperature reactivity feedback can still be compared.

In the present analyses, the developed reactor model is configured to represent a standardized AP1000 PWR design. The design data and parameters are reported in the AP1000 Design Control Document (Westinghouse Electric Company, 2011) and the Core Reference Report (Hone et al., 2015). The reported temperature reactivity feedback effects for the AP1000 are those of $\rho_{f(T)}$ and $\rho_{m(T)}$. For the latter, the moderator temperature feedback coefficient $\alpha_m(T)$ is reported as a function of the soluble boron concentration in parts-per-million (ppm).

Fig. 4.1 compares the reported fuel temperature reactivity feedback coefficient, $\alpha_f(T)$, as a function of the fuel temperature (Hone et al. 2015) as well as the applicable polynomial function fit used in the reactor point kinetics model. In this figure, the reported reactivity values are in SI units of ρ/K. The values of the feedback coefficient shown are for both Beginning-of-Life (BOL)

and End-of-Life (EOL) fuel compositions (Fig. 4.1). As the date in this figure shows, $\alpha_f(T)$ becomes less negative with increasing fuel temperature both at BOL and EOL. However, fuel temperature reactivity the feedback coefficient is negative at EOL than at BOL. The reported values of the fuel temperature reactivity feedback coefficients for the AP1000 at BOL and EOL are correlated respectively, as:

$$\alpha_f(T) = -1.0624 \times 10^{-11}\, T_f^{\,2} + 2.8632 \times 10^{-8}\, T_f - 4.3446 \times 10^{-5} \quad (4.1)$$

$$\alpha_f(T) = -3.1764 \times 10^{-11}\, T_f^{\,2} + 6.9219 \times 10^{-8}\, T_f - 6.7265 \times 10^{-5} \quad (4.2)$$

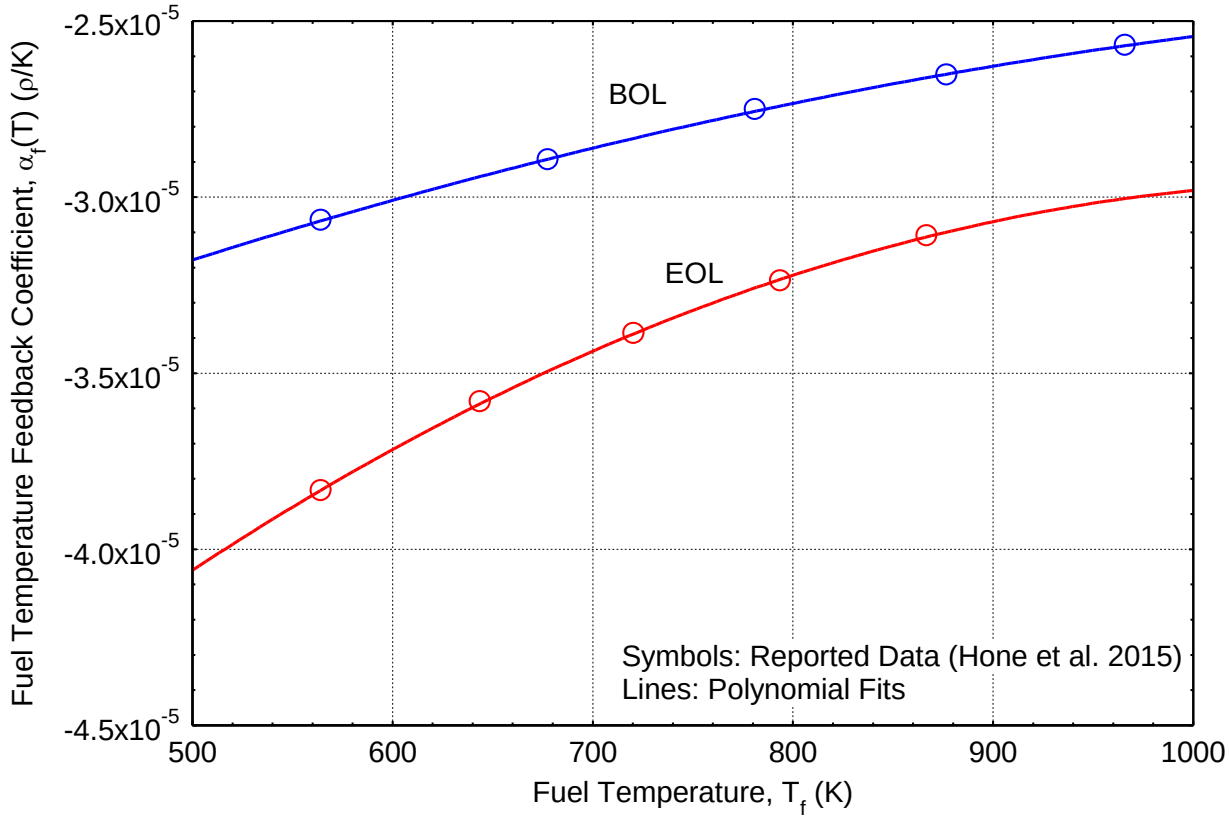

Fig. 4.1: Reported values of the AP1000 reactor fuel temperature reactivity feedback coefficient.

The present data in Fig. 4.2 is of the reported BOL moderator temperature reactivity feedback coefficient, $\alpha_m(T)$, as a function of temperature and the soluble boron concentration (Hone et al., 2015), The developed polynomial fits of this data are implemented in the present reactor point kinetics component of the developed Matlab Simulink reactor model. In this figure the reported reactivity values are also converted to SI units of ρ/K.

The results in Fig. 4.2 show that for a given moderator temperature $\alpha_m(T)$ becomes more positive with increased concentration of the soluble boron. For a given soluble boron concentration, $\alpha_m(T)$ initially become more positive with temperature before peaking and more negative with further increase in temperature (Fig. 4.2). The reported values of the moderator temperature reactivity feedback coefficient for the AP1000 are presented and fitted in Fig. 2.4 as a function of the soluble boron concentration at different moderator bulk temperatures, T_b, as:

$$\alpha_{m(T)} = a_1\, T_b^{\,4} + a_2\, T_b^{\,3} + a_3\, T_b^{\,2} + a_4\, T_b + a_5, \quad (4.3)$$

In this expression, the coefficients a_1, a_2, a_3, a_4, and a_5 are expressed as functions of the concentration of the soluble boron in the moderator, S, in ppm, as:

$$a_1 = -6.7100 \times 10^{-27}\, S^4 + 4.1314 \times 10^{-23}\, S^3 - 8.6231 \times 10^{-20}\, S^2 + 5.6049 \times 10^{-17}\, S + 1.0602 \times 10^{-14}, \quad (4.4)$$

$$a_2 = 1.2432 \times 10^{-23}\, S^4 - 7.5495 \times 10^{-20}\, S^3 + 1.5249 \times 10^{-16}\, S^2 - 8.1803 \times 10^{-14}\, S - 4.8114 \times 10^{-11}, \quad (4.5)$$

$$a_3 = -8.3112 \times 10^{-21}\, S^4 + 4.9712 \times 10^{-17}\, S^3 - 9.7004 \times 10^{-14}\, S^2 + 4.1356 \times 10^{-11}\, S + 4.5754 \times 10^{-8}, \quad (4.6)$$

$$a_4 = 2.4690 \times 10^{-18}\, S^4 - 1.4582 \times 10^{-14}\, S^3 + 2.7561 \times 10^{-11}\, S^2 - 8.7865 \times 10^{-9}\, S - 1.6448 \times 10^{-5}, \quad (4.7)$$

$$a_5 = -2.6578 \times 10^{-16}\, S^4 + 1.5476 \times 10^{-12}\, S^3 - 2.8223 \times 10^{-9}\, S^2 + 5.5708 \times 10^{-7}\, S + 2.0520 \times 10^{-03}, \quad (4.8)$$

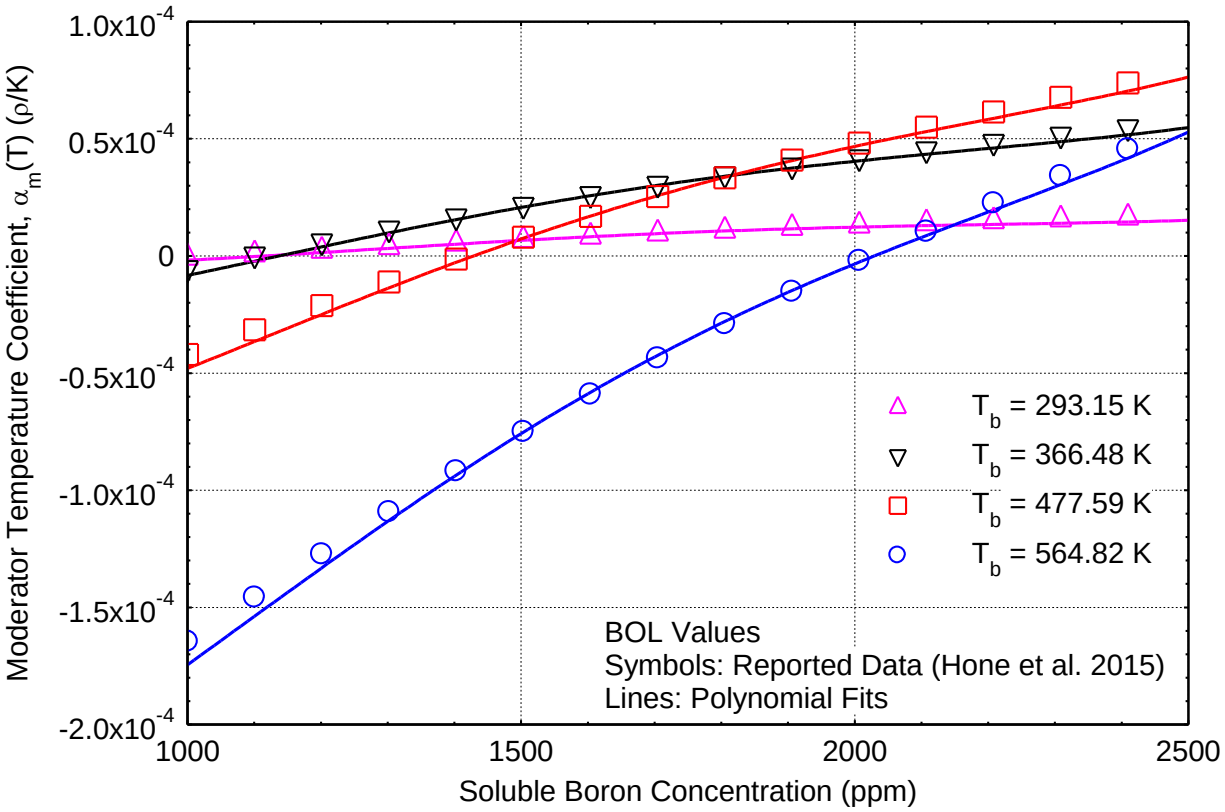

Fig. 4.2: Reported values of AP1000 moderator temperature reactivity feedback coefficient

Figure 4.3 compares the values of the fuel temperature reactivity feedback calculated by the developed reactor model to the reported values for the AP1000 PWR. The calculated values of $\rho_f(T)$ as function of the calculated reactor thermal power are in good agreement with the reported values to within ~5%. The calculated average fuel temperature, T_f , by the present thermal-

hydraulics model of the reactor is close to that estimated for the AP1000 design (Hone et al., 2015). The closest agreement is at 100% nominal power, with the calculated values are slightly more negative than those reported (Fig. 4.3). This indicates that the calculated fuel temperatures by the present reactor model are slightly higher than those reported for the AP1000 PWR. However, the close agreement in Fig. 4.3 suggests that the modeling approach and assumptions in the present reactor thermal-hydraulic model are appropriate for determining the average fuel temperature within the reactor core with acceptable accuracy.

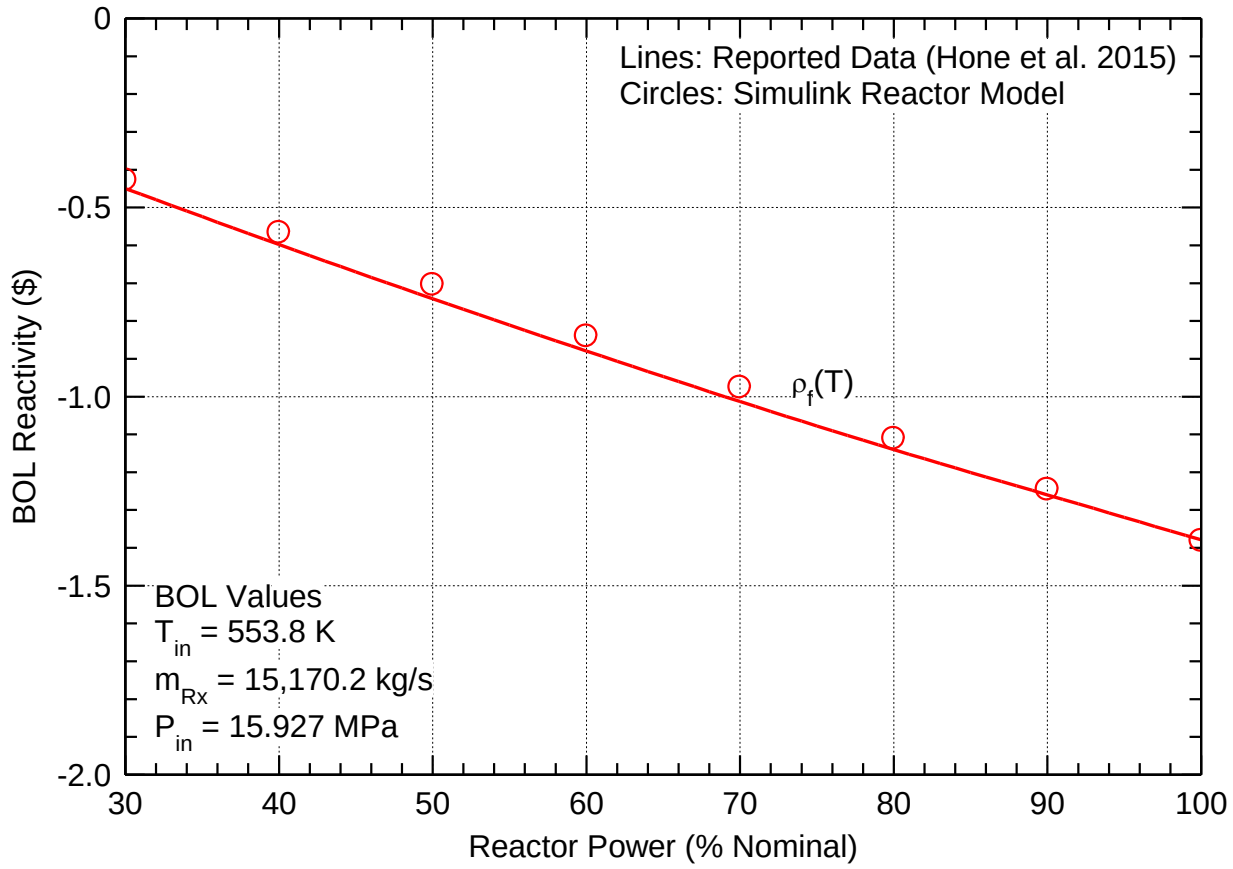

Fig. 4.3: Comparison of calculated values the fuel temperature reactivity feedback using the present point kinetics model to those reported for the AP1000 PWR.

4.1.2 Comparison of Loop Pressure Losses

The calculated pressure losses in the overall momentum balance of the primary loop model are compared to the reported values in the Design Control Document for the AP1000 during nominal operation (Westinghouse Electric Company, 2011). This report lists two values: one for the pressure losses across the reactor core fuel bundles, and the second is of the total pressure losses in the reactor vessel from the inlet nozzle to the outlet nozzle. The reported pressure losses across the fuel bundles are 266.827 kPa at nominal reactor operation, while the reported total pressure losses in the reactor vessel are 446.780 kPa. The reported total pressure losses across the entire primary loop are 111.25 m or 811.832 kPa.

The calculated pressure losses values using the developed reactor and primary loop models are presented in Figure 4.4. The calculated reactor core pressure losses in the primary loop Model are the sum of the friction pressure losses across the fuel bundles, $\Delta p_{f,co}$ (Eq. 2.21), and due to the spacer grids, Δp_{sp} (Eq. 2.26). The calculated total pressure losses is the reactor the

vessel are the sum of the reactor internal pressure losses, Δp_{Rx} (Eq. 2.25), and the pressure losses for the inlet nozzle, Δp_{in} (Eq. 2.31), and outlet nozzle, Δp_{out} (Eq. 2.32). At nominal operating conditions, the present reactor model calculates pressure losses across the core fuel bundles of 263.145 kPa, which is only 3.68 kPa lower that the reported value, or within 1.38%.

The calculated total pressure losses for the reactor vessel of 412.688 kPa are 34.092 kPa lower than the reported value of 466.780 kPa, or within 7.63%. This difference may be partially attribute to the estimated pressure loss in the lower core support structure, for which only few details are provided in the reactor design documents for the lower core support and the orifices structure. Instead, the effective diameter and shape of the orifices are guesstimated from the provided fuel bundle dimensions.

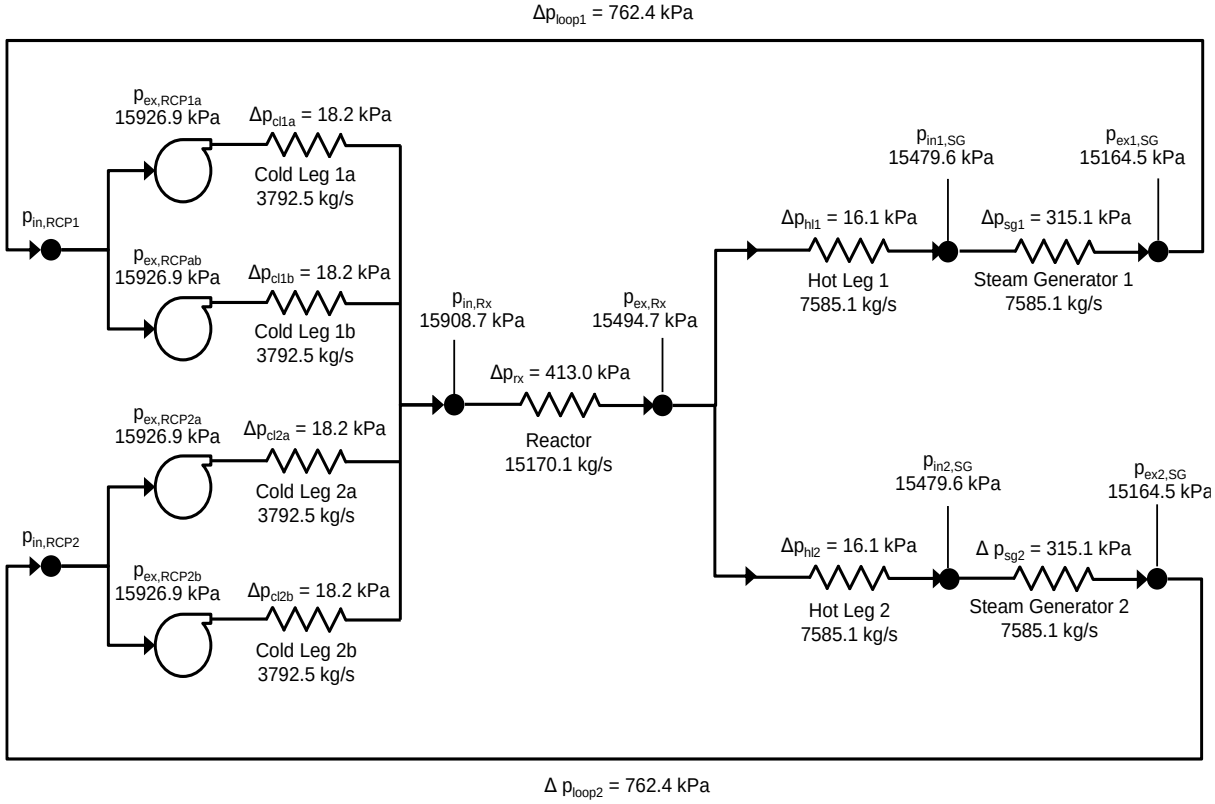

Fig. 4.4: Calculated pressure losses in primary coolant loop of reference design of AP1000 PWR.

The calculated total pressure losses in the primary loop, $\Sigma\Delta P_{loss}$, are 762.4 kPa, which is 6.09% lower than of the reported value of 811.8 kPa. Overall, comparisons results confirm the soundness of the present modeling approach for the reactor and the primary loop models for satisfactory agreements between the reported and calculated values of the pressure losses in the reactor and primary coolant loop of the reference AP1000 design.

4.1.3 Validation of Reactor Coolant Pump Model

To validate the performance of the developed primary coolant pump model the calculated performance results are compared to the test reported data for the centrifugal coolant pumps in the Loss-of-Flow-Test (LOFT) experimental facility (Reeder, 1978). The LOFT facility used two canned rotor type vertical shaft centrifugal pumps with water bearings (Reeder, 1978) in parallel to circulate the coolant through the electrically heated reactor core. Table 4.1 lists the key

dimensions and design rated performance values. These values are used to represent the LOFT facility pump in the present pump model. The homologous head and torque and efficiency curves for the LOFT facility pump (Fig. 2.12) are used in input to the present model as lookup tables.

Table 4.1: Reported design parameters for the LOFT facility centrifugal pumps (Reeder, 1978).

Parameter	Value
Pump suction equivalent diameter, D_h	0.21584 m
Inlet cross sectional area, A_{cs}	0.036589 m^2
Internal volume	0.099 m^3
Rated speed, ω_R	369.66 rad/s (3530 rpm)
Rated head, H_R	96 m
Rated flow rate, Q_R	0.315 m^3/s
Rated torque, τ_R	500 N-m
Rated water density, ρ_R	614 kg/m^3
Moment of inertia, MOI	10 kg-m^2 for $\omega > 70$ rad/s, 1.43 kg-m^2 for $\omega < 70$ rad/s

Figure 4.5 presents the reported supply and demand curves for the LOFT facility coolant pump while operating at ambient coolant temperature (300 K) (Reeder, 1978). The volumetric flow rate in Fig. 4.5 per pump is half the total volumetric flow rate for the primary loop of the LOFT facility, while the pump head would be equal for the two pumps. The results generated by the developed reactor coolant pump model are for a 300 K suction inlet temperature for constant rotational speeds of 1,000, 1,500, 2,000, 2,500, 3,000, 3,250, and 3,550 RPM are compared with the reported curves for the LOFT facility in Fig. Fig. 4.5. For each RPM, the value the inlet flow rate is varied up to the point of intersection with the reported pump demand curve.

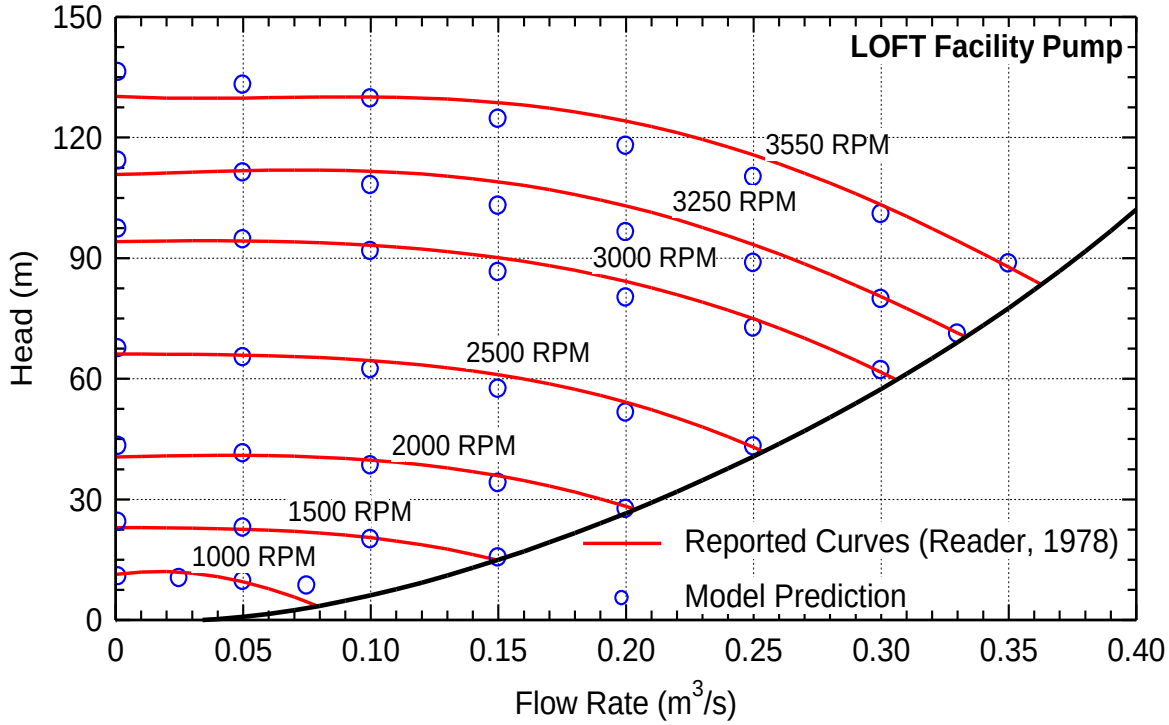

Fig. 4.5: Comparison of calculated supply curves and reported data for the LOFT facility pumps at different shaft rotation speeds from 1,000 to 3,550 RPM

The comparison results in Fig. 4.5 show that the present pump model tends to slightly over-predict the pump head at low flow rates by up to ~7%. In the middle range of the flow rates, the model under-predicts the pump head by as much as 6.5 %, and the predicts are in closer agreement with the reported supply curves at the points of intersection with the demand curve (Fig. 4.5). The model predictions are generally in good agreement with reported curves, particularly for the low and mid-range flow rates to within ~ 7%.

Table 4.2: Comparisons of calculated and reported thermal energy dissipation by LOFT pumps.

Parameter	**Value**
Pump Speed, ω	245.3895 rad/s (2343.3 RPM)
Pump Flow	0.239 m^3/s
Suction Inlet Temperature	300 K
Reported Thermal Dissipation to Flow	160 J/kg
Calculated Thermal Dissipation to Flow	141.96 J/kg
Difference	-18.04 j/kg (-11.3%)

Table 4.2 compares the calculated and reported thermal power dissipation to the flow by the LOFT facility pumps. The reported energy dissipation to the flow by the LOFT pump when operating at its nominal full conditions: ω = 245.3895 rad/s (2,343.3 RPM), $T_{suction}$ = 300 K, and Q_{in} = 0.239 m^3/s is 160 J per kg of flow (Reeder, 1978). The calculated thermal energy dissipation by the present pump model at these conditions is141.96 J/kg, which ~11.3% lower than reported for the LOFT pump. Considering performance and measurement uncertainties and that the energy dissipation for the coolant pumps for large PWR plant is typically < 0.5% of the reactor thermal power, the current agreement between the predictions of the present pump model and the reported value for the LOFT facility pump is acceptable.

4.1.4 Validation of Pressurizer Model

The developed pressurizer model is validated by comparing predictions to reported transient data from two experiments; one for the Shippingport PWR (Redield et al,1968), and a small pressurizer at a MIT scaled experimental facility (Kim, 1984). The pressurizer for the Shippingport PWR plant is cylindrical, 1.37m in diameter, 5.1m tall, and of a total volume of 7.419m^3. At steady state full power operation, the system pressure is maintained at 14.2 MPa. It is controlled using three banks of electrical heaters, a spray system, and relief valves. The shippingport pressurizer's control parameters are summarized in Table 4.3 (Redield et al,1968).

The Shippingport test has a first surge-in which raised the water level in the pressurizer by 0.64 m, within two minutes after the start of the transient. It is followed by a drop of the water level of an equal magnitude. The second change decreases the water level in the pressurizer by 0.46 m, which is subsequently followed by a surge-out of approximately the same magnitude as the first surge in event.

Figure 4.6 compares the predictions of present model predictions to the reported test results for the Shippingport transient test, indicating good agreement. In this figure, the developed pressurizer model is also compared to the reported modeling results of Pini et al. (2018) using the RELAP5 system code. It can be seen that the predictions of the developed physics-based transient mode of the pressurizer model are in closer agreement with the reported experimental data for the Shippingport test than the reported RELAP5 code predictions of Pini et al. (2018).

Table 4.3: Shippingport pressurizer pressure controller parameters

Spray water from cold leg					
Spray flow (kg/s)	1.909	Turn-on pressure (MPa)	14.272	Turn-off pressure (MPa)	13.962
Electrical heaters					
Heating power bank 1 (kW)	40	Turn-on temperature (K)	605.4	Turn-off temperature (K)	608.7
Heating power bank 2 (kW)	80	Turn-on pressure (MPa)	13.348	Turn-off pressure (MPa)	13.79
Heating power bank 3 (kW)	250	Turn-on pressure (MPa)	13.141	Turn-off pressure (MPa)	13.893

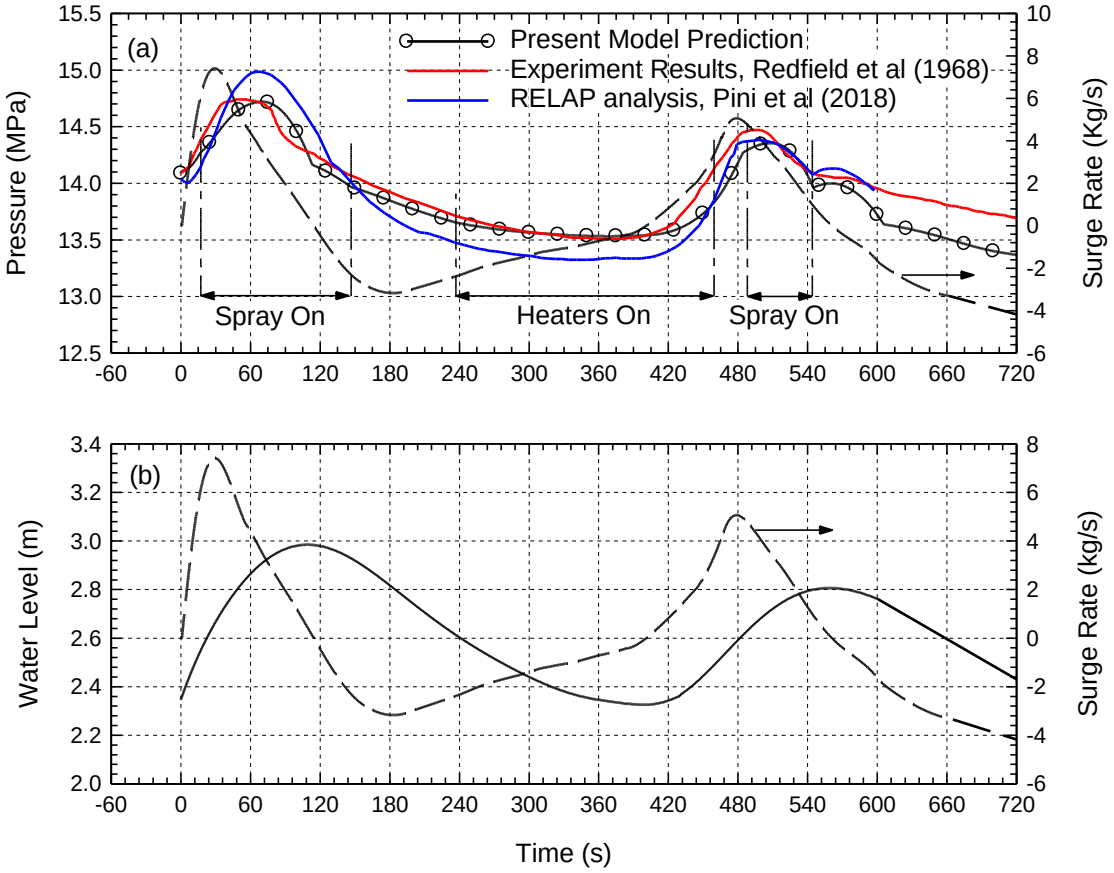

Fig. 2.6: Comparison of Shippingport PWR pressurizer response during load-drop transient; (a) Pressure change, (b) Water level change.

The predictions of the present pressurizer model are also compared to the reported experimental results of a small-scale MIT pressurizer experimental facility during a partially full surge-in transient (Kim, 1984). This experiment was done on a cylindrical stainless steel pressure tank with a height of 1.14 m and inner diameter of 0.20 m. The thickness of the tank wall is 0.0127 m. The pressure in the tank is controlled with variable power electrical heaters installed within the pressurizer.

The partial full surge-in the experiment is intended to simulate the surge-in transient without a liquid spray, starting from an equilibrium state (Kim, 1984). The tank was filled with saturated water (at ~690 kPa) to about 0.381 m height (1/3 of the tank height). Then the water surge into the pressurizer through the surge line at ~0.27 kg/s continued until the water level reached about 0.77 m (2/3 of the tank height). This resulted in a measured pressure change of 170 kPa (from 690 to 860 kPa) (Kim, 1984). After the surge-in stopped, the heat losses to the environment from the tank caused the pressure to slowly decrease (Kim, 1984).

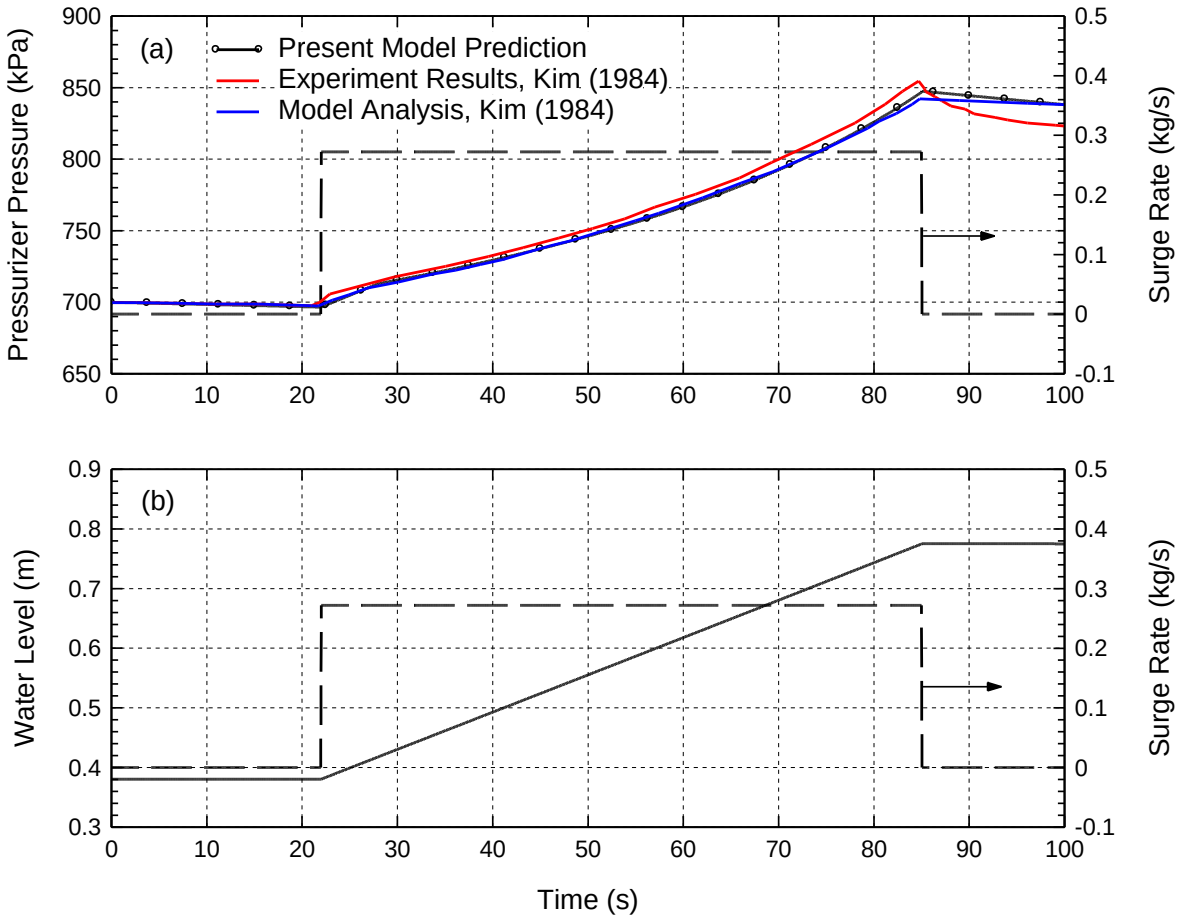

Fig. 4.7: Comparison of MIT scaled pressurizer experiment response during a partial surge-in transient; (a) Pressure change, (b) Water level change.

Figure 4.7a compares the present pressurizer model predictions to the reported experiment results and model predictions performed by Kim (1984) for a surge-in transient. Fig. 4.7b shows the change in the water level in the pressure tank during the transient. The transient results calculated using the present model are in adequate agreement with the reported experimental data and the analytical predictions by Kim (1984). There is a small difference between the present model predictions and the experimental data after surge-in stops (Fig. 4.7a). Kim (1984) estimated a total heat loss of 1.1 kW during the test, which is used in the present pressurizer. The heat losses is not likely to be constant during the experiment, and since heat losses to the environment are the most important mechanism after the surge-in stops, this assumption may be the cause for the difference between the present model and experiments. The validation results of

the developed physics-based pressurizer model show adequate agreement between the model predictions and the reported test data and modeling results.

4.2 Representative PWR Transient Analyses

The developed fast-running and transient reactor can easily be configured to represent different PWR designs, with geometrical and reactor kinetics parameters. A representative PWR design is used to investigate the developed PWR plant model. This PWR design is similar in layout to the Westinghouse AP-1000 and the Combustion Engineering System 80+ reactor designs (Westinghouse Electric Company, 2011; Palo Verde Nuclear Generating Station, 2017). The representative PWR plant in Fig. 2.1 has two primary loops, each with a hot leg and two cold legs, a steam generator, and two reactor coolant pumps. The input parameters for the representative PWR are given in Table 4.4.

Table 4.4: Representative value of input parameters to the developed PWR plant model.

Input Parameters	Value
Reactor Model	
Rod Axial Nodes/Fuel Assemblies/Assembly Rods/Guide Tubes	2 / 157 / 264 / 25
Fuel Rod Pitch / Pellet Diameter (m)	0.21402 / 8.19
Cladding Outer Diameter / Thickness (mm)	9.5 / 0.57
Fuel Rod Length / Gas Plenum Length (m)	4.58318 / 4.2672
Fuel Rod Assembly P/d	1.3262
Guide Tube Outer Diameter / Wall Thickness (mm)	12.2428 / 0.508
Number of Assembly Spacers	12
Resistance for Assembly Spacers, K_{spa} / Core Support, K_{sup}	1.57 / 5.27
Flow Area in Core Lower Support Structure (m^2)	7.191343
Core Barrel Inner Diameter / Downcomer Outer Diameter (m)	3.39725 / 4.0386
Downcomer Inner Diameter (m)	3.49885
Distance from Inlet to Lower Plenum (m)	6.54020
Distance from Core Exit to lower Plenum (m)	6.08841
Cold Leg / Hot Leg Inner Diameter (m)	0.5588 / 0.7874
Steel Mass of in Reactor Vessel (kg)	246383
Total Coolant Volume in Reactor (m^3)	109.211263
Reactor Initial Power (W) / Normalized axial Power Profile	1.0 / 0.5
Delayed Neutron Fraction x 10^3	0. 2475 1.6425 1.47, 2.9625, 0.8625, 0.313
Delayed Neutron Group Lambda x 10^2	1.24, 3.05, 11.1, 30.1, 113, 300
Prompt Neutron Lifetime x 10^5 (s)	1.98
Initial Source Strength	1.0 x 10^6
Reference Temperature for Reactivity Feedback (K)	564.8167
Boron Reactivity Worth x 10^3 ($/ppm)	-7.133654
Initial Boron Concentration (ppm)	1321
The moderator temperature reactivity Coefficient $\rho_m(T)$, is determined using a quadratic fit expressed as: $\rho_m(T) = A*T^4+B*T^3+C*T^2+D*T+E$. In this expression, coefficients A, B, C, D and E are polynomial functions of soluble boron concentration, S (ppm), as: $= c_1*S^4+c_2*S^3+c_3*S^2+c_4*S+c_5$,	

Input Parameters	**Value**
Moderator Temperature Coefficient A-c1	$-6.71\text{x}10^{-27}$
Moderator Temperature Coefficient A-c2	$4.1314\text{x}10^{-23}$
Moderator Temperature Reactivity Coefficient: A-c_3	$-8.6231\text{x}\ 10^{-20}$ / $5.6049\text{x}10^{-17}$
A-c_5 / B-c_1	$1.0602\text{x}10^{-14}$ / $1.2432\text{x}10^{-23}$
B-c_2 / B-c_3	$-7.5495\text{x}10^{-20}$ / $1.5249\text{x}10^{-16}$
B-c_4 / B-c_5	$-8.1803\text{x}10^{-14}$ / $-4.8114\text{x}10^{-11}$
C-c_1/ C-c_2	$-8.3112\text{x}10^{-21}$ / $4.9712\text{x}10^{-17}$
C-c_3 / C-c_4	$-9.7004\text{x}10^{-14}$ / $4.1356\text{x}10^{-11}$
C-c_5 / D-c_1	$4.5754\text{x}10^{-8}$ / $2.4690\text{x}10^{-18}$
D-c_2 / D-c_3	$-1.4582\text{x}10^{-14}$ / $2.7561\text{x}10^{-11}$
D-c_4 / D-c_5	$-8.7865\text{x}10^{-9}$ / $-1.6448\text{x}10^{-5}$
E-c_1 / E-c_2	$-2.6578\text{x}10^{-16}$ / $1.5476\text{x}10^{-12}$
E-c_3 / E-c_4	$-2.8223\text{x}10^{-9}$ / $5.5708\text{x}10^{-7}$
E-c_5	$2.0520\text{x}10^{-3}$
Fuel temperature reactivity coefficient, $\rho_f(T)$,is calculated using a quadratic fit, as: $\rho_f(T) = A*T^4 + B*T^3 + C*T^2 + D*T + E$.	
Fuel Temperature Reactivity Coefficient A, B	0, 0
C, D	$-1.0624\text{x}10^{-11}$, $2.8632\text{x}10^{-8}$
E	$-4.3446\text{x}10^{-5}$
Cladding / Structure Feedback Coefficient/ Reactor heat losses	0 / 0 / 0
Fraction of Deposited Reactor Power in Fuel	0.974
Fuel Burnup (GWd/MTU)	0
Fuel Assembly Flow Fraction	1
UO_2 / Zircaloy Cladding Surface Roughness (m)	$3.3\text{x}10^{-6}$ / $1.8\text{x}10^{-6}$
UO_2 / Zircaloy Emissivity	0.85, 0.2
Temperature Jump Distances at Fuel and Clad Surfaces (m)	$2\text{x}10^{-6}$
Fuel Rod Gap Closure (1 for open, 0 for closed)	1
Fuel-Clad Interfacial Pressure (Pa)	0
Pressurizer Model	
Height of Straight Wall (m)	9.9822
Wall Inner / Outer Diameter (m)	2.54 / 2.794
Active Heater Bottom Elevation from Bottom (m)	1.4
Active Heater Top Elevation from Bottom (m)	3.93
Wall Thermal Conductivity (W/m.K) / Density (kg/m^3)	25.0 / 7854
Wall Specific Heat Capacity (J/kg.k)	559
Surge Line Inner Diameter / Length (m)	0.4572 / 25.3919331
Steam Generator Model	
Number of Tubes	10025
Tube Outer Diameter / Wall Thickness (m)	0.0174752 / 0.001016
Tube Triangular Pitch (m)	0.024892
Tubesheet Thickness (m)	0.790702
Average Tube Length (m) / Turn Angle (°)	22.453848 / 180
Mean Radius of Curvature of Tubes (m)	1.38862
Steam Generator Height (m)	22.460204

Input Parameters	Value
Upper Shell Inner Diameter (m)	5.334
Lower Shell Inner Diameter / Downcomer Width (m)	4.191 / 0.127
Volume of Water in SG Tubes / Plenums (m^3)	42.16379 / 16.650308
Height of Feedwater Nozzles / Separator Deck (m)	15.272004 / 16.772004
Location of Lower / Upper Narrow Range Level Tap (m)	15.272004 / 18.929604
Turbine and Feedwater Pump Efficiency	0.9
Generator and Turbo-Generator Shaft Efficiency	0.95
Pump Model	
RCP Height (m)	6.7056
RCP Unit Mass, Dry (kg)	90718.48
Rated Pump Speed (rpm)	1100
Rated Head (m) / Volumetric Flow (m^3/s)	115 / 5.1
Rated Total Torque (N-m)	$80.5x10^4$
Rated Fluid Density (kg/m^3)	734
Equivalent Hydraulic Diameter (m)	0.6604
Motor Efficiency / Control Volume (m^3)	0.95 / 0.8
Suction / Discharge Inner Diameter (m)	0.6604 / 0.5588
Primary Loop Model	
Number of Hot Legs	2
Hot Leg Inner Diameter (m)	0.7874
Hot Leg Length (m) / Turn Angle (°)	5.3571648 / 32
Hot Leg Mean Turn Radius (m)	1.5932245
Hot Leg Wall Thickness (m)	0.08255
Number of Cold Legs	4
Cold Leg Inner Diameter / Length (m)/ Turn Angle (°)	0.5588 / 7.4409605 / 60
Cold Leg Mean Turn Radius / Wall Thickness (m)	2.8378727 / 0.065024

The PLCs embedded within the Simulink model of the PWR plant are tuned to produce a smooth response to operational transients. The PI controller of the water level PLC in the steam generator is set with a proportional constant of 0.02 and an integral constant of 0.6. The pressurizer water level controller is set with a proportional constant of -2800 and an integral constant of -50. The reactor regulator PLC is not used in this implementation as we wanted to investigate the natural response characteristics of the developed reactor model. Details of the analysis for determining these values are provided in a companion Task 3 Report (El-Genk, et al., 2020b *in progress*).

4.3 Reactor Startup Transient

This subsection presents and discusses the transient results of a startup of representative PWR plant using the developed physics-based modeling capabilities described earlier in this report. The implemented scenario the reactor startup is shown in Fig. 4.8. The scenario begins at time t_0 with the PWR plant at hot zero power (reactor power = 1 W). At low power levels, the reactor is kept subcritical to avoid a spike in the positive temperature reactivity feedback. At time t_0: (a) all four reactor coolant pumps are running at 100% of nominal flow and dissipating 15 MW_{th} into the primary loop, (b) the pressurizer, placed in automatic control mode, maintains a system pressure of 15.41 MPa, (c) the reactor primary coolant loop is a mean temperature of

564.8 K due to the thermal dissipation from the reactor coolant pumps, and (d) the heat in the primary loop is removed in the steam generators to the secondary loop.

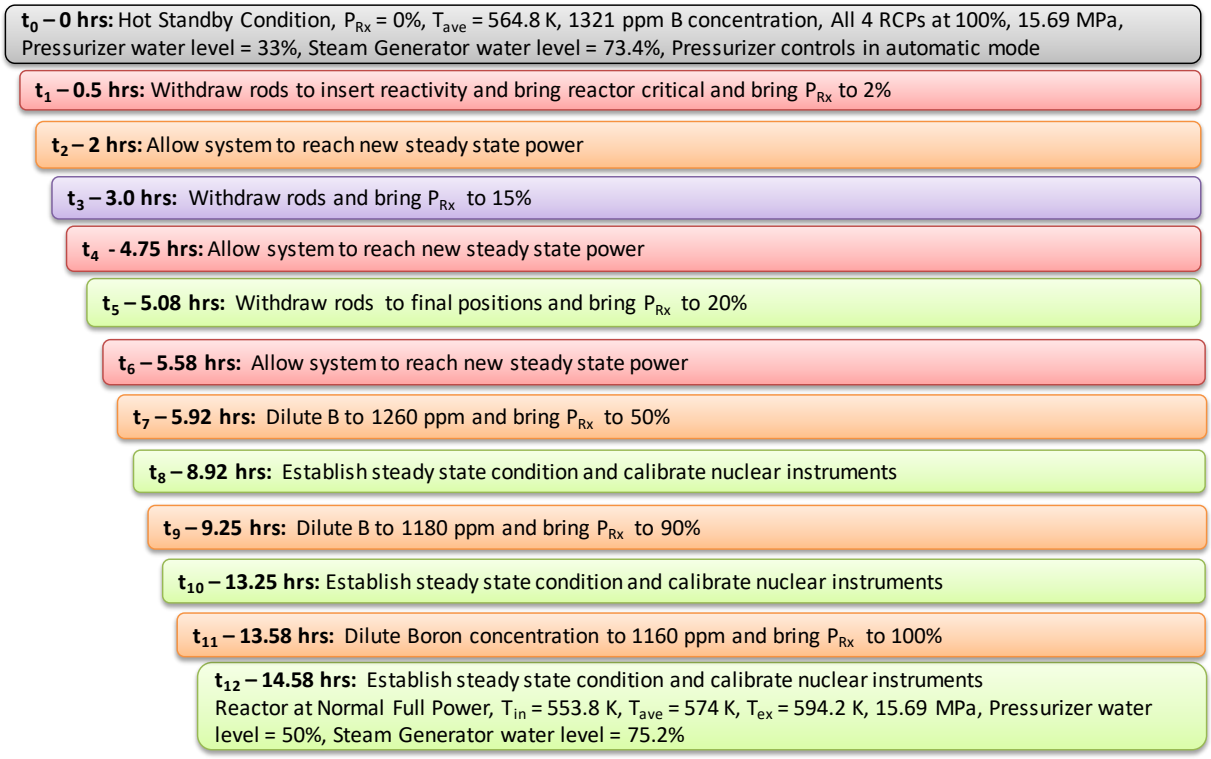

Fig. 4.8: Performed startup scenario of a representative PWR plant.

The reactor startup is initiated at time t_1 by withdrawing the control element assemblies to insert 2.07¢ of external reactivity to bring the reactor to a critical state and operate at thermal power of 2% of nominal by time t_2. Simultaneously, the secondary loop condition is adjusted to increase the steam load to the turbine to 2% of nominal full power. At t_3, the control element assemblies are withdrawn further to insert 20.84¢ of external reactivity and the steam generator steam production increased to that for 15% of nominal full power. These conditions are held until reaching steady state operation at time t_4. At t_5, the control elements are withdrawn further to insert a total of 27.77¢ of external reactivity, and at t_6 the reactor power reaches 20% of nominal full power. The control element assemblies reach final disposition for this scenario, and further reactivity insertion is accomplished by diluting the concentration of soluble boron in the primary coolant.

At time t_7, the boron concentration in the primary loop initially at 1321 ppm decreased to 1260.6 ppm to bring the reactor power up to 50% of nominal. Starting at time t_8, the reactor power is held constant at 50% for the operators to calibrate the nuclear instrumentation. At time t_9, the soluble boron concentration in the primary loop is further decreased to 1180.1 ppm to increase the reactor power to 90% of nominal. This power is held constant at time t_{10} to allow the nuclear instrumentation to be checked and calibrated again prior to bringing the reactor to full power operation conditions. At time t_{11} the boron concentration in the primary loop drops to 1060 ppm and the reactor thermal power reaches 100% of nominal full power at t_{12}. During this

startup scenario, the condition of the secondary loop of the plant is simultaneously adjusted to increase the steam load to the turbine, commensurate with the reactor thermal power.

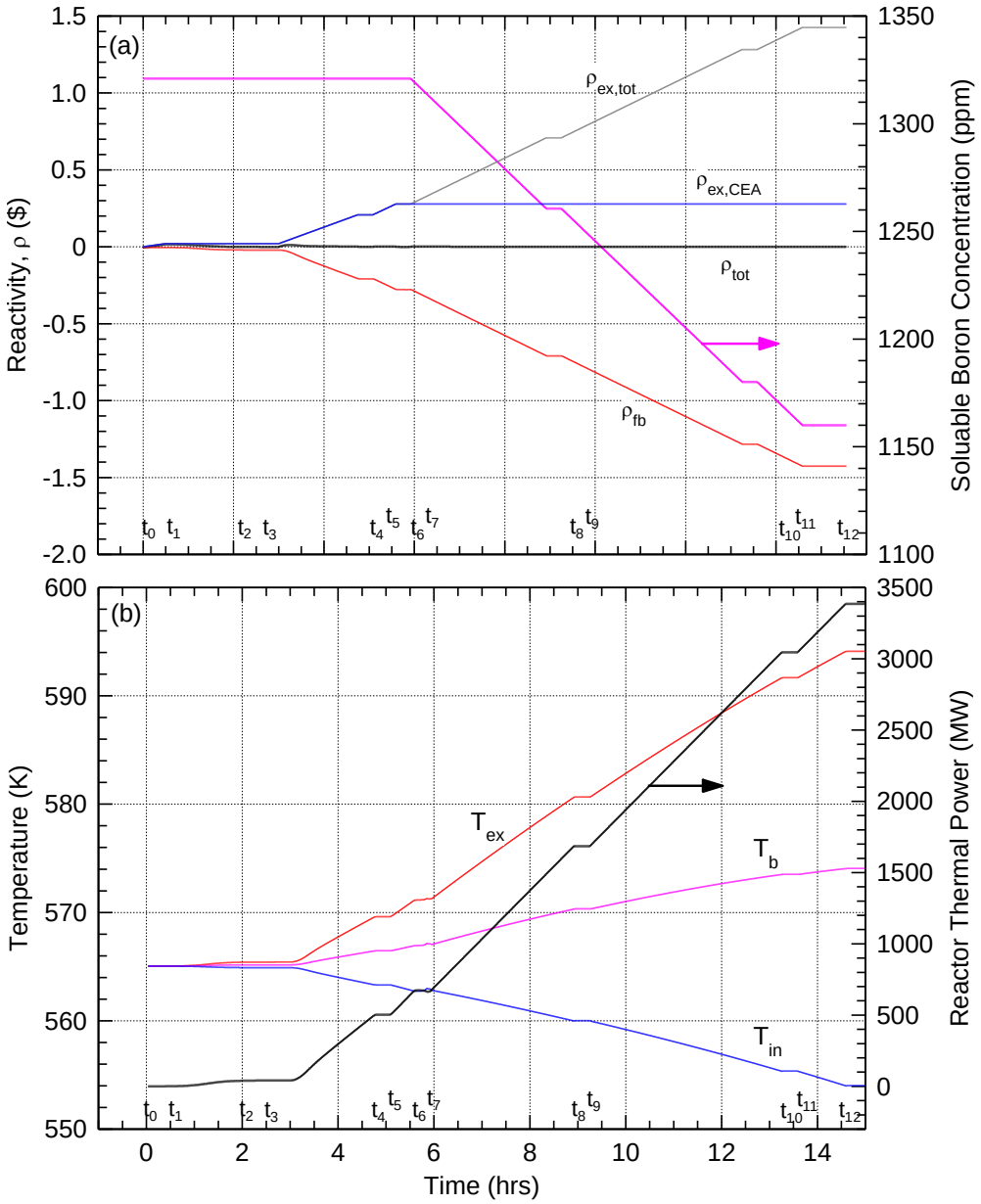

Fig. 4.9: Calculated transient response of the reactor state variables during the performed startup scenario (Fig. 4.8) of a representative PWR plant.

The determined transient values of select state variables using the developed capabilities in this work in a representative PWR plant during the described startup sequence (Fig. 4.8) are presented in Figs. 4.9- 4.11. The results in Fig. 4.9a-b are of the calculated transient response of the select state variable by the developed reactor model. The results in Fig. 4.10a-b are of the calculated transient the response of the state variables for the steam generator model, and those in Fig. 4.11a-c are of the response of state variables for pressurizer.

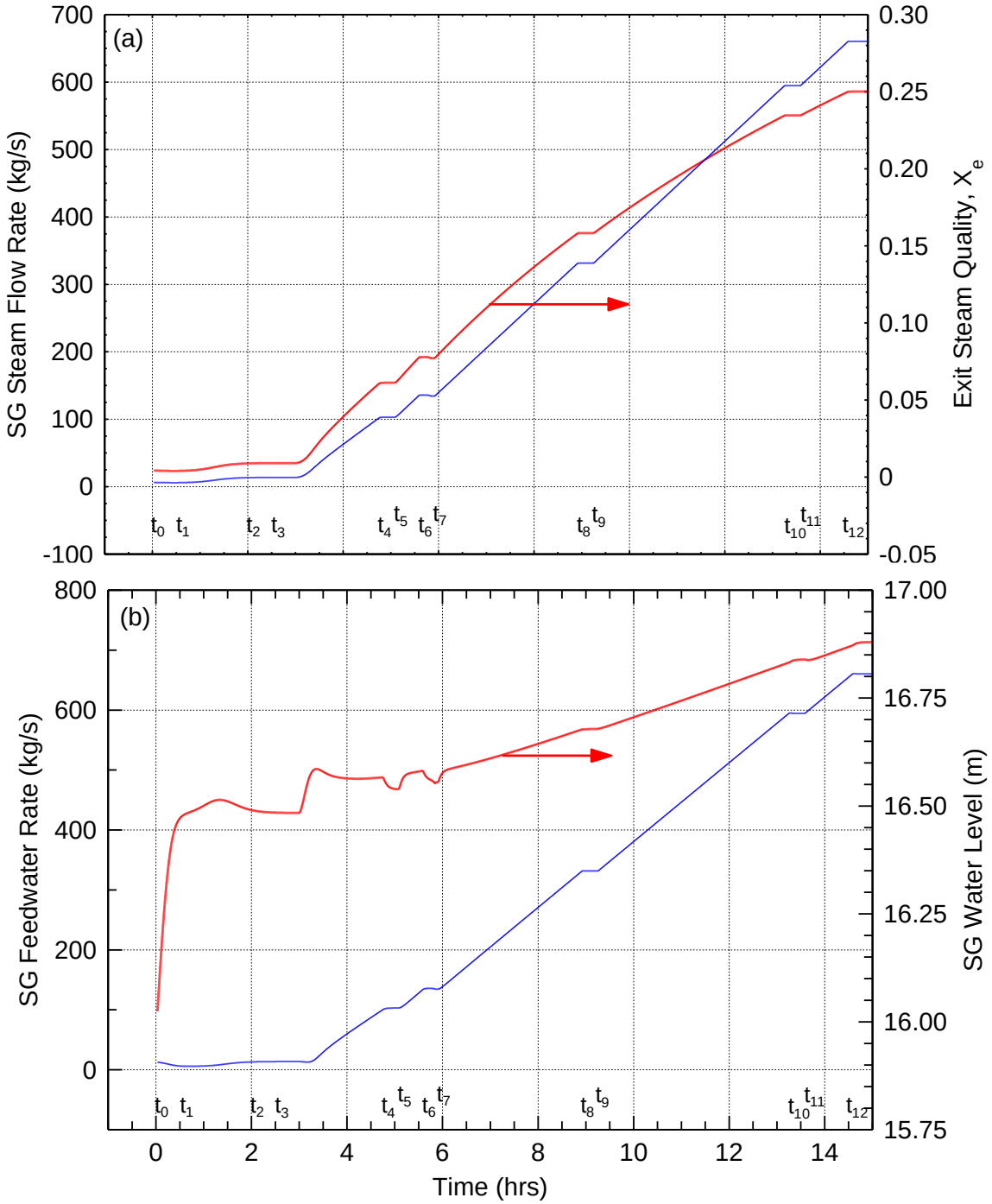

Fig. 4.10: Calculated transient response of the steam generator state variables during the performed startup scenario (Fig. 4.8) of a representative PWR plant.

In the simulated start up transient in these figures, increasing the reactor thermal power increases the heat generation rate in the fuel, increasing its temperature as well as the bulk temperature of the water coolant in the reactor. These temperature increases introduce negative reactivity feedback, which remains in balance with the positive external reactivity insertion, to maintain the total reactivity in the reactor core near zero (Fig. 4.9a). The increase in the bulk

temperature of the moderator is due to the increase in the reactor exit temperature and the temperature rise across the reactor core fuel assemblies with increased reactor thermal power (Fig. 4.9b). The corresponding decrease in the coolant inlet temperature to the reactor is caused by the increased steam production in the steam generator to the turbine in secondary side of the PWR plant (Fig. 4.10a).

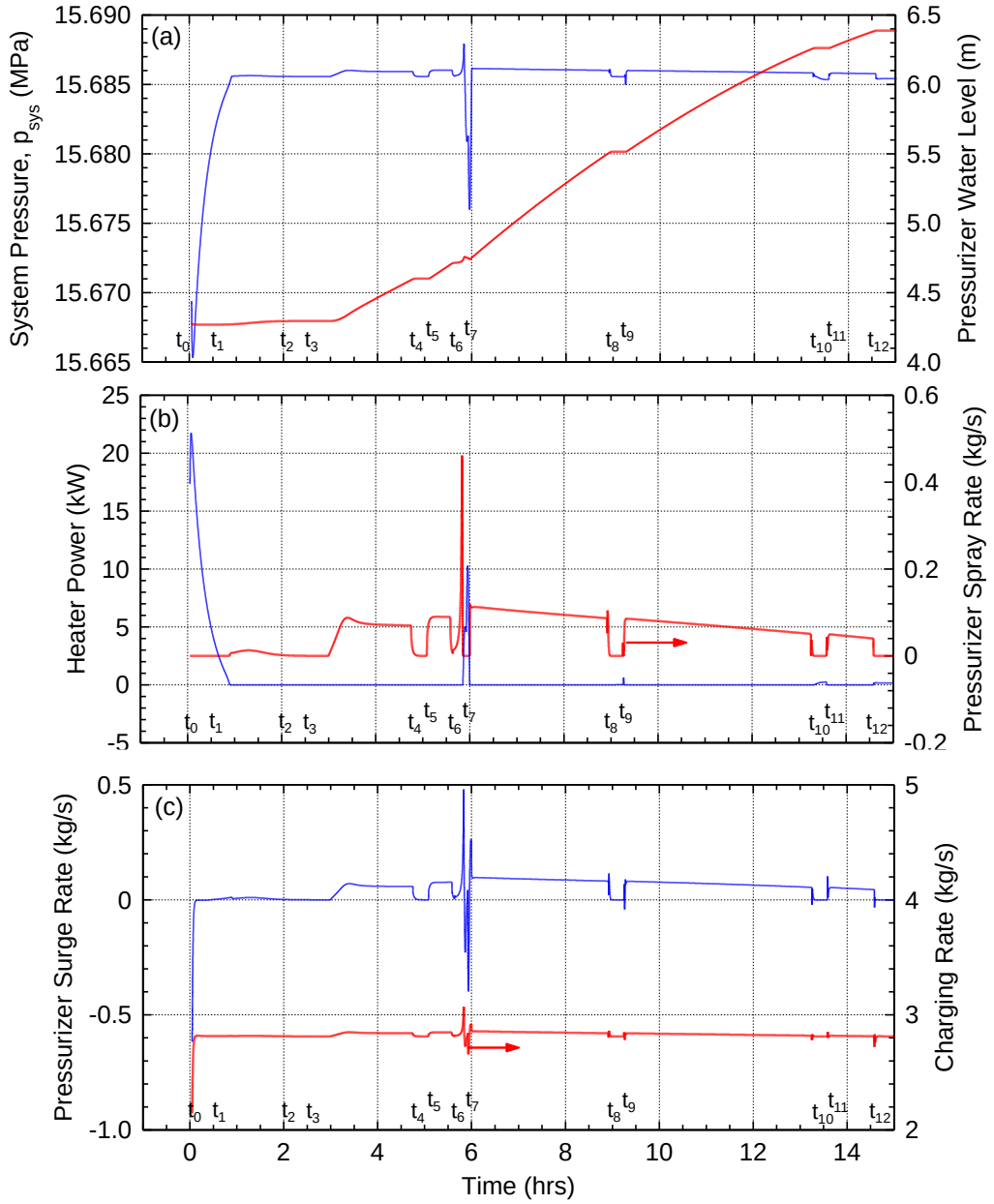

Fig. 4.11: Calculated transient response of the pressurizer state variables during the performed startup scenario (Fig. 4.8) of a representative PWR plant.

The increase in the steam flow rate commensurate with the increase in load demand is reflected in part by the increase in the steam quality exiting the U-tube bundle in the steam generator (Fig. 4.10a). As the steam exit quality increases, less saturated liquid is recirculated back through the downcomer of the steam generator to the central up-flow region. The feedwater

control PLC adjusts the rate of the feedwater to maintain the water level in the steam generator at the programed setpoint. The magnitude of such an adjustment depends on the value of the reactor thermal power during the startup transient (Fig. 3.8). During the startup sequence the pressurizer PLCs maintain the system pressure and internal water level to within their programed setpoints (Fig. 3.6 and 3.7). The change in the system pressure during the startup transient is generally small, with the exception to that occurred at t_7, following the reduction of the soluble boron concentration in the primary loop to increase the reactor power to 50% of nominal.

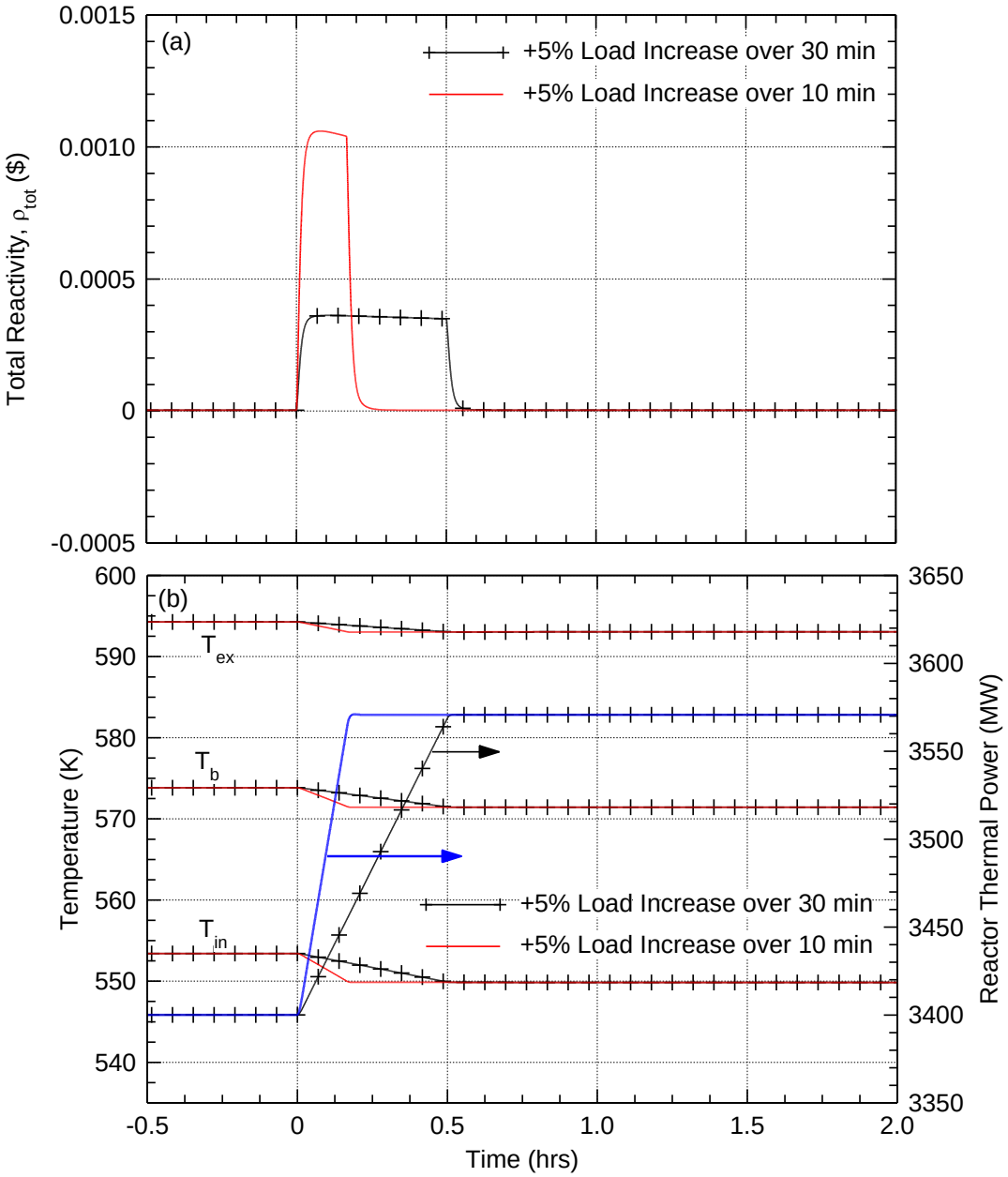

Fig. 4.12: Calculated transient response of the reactor state variables in a representative PWR plant following a 5% increase in load demand.

The water level PLC for the pressurizer increases the charging rate of the primary loop, which in conjunction to the thermal expansion of the coolant with increase reactor power in the

conducted startup transient, causes a surge in of the water from the primary loop into the pressurizer (Fig. 4.11c). This increase in pressure (Fig. 4.11a) causes the pressurizer pressure PLC to increase the rate of spray of subcooled water from the cold leg of the primary loop into the top region of saturated steam. Such an action decreases the pressure spike and eventually brings the pressure back to nominal (Fig. 4.11b).

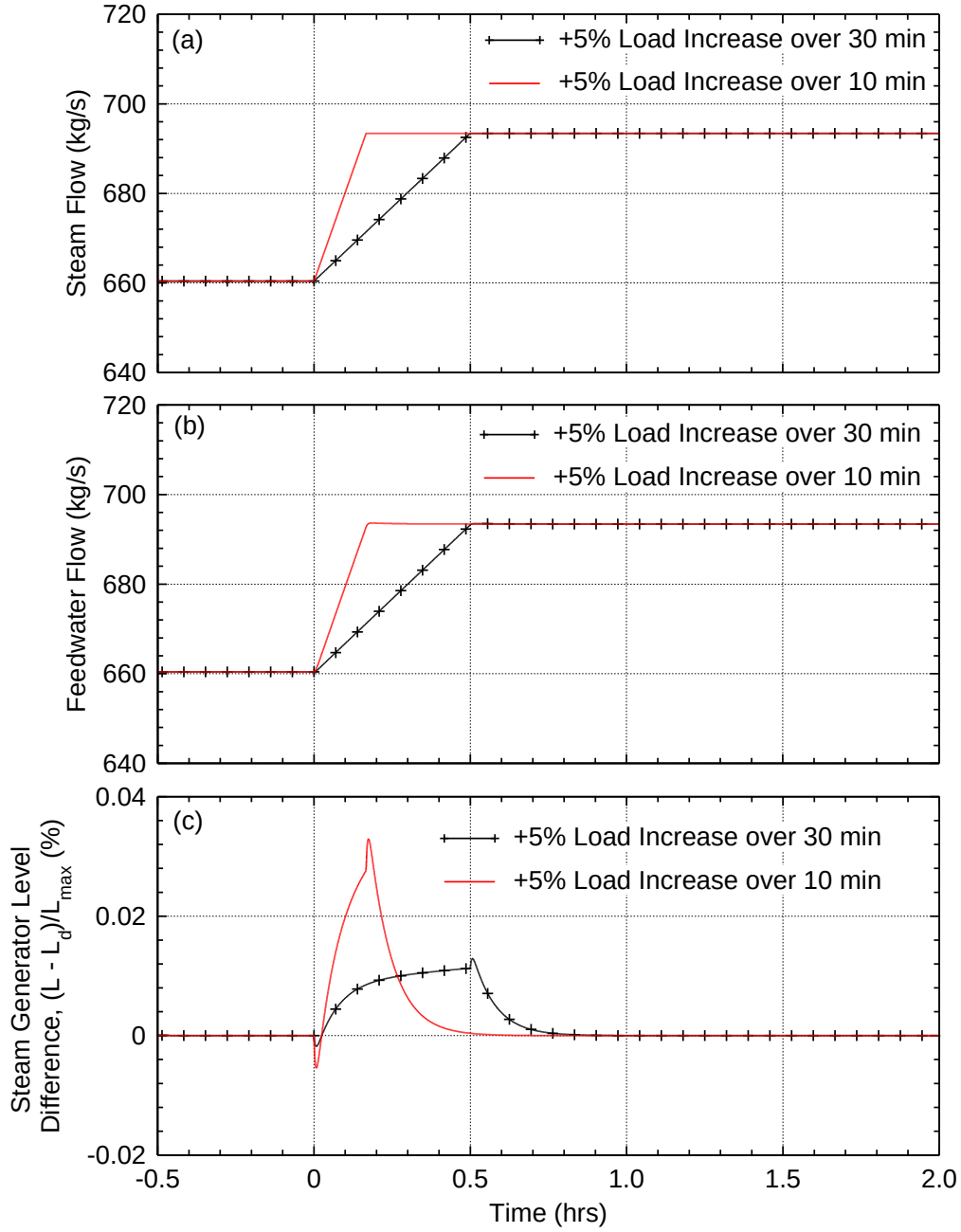

Fig. 4.13: Calculated transient response of the steam generator state variables in a representative PWR plant following a 5% increase in load demand on the turbine in the secondary loop.

The resulting decrease in the water spray, associated with a decrease in the charging rate into the primary loop, cause surge out from the pressurizer into the primary (Fig. 4.11c), results in sharp drop in pressure (Fig. 4.11a). This relatively small drop in the system pressure (~0.01

MPa) demonstrates that the pressurizer's PLCs, which work independently, could maintain smooth reactor operation. The pressure and the water level PLCs for the pressurizer control the power supply to the proportional heater banks and the water charging pumps in the primary loop, which eventually brings the pressure back to the setpoint (Fig. 4.11).

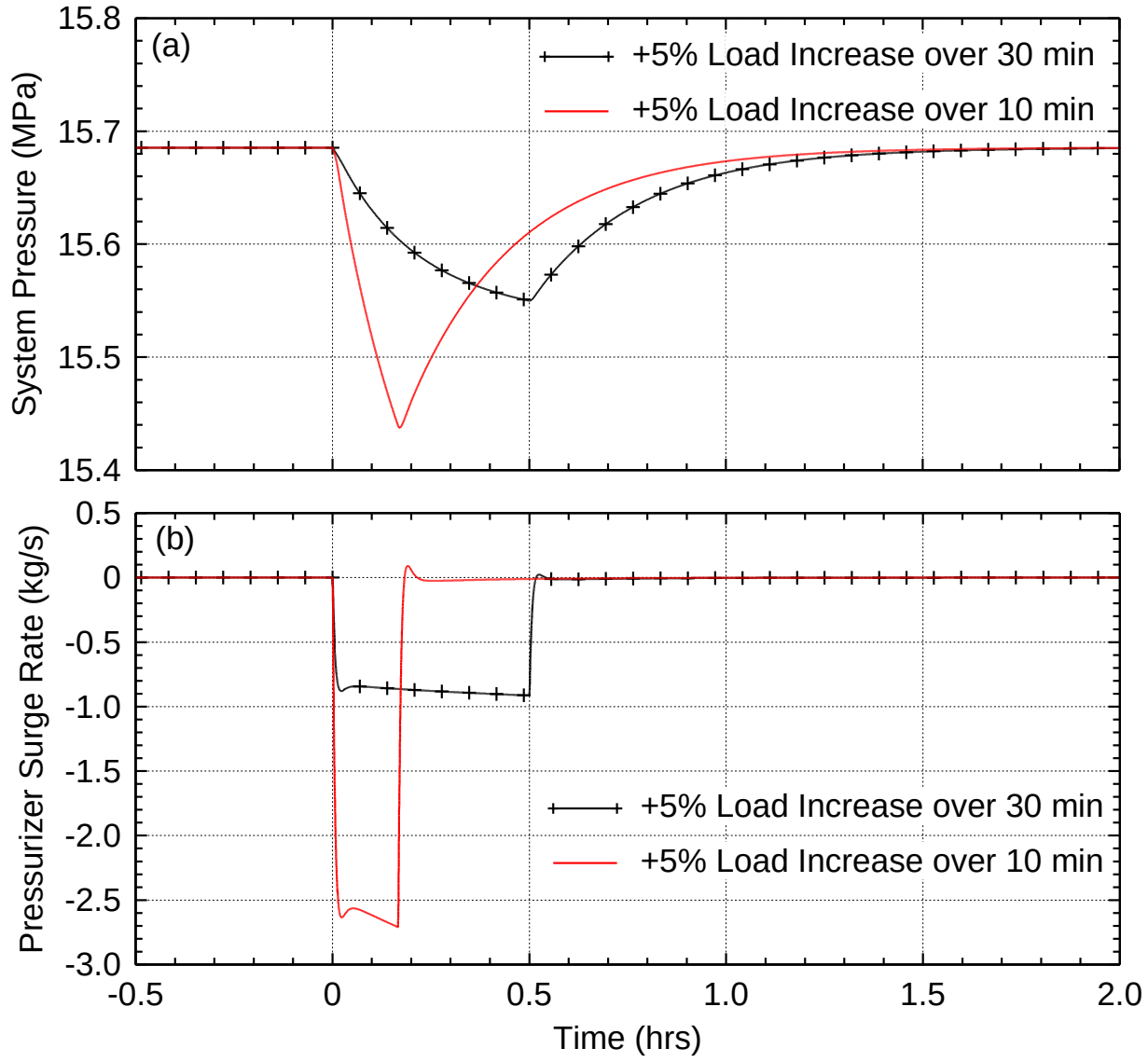

Fig. 4.14: Calculated transient response of the pressurizer state variables in a representative PWR plant following a 5% increase in load demand on the turbine in the secondary loop.

4.4 Transient Response Following an Increase in Load Demand

The calculated transient values of the state variables using the present model, following a 5% increase in the load demand for the turbine in the secondary loop, are presented in Figs. 4.12-4.15. At the start of this transient, time = 0, the plant is at steady state nominal condition and the reactor power is 100% of nominal power. The steam load demand is then increased by 5% in a linear ramp and then held constant at to 105% of nominal. This analysis also investigates the effect of changing the ramp time of the load by 5% to 10 and 30 minutes. Figs. 4.12, and 4.13 present the calculated transient state variables for the reactor and the steam generator,

respectively, following an increase in the load demand at different rates by 5%. Figs. 4.14 and 4.15 present the corresponding transient response of the state variables for the pressurizer.

Increasing the load demand increases the steam flow rate (Fig. 4.13a), which momentarily decreases the water level in the steam generators as well as the temperature of the primary loop water returning to the reactor (Fig. 4.12b). The lower temperature introduces a positive reactivity, by the fuel and moderator (Fig. 4.12a), which increases the reactor thermal power (Fig. 4.12b). During this transient the external reactivity is kept constant. The decrease in the water level in the steam generator following the increase in the load demand (Fig. 4.11c) causes the feedwater control PLC to increase the rate of feedwater to the steam generator by adjusting the throttle valve (Fig. 4.13b). It is followed by an increase in the water level in the steam generator above the desired level, L_d, This water level return gradually to the desired level as the feedwater flow rate reach a high steady state value commensurate with the increase in the load demand, bringing the water level back to the control setpoint (Fig. 4.13c).

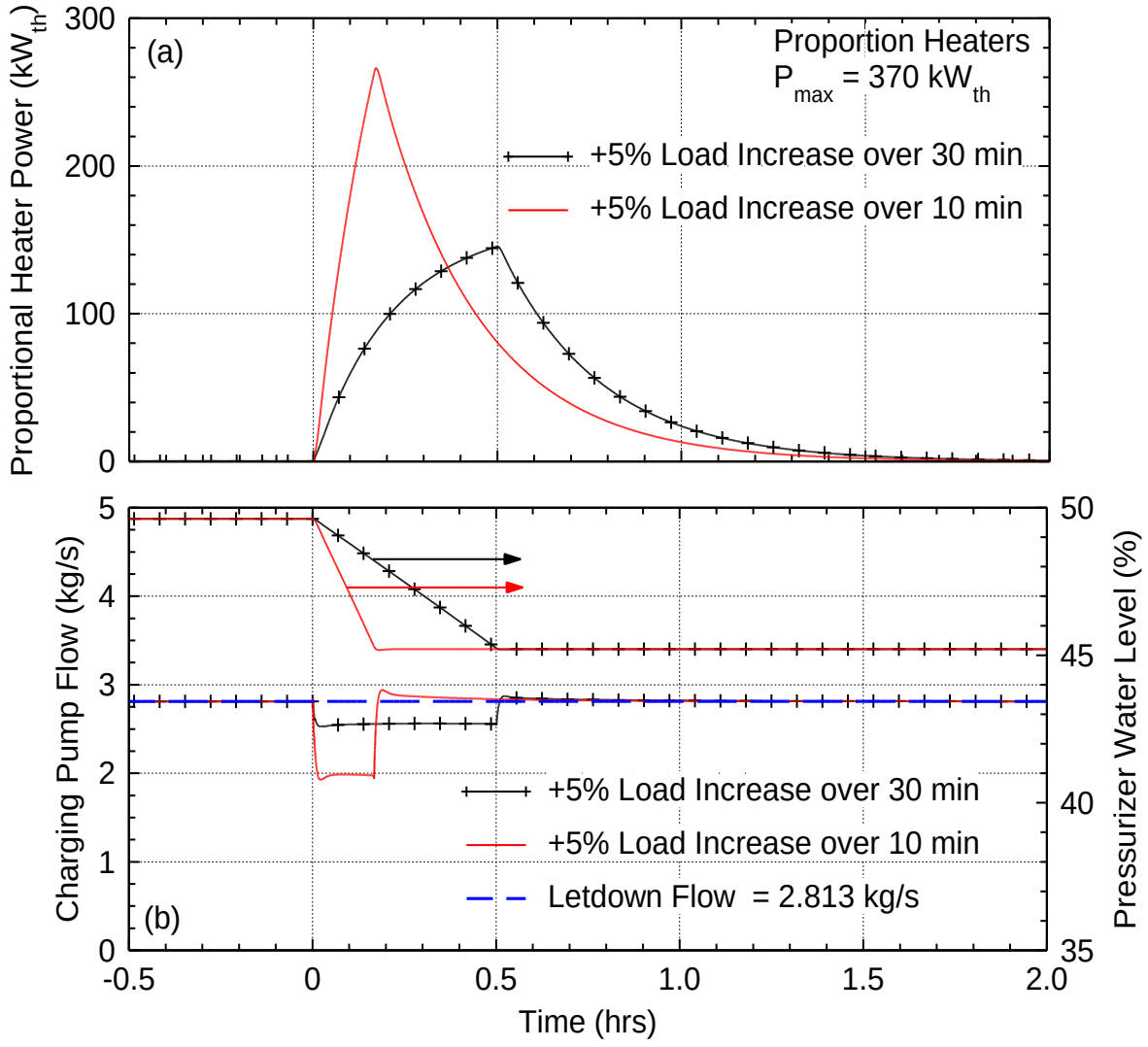

Fig. 4.15: Calculated transient response of the pressurizer's proportional heaters and the charging pump in a representative PWR plant following a 5% increase in load demand.

The decrease in the coolant temperatures (Fig. 4.12b) result in thermal contraction which causes a surge out from the pressurizer (Fig. 4.14b) and deceases the system pressure (Fig. 4.14a). The pressurizer pressure PLC increases the power to the proportional heater banks (Fig. 4.15a), which increases the system pressure back to the control setpoint. The decrease in the coolant temperature also decreases the water level setpoint for the pressurizer water level PLC (Fig. 3.7) which causes the PLC to decrease the charging rate to bring the water level to the new desired level (Fig. 4.15b). The short ramp duration of increasing load demand over 10 min results in larger changes for the state variables during the transient. This is due in part to the thermal inertia of the materials and the coolant in the primary loop as well as the response of the plant operation PLCs.

The longest ramp duration of 30 min effectively decreases the size and the duration of the spikes in the calculated state variables, partially due to the relatively fast response of the PLCs. Therefore, it desirable that the setup parameters for the PLCs ensure that the controllers respond quickly during fast transients, this reduces over- and under spikes in the state variables their oscillatory behavior during operation transients. The present results of the changes in the state variables of a PWR following a 5% increase in load demand show that the selected parameters for the PLCs are adequate for limiting the oscillation and spikes in the state variable of the plant, including those for the pressurizer and the steam generator.

4.5 Summary

This section compared the predictions of the developed primary coolant loop model and of the developed physics based models of various components in the loop to reported design values for AP1000 reactor and to experimental results from scaled test facilities of the pressurizer and the primary coolant pumps. The predictions of these models are generally in good agreement with reported values. The calculated pressure losses in the reactor core fuel assemblies, across the reactor vessel, and total in the primary coolant loop are within 1.38%, 7.65%, and 6.1% of the reported values, respectively. The pressure head by the primary pump to the flowing water in the primary loop is within 7% of the reported value for the pump tested in the LOFT facility.

This section also presented the transient results and values of the state variables calculated using the developed, physics based dynamic model of a representative PWR plant detailed in Section 2. The performed transients are those of a reactor startup and following a 5% increase in plant load demand. In these transient, the PLCs embedded within the Simulink model of the PWR plant are tuned to produce a smooth response during these transients. The PI controller of the water level PLC in the steam generator is set with a proportional constant of 0.02 and an integral constant of 0.6. The pressurizer water level controller is set with a proportional constant of -2800 and an integral constant of -50.

The results show that the PWR plant model and the connected PLCs maintain a smooth startup from hot zero power condition to 100% nominal power operation with small spikes in the calculated state variables. The transient results following a +5% increase in load demand show that faster transient of 10 minute duration to apply the increase in the load demand produces larger spikes and oscillations in the values of the calculated state variables than for the transient with a longer duration of 30. The results confirm that the selected parameters for the PLCs are adequate for limiting the oscillation and spikes in the state variables of the plant during operation transients.

5. Summary and Conclusions

This report details the work performed at UNM-ISNPS on developing a physics-based dynamic model of a representative PWR plant, which is a part of the Nuclear Instrumentation & Control Simulation (NICSim) project funded by DOE NEUP award in 2018 to the University of New Mexico. This effort is carried out in collaboration with Sandia National Laboratory. The developed dynamic models are those of the primary coolant loops and of the coupled components of the pressurizer, the steam generator, the primary coolant pumps and the associated PLCs. The developed physics based PWR plant models for the NICSim platform include: (a) a dynamic reactor model with coupled point kinetics and thermal-hydraulics, (b) a 3-region pressurizer model, (c) a steam generator model, and (d) a model for the reactor coolant pumps. The reactor 6-point kinetics equations are solved using a robust and efficient exponential matrix technique developed at UNM-ISNPS, which is efficient, highly stable, accurately predicts the transient changes due to rapid reactivity insertions, regardless of the time step size up to several seconds, or even longer.

The integrated physics based dynamic PWR plant model functions integrated with the controllers of the safety PLCs in the plant protection and safety monitoring I&C system, and the controller PLCs in the plant operation I&C system. This effort developed a CPC PLC for performing the reactor trip function and an engineered safety features actuation system PLC for autonomously actuating the plants engineered safety features. Additional PLCs within the plant's operation I&C system are also developed. PLCs are developed for the reactor's regulation, controlling the pressurizer's pressure and water level, controlling the water level in the steam generator, and controlling the operation of reactor coolant pumps. The controllers continuously receive state variables from the PWR primary loop model and return control signals to adjust plant operation such that the values of the various state variable are within the programed setpoints.

This report compared the predictions of the developed primary coolant loop model and of the developed physics based models of various components in the loop to reported design values for AP1000 reactor and to experimental results from scaled test facilities of the pressurizer and the primary coolant pumps. The predictions of these models are generally in good agreement with reported values. The calculated pressure losses in the reactor core fuel assemblies, across the reactor vessel, and total in the primary coolant loop are within 1.38%, 7.65%, and 6.1% of the reported values, respectively. The calculated pressure head and thermal energy dissipation by the primary pump to the flowing water in the primary loop are within 7% and 11.3%, respectively, of the reported values for the pump tested in the LOFT facility.

In addition, this report presented the transient results and values of the state variables calculated using the developed, physics based dynamic model of a representative PWR plant detailed in Section 2. The performed transients are those of a reactor startup and following a 5% increase in plant load demand. In these transient, the PLCs embedded within the Simulink model of the PWR plant are tuned to produce a smooth response during these transients. The PI controller of the water level PLC in the steam generator is set with a proportional constant of 0.02 and an integral constant of 0.6. The pressurizer water level controller is set with a proportional constant of -2800 and an integral constant of -50.

The transient results of a reactor startup and following a 5% increase in load demand confirmed the robustness the reliance of the developed physics-based models for a representation PWR plant and components. The PWR plant models and the connected PLCs maintain a smooth startup from hot zero power condition to 100% nominal power operation with small spikes in the

calculated state variables. The results confirm that the selected parameters for the PLCs are adequate for limiting the oscillation and spikes in the state variables of the plant during transient operations.

The research described in this progress report developed and demonstrated important elements to be implemented in the NICSim platform. The developed and validated physics-based dynamic model of a representative PWR plant is a core element of this platform. This PWR plant model will be integrated together with the emulated PLCs, developed and tested in a companion technical report of technical task 3, into the NICSim platform.

The validation of the PLC emulation and the developed interface program will enable future simulation of different operation and safety I&C system architectures, linked to the dynamic, physics-based model a PWR power plant. Future implementation and successful completion of this work include investigating the physical impacts of targeted cyber-attacks on the plant I&C system architectures, aiding in training plant operators for identifying signs of a potential cyber-attack, and helping develop metrics to quantify how a cyber-attack may propagate throughout I&C system networks of a nuclear power plant.

6. Acknowledgements

This research is being performed using funding received from the DOE Office of Nuclear Energy's Nuclear Energy University Program under Contract No. Nu-18-NM-UNM-050101-01 to the University of New Mexico. Any opinions, findings, and conclusions or recommendations expressed in this publication are those of the author(s) and do not necessarily reflect the views of the U.S. Department of Energy.

Sandia National Laboratories is a multi-mission laboratory managed and operated by National Technology and Engineering Solutions of Sandia, LLC, a wholly owned subsidiary of Honeywell International, Inc., for the U.S. DOE's National Nuclear Security Administration under contract DE-NA-0003525. The views expressed in the article do not necessarily represent the views of the U.S. DOE or the United States Government.

7. References

Altamimi, R., El-Genk, M.S., Schriener, T.M., 2020, "Pressurizer Model and PLCs for Investigation of Cybersecurity of PWR Plants". In Trans. ANS 2020.

Alves, T.R., Buratto, MM, Mauricio de Souza, F., and Rodrigues, T.V., 2014. "OpenPLC: An open source alternative to automation," in proceedings IEEE Global Humanitarian Technology Conference (GHTC 2014), San Jose, CA, USA, DOI: 10.1109/GHTC.2014.6970342

Bell, I., Wronski, J., Quolin, S., Lemort, V., 2015, "Pure and Pseudo-pure Fluid Thermophysical Property Evaluation and the Open-Source Thermophysical Property Library CoolProp," Ind. Eng. Chem. Res. 2014, 53(6), pp. 2498–2508

Dragos, Inc., 2017. CRASHOVERRIDE, Analysis of the Threat to Electric Grid Operations version 2.20170613, www.DRAGOS.com.

El-Genk, M.S, Schriener, T.M., Lamb, C., Fasano, R., Hahn, A., 2019, Implementation and Validation of PLC Emulation and Data Transfer, Report No. UNM-ISNPS-02-2019, Institute for Space and Nuclear Power Studies, The University of New Mexico, Albuquerque, NM, USA

El-Genk, M.S., Schriener, T.M., Altamimi, R., Hahn, A., Lamb, C., Fasano, R., 2020a. "NICSim: Nuclear Instrumentation & Control Simulation For Evaluating Response To Cyber Attacks," Proceedings of the 2020 28th Conference on Nuclear Engineering Joint with the ASME 2020 Power Conference ICONE28-POWER2020, August 2-6, 2020, Anaheim, California, USA, paper ICONE28-POWER2020-14645

El-Genk, M.S, Schriener, T.M., Hahn, A., Altamimi, R., Lamb, C., Fasano, R., 2020b, PWR Plant Emulated Programmable Logic Controllers for Protection and Safety Monitoring and Operation I&C System for Cybersecurity Applications, *in progress*

El-Genk, M. S., Tournier J.-M., 2016, "A Point Kinetics Model and Dynamic Simulation of Next Generation Nuclear Reactor," J. Progress in Nuclear Energy, 92, pp. 91-103.

Fasano, R., Lamb, C., El-Genk, M.S., Schriener, T.M., Hahn, A., 2020. "Emulation methodology of programmable logic controllers for cybersecurity applications," Proceedings of the 2020 28th Conference on Nuclear Engineering Joint with the ASME 2020 Power Conference

ICONE28-POWER2020, August 2-6, 2020, Anaheim, California, USA, paper ICONE28-POWER2020-11150

Hahn, A., Schriener, T.M., El-Genk, M.S., 2020. "Selection and validation of fast and synchronous interface to the controller of a space nuclear reactor power system," Proceedings of the 2020 28th Conference on Nuclear Engineering Joint with the ASME 2020

Hahn, A., Schriener, T.M., El-Genk, M.S., 2020. "Selection and validation of fast and synchronous interface to the controller of a space nuclear reactor power system," Proceedings of the 2020 28th Conference on Nuclear Engineering Joint with the ASME 2020 Power Conference ICONE28-POWER2020, August 2-6, 2020, Anaheim, California, USA, paper ICONE28-POWER2020-16237

Haskins, D.A., El-Genk, M.S., 2017. "Natural Circulation Thermal-hydraulics Model and Analyses of "SLIMM"- A Small Modular Reactor," Annals of Nuclear Energy, 101, pp. 516-527.

Hone, M., McCloskey, Eisenhauer, J., Null, R., MacDonald, A., 2015. AP1000 Core Reference Report, Westinghouse technical report WCAP-17524-NP-A, APP-GW-GLR-156, rev 1, Westinghouse Electric Company LLC, Cranberry Township, PA

Idel'chik, I.E. 1960. "Handbook of Hydraulic Resistance, Coefficients of Local Resistance and of Friction, 1960." English version, AEC-TR-6630 (1966).

International Association for the Properties of Water and Steam, 2007, The International Association for the Properties of Water and Steam Revised Release on the IAPWS Industrial Formulation 1997 for the Thermodynamic Properties of Water and Steam, Lucerne, Switzerland, IAPWS R7-97(2012)

Jens, W.H., Lottes, D.A., 1951. "Analysis of Heat Transfer, Burnout, Pressure Drop, and Density Data for High Pressure Water," Argonne National Laboratory, Chicago, IL, ANL-4627.

Karnouskos, S., 2011. "Stuxnet Worm Impact on Industrial Cyber-Physical System Security," in proceedings IECON 2011 - 37th Annual Conference of the IEEE Industrial Electronics Society, Melbourne, VIC, Australia, 7-10 November, 2011, DOI: 10.1109/IECON.2011.6120048.

Kim, S.N., 1984. An experimental and analytical model of a PWR pressurizer during transients, Doctoral dissertation, Massachusetts Institute of Technology, Cambridge, MA.

Korsah, K., et al., 2008. Instrumentation and Controls in Nuclear Power Plants: An Emerging Technologies Update, US NRC Technical Report NUREG/CR-6992, Washington, DC.

Mason, E.A., S.C. Saxena, 1958, "Approximate formula for the thermal conductivity of gas mixtures." The Physics of fluids 1(5), pp. 361-369.

National Research Council, 1997. Digital Instrumentation and Control Systems in Nuclear Power Plants, Safety and Reliability Issues, Final Report, National Academy Press, Washington, D.C.

Nuclear Energy Institute, 2010, "Cyber Security Plan of Nuclear Power Reactors," NEI Technical Report NEI 08-09 [Rev.6].

Nuclear Safety Analysis Division, 2001, "RELAP5/MOD3.3 Code Manual Volume II: User's Guide and Input Requirements," Information Systems Laboratories, Inc., Rockville, Maryland

Palo Verde Nuclear Generating Station, 2017. Palo Verde Nuclear Generating Station Units 1, 2, and 3 Updated Final Safety Analysis Report, Rev. 19 Corrected (Redacted per RIS 2015-17)

Perlroth, N., 2019. "Hackers are Targeting Nuclear Facilities, Homeland Security Dept. and F.B.I. Say", New York Times, June 19, 2019.

Pini, A., Cammi, A., Colombo, L., Tigliole, A.B., 2018. A non-equilibrium control oriented model for the pressurizer dynamics. Progress in Nuclear Energy, 106, pp.102-119.

Redfield, J.A., Prescop, V., Margolis, S.G., 1968. Pressurizer performance during loss-of-load tests at Shippingport: Analysis and test. Nuclear Applications, 4(3), pp.173-181.

Reeder, D.L., 1978. LOFT System and Test Description (5.5 ft Nuclear Core 1 LOCES), Idaho National Engineering Laboratory, Idaho Falls, ID, NUREG/CR-0247

Sandia National Laboratories, 2016. SCEPTRE, Sandia Document SAND2016-8095C.

Schindhelm, E.P., Single, R.E., 2010. AP1000 Protection and Safety Monitoring System Architecture Technical Report, Technical Report WCAP-16675-NP, APP-GW-GLR-147, rev 2, Westinghouse Electric Company LLC, Cranberry Township, PA

Southern Nuclear Operating Company, 2018. Vogtle Electric Generating Plant 3 and 4 Updated Final Safety Analysis Report, Revision 6, ND-18-0656, Southern Nuclear Operating Company, Inc., Birmingham, Alabama

Su, B., & El-Genk, M. S., 1993, "Forced convection of water in rod-bundles," International Communications in Heat and Mass Transfer (United States), 20(2).

The MathWorks, Inc., 2018. Simulink Version 9.2 (R2018b).

US Department of Homeland Security, 2015, "Nuclear Sector Cybersecurity Framework Implementation Guidance."

US Nuclear Regulatory Commission, 2007. "Reactor Concepts Manual: Pressurized Water Reactor (PWR) Systems," US Nuclear Regulatory Commission Technical Training Center, Washington DC, Educational Teaching Material 603.

VMware, 2019. VMware Workstation 15 Pro.

Westinghouse Electric Company, 2011. AP1000 Design Control Document Revision 19, Westinghouse Electric Company LLC, Pittsburgh, PA

Appendix A: Pressure Loss Model Diagrams from Idel'Chik (1960)

Presented here are the hydraulic resistance diagrams from Idel'Chik (1960) used in the PWR primary loop pressure loss models.

Entrance to a straight conduit through a perforated plate with thick-edged orifices $\left(\frac{l}{d_h} > 0.015\right)$	Section III Diagram 3-18

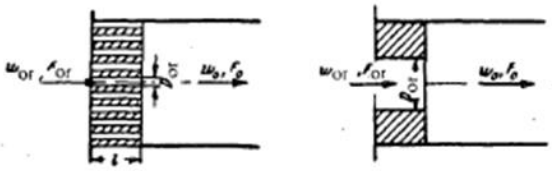

$$d_h = \frac{4f_{or}}{\Pi_{or}};$$

Π_{or} = perimeter
f_{or} = area of one orifice
F_{or} = free grid (washer) section

$$\bar{f} = \frac{F_{or}}{F_0} = \frac{\Sigma f_{or}}{F_0}$$

1) $\mathrm{Re} = \frac{w_{or} d_h}{\nu} > 10^5$:

$$\zeta = \frac{\Delta H}{\frac{\bar{w}_0^2}{2g}} \cong \left[0.5 + (1-\bar{f})^2 + \tau(1-\bar{f}) + \lambda \frac{l}{d_h}\right]\frac{1}{\bar{f}^2} = \left(\zeta_0 + \lambda \frac{l}{d_h}\right)\frac{1}{\bar{f}^2}.$$

where τ is determined from the curve $\tau = f\left(\frac{l}{d_h}\right)$; λ is determined as a function of Re and $\bar{\Delta} = \frac{\Delta}{d_h}$ from diagrams 2-2 – 2-5; Δ is taken from Table 2-1; ν is taken from § 1-3,b.

2) $\mathrm{Re} < 10^5$ (approximate)

$$\zeta = (\zeta_\varphi + \bar{\varepsilon}_0^{\mathrm{Re}}\zeta_0)\frac{1}{\bar{f}^2},$$

where ζ_φ and $\bar{\varepsilon}_0^{\mathrm{Re}}$ are found from diagram 4-10;

$$\zeta_0 = 0.5 + (1-\bar{f})^2 + \tau(1-\bar{f})$$

l/d_h	0	0.2	0.4	0.6	0.8	1.0	1.2	1.6	2.0	2.4
τ	1.35	1.22	1.10	0.84	0.42	0.24	0.16	0.07	0.02	0

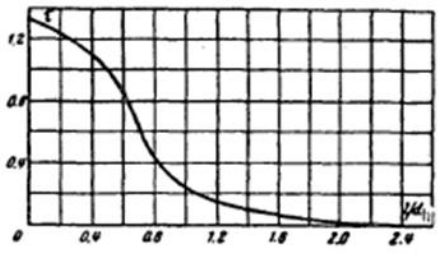

Fig. A.1: Pressure loss diagram used to calculate hydraulic resistance of lower core orifice plate (Idel'Chik 1960)

Thickened grid (perforated plate or laths) $\left(\frac{l}{d_h} > 0.015\right)$	Section VIII Diagram 8-4

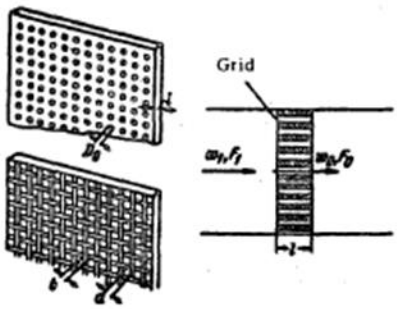

$d_h = \frac{4f_0}{\Pi_0}$; Π_0 – perimeter;

$\bar{f} = \frac{F_0}{F_1}$;

1. $Re = \frac{w_0 d_h}{\nu} \geq 10^5$:

$$\zeta = \frac{\Delta H}{\frac{\gamma w_1^2}{2g}} = \left[(0.5 + \varepsilon\sqrt{1-\bar{f}})(1-\bar{f}) + (1-\bar{f})^2 + \lambda\frac{l}{d_h}\right]\frac{1}{\bar{f}^2} = \left(\zeta_0 + \lambda\frac{l}{d_h}\right)\frac{1}{\bar{f}^2}.$$

where $\varepsilon = f\left(\frac{l}{d_h}\right)$ is taken from the table or, more accurately, from the graph of diagram 4-11;

$$\zeta_0 = (0.5 + \varepsilon\sqrt{1-\bar{f}})(1-\bar{f}) + (1-\bar{f})^2;$$

λ is determined from diagrams 2-1 to 2-5 as a function of Re and $\bar{\Delta} = \frac{\Delta}{D_h}$.

At $\lambda = 0.02$ the values of ζ are determined from the curves $\zeta = f(\bar{f})$ corresponding to different $\frac{l}{d_h}$ or from the table;

ν is taken from § 1-3, b;
$\bar{\Delta}$ is taken from Table 2-1;

2. $Re < 10^5$ (approximately):

$$\zeta_{Re} = \frac{\Delta H}{\frac{\gamma w_1^2}{2g}} = \left(\zeta_\varphi + \varepsilon_0^{Re}\zeta_0 + \lambda\frac{l}{d_h}\right)\frac{1}{\bar{f}^2}.$$

where ζ_0 is determined as at $Re > 10^5$; ζ_φ and ε_0^{Re} – cf. diagram 8-2.

Fig. A.2: Pressure loss diagram used to calculate hydraulic resistance of fuel assembly spacer grids (Idel'Chik 1960)

Thickened grid (perforated plate or laths) $\left(\frac{l}{d_h} > 0.015\right)$ (continued)	Section VIII
	Diagram 8-4

Values of ζ

$\frac{l}{d_h}$	τ	$\bar{T}$ 0.02	0.04	0.06	0.08	0.10	0.15	0.20	0.25	0.30	0.40	0.50	0.60	0.70	0.80	0.90	1.0
0	1.35	7 000	1 670	730	400	245	96.0	51.5	30.0	18.2	8.25	4.00	2.00	0.97	0.42	0.13	0
0.2	1.22	6 600	1 600	687	374	230	94.0	48.0	28.0	17.4	7.70	3.75	1.87	0.91	0.40	0.13	0.01
0.4	1.10	6 310	1 530	660	356	221	89.0	46.0	26.5	16.6	7.40	3.60	1.80	0.88	0.39	0.13	0.01
0.6	0.84	5 700	1 380	590	322	199	81.0	42.0	24.0	15.0	6.60	3.20	1.60	0.80	0.36	0.13	0.01
0.8	0.42	4 680	1 130	486	264	164	66.0	34.0	19.6	12.2	5.50	2.70	1 34	0.66	0.31	0.12	0.02
1.0	0.24	4 260	1 030	443	240	149	60.0	31.0	17.8	11.1	5.00	2.40	1.20	0.61	0.29	0.11	0.02
1.4	0.10	3 930	950	408	221	137	55.6	28.4	16.4	10.3	4.60	2.25	1.15	0.58	0.28	0.11	0.03
2.0	0.02	3 770	910	391	212	134	53.0	27.4	15.8	9.90	4.40	2.20	1.13	0.58	0.28	0.12	0.04
3.0	0	3 765	913	392	214	132	53.5	27.5	15.9	10.0	4.50	2.24	1.17	0.61	0.31	0.15	0.06
4.0	0	3 775	930	400	215	132	53.8	27.7	16.2	10.0	4.60	2.25	1.20	0.64	0.35	0.16	0.08
5.0	0	3 850	936	400	220	133	55.5	28.5	16.5	10.5	4.75	2.40	1.28	0.69	0.37	0.19	0.10
6.0	0	3 870	940	400	222	133	55.8	28.5	16.6	10.5	4.80	2.42	1.32	0.70	0.40	0.21	0.12
7.0	0	4 000	950	405	230	135	55.9	29.0	17.0	10.9	5.00	2.50	1.38	0.74	0.43	0.23	0.14
8.0	0	4 000	965	410	236	137	56.0	30.0	17.2	11.1	5.10	2.58	1.45	0.80	0.45	0.25	0.16
9.0	0	4 080	985	420	240	140	57.0	30.0	17.4	11.4	5.30	2.62	1.50	0.82	0.50	0.28	0.18
10	0	4 110	1 000	430	245	146	59.7	31.0	18.2	11.5	5.40	2.80	1.57	0.89	0.53	0.32	0.20

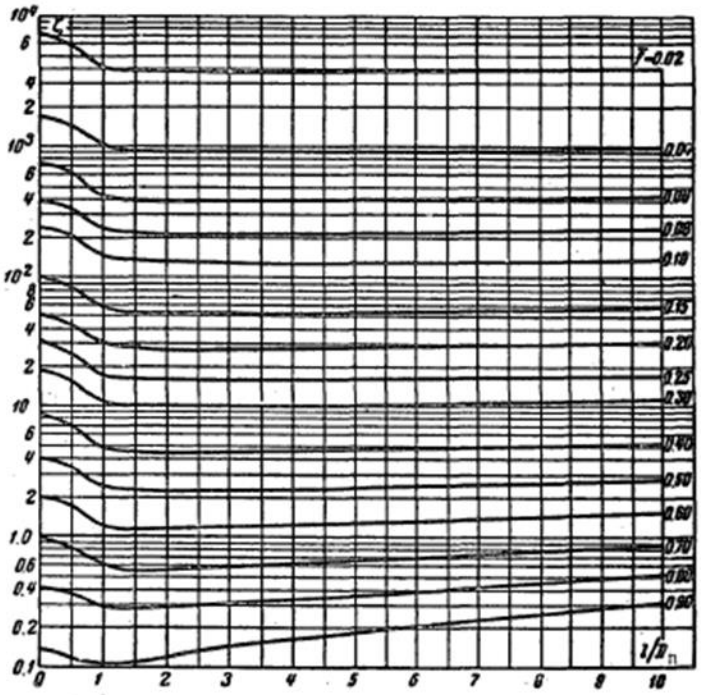

Fig. A.3: Pressure loss diagram used to calculate hydraulic resistance of fuel assembly spacer grids (cont.) (Idel'Chik 1960)

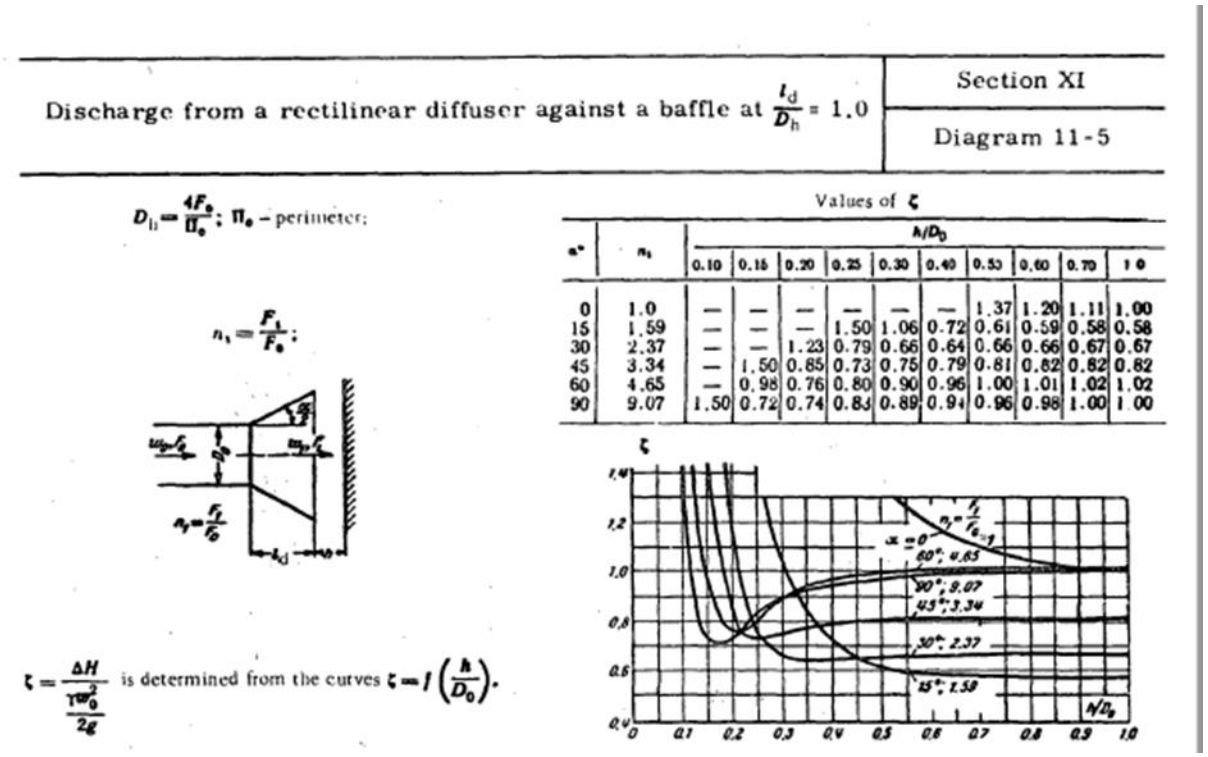

Discharge from a rectilinear diffuser against a baffle at $\frac{l_d}{D_h} = 1.0$

Section XI

Diagram 11-5

$D_h = \frac{4F_0}{\Pi_0}$; Π_0 – perimeter;

$n_1 = \frac{F_1}{F_0}$;

$\zeta = \frac{\Delta H}{\frac{\gamma w_0^2}{2g}}$ is determined from the curves $\zeta = f\left(\frac{h}{D_0}\right)$.

Values of ζ

$\alpha°$	n_1	h/D_0 0.10	0.15	0.20	0.25	0.30	0.40	0.50	0.60	0.70	1.0
0	1.0	—	—	—	—	—	—	1.37	1.20	1.11	1.00
15	1.59	—	—	—	1.50	1.06	0.72	0.61	0.59	0.58	0.58
30	2.37	—	—	1.23	0.79	0.66	0.64	0.66	0.66	0.67	0.67
45	3.34	—	1.50	0.85	0.73	0.75	0.79	0.81	0.82	0.82	0.82
60	4.65	—	0.98	0.76	0.80	0.90	0.96	1.00	1.01	1.02	1.02
90	9.07	1.50	0.72	0.74	0.84	0.89	0.94	0.96	0.98	1.00	1.00

Fig. A.4: Pressure loss diagram used to calculate hydraulic resistance of reactor vessel inlet nozzles for flow entering through cold legs into annular downcomer (Idel'Chik 1960).

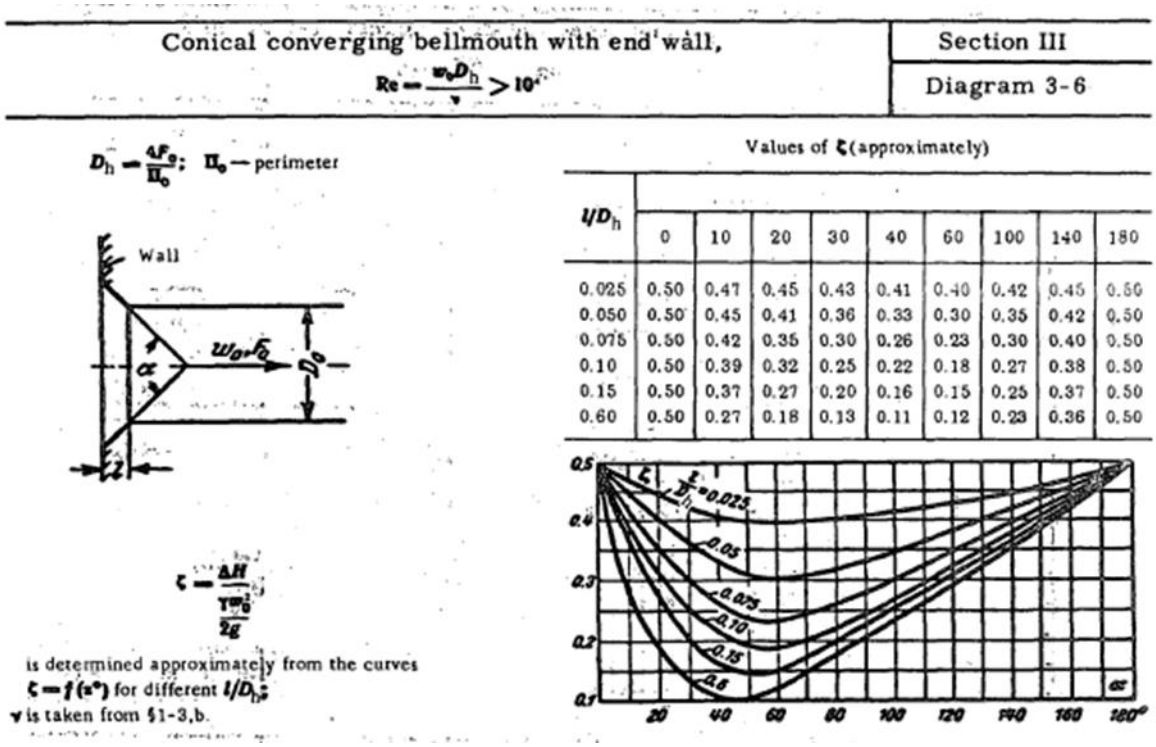

Conical converging bellmouth with end wall, $Re = \frac{w_0 D_h}{\nu} > 10^5$

Section III

Diagram 3-6

$D_h = \frac{4F_0}{\Pi_0}$; Π_0 — perimeter

$\zeta = \frac{\Delta H}{\frac{\gamma w_0^2}{2g}}$

is determined approximately from the curves $\zeta = f(\alpha°)$ for different l/D_h;

ν is taken from §1-3,b.

Values of ζ (approximately)

l/D_h	0	10	20	30	40	60	100	140	180
0.025	0.50	0.47	0.45	0.43	0.41	0.40	0.42	0.45	0.50
0.050	0.50	0.45	0.41	0.36	0.33	0.30	0.35	0.42	0.50
0.075	0.50	0.42	0.35	0.30	0.26	0.23	0.30	0.40	0.50
0.10	0.50	0.39	0.32	0.25	0.22	0.18	0.27	0.38	0.50
0.15	0.50	0.37	0.27	0.20	0.16	0.15	0.25	0.37	0.50
0.60	0.50	0.27	0.18	0.13	0.11	0.12	0.23	0.36	0.50

Fig. A.5: Pressure loss diagram used to calculate hydraulic resistance of reactor vessel outlet nozzles for flow leaving upper plenum and entering the hot legs (Idel'Chik 1960).

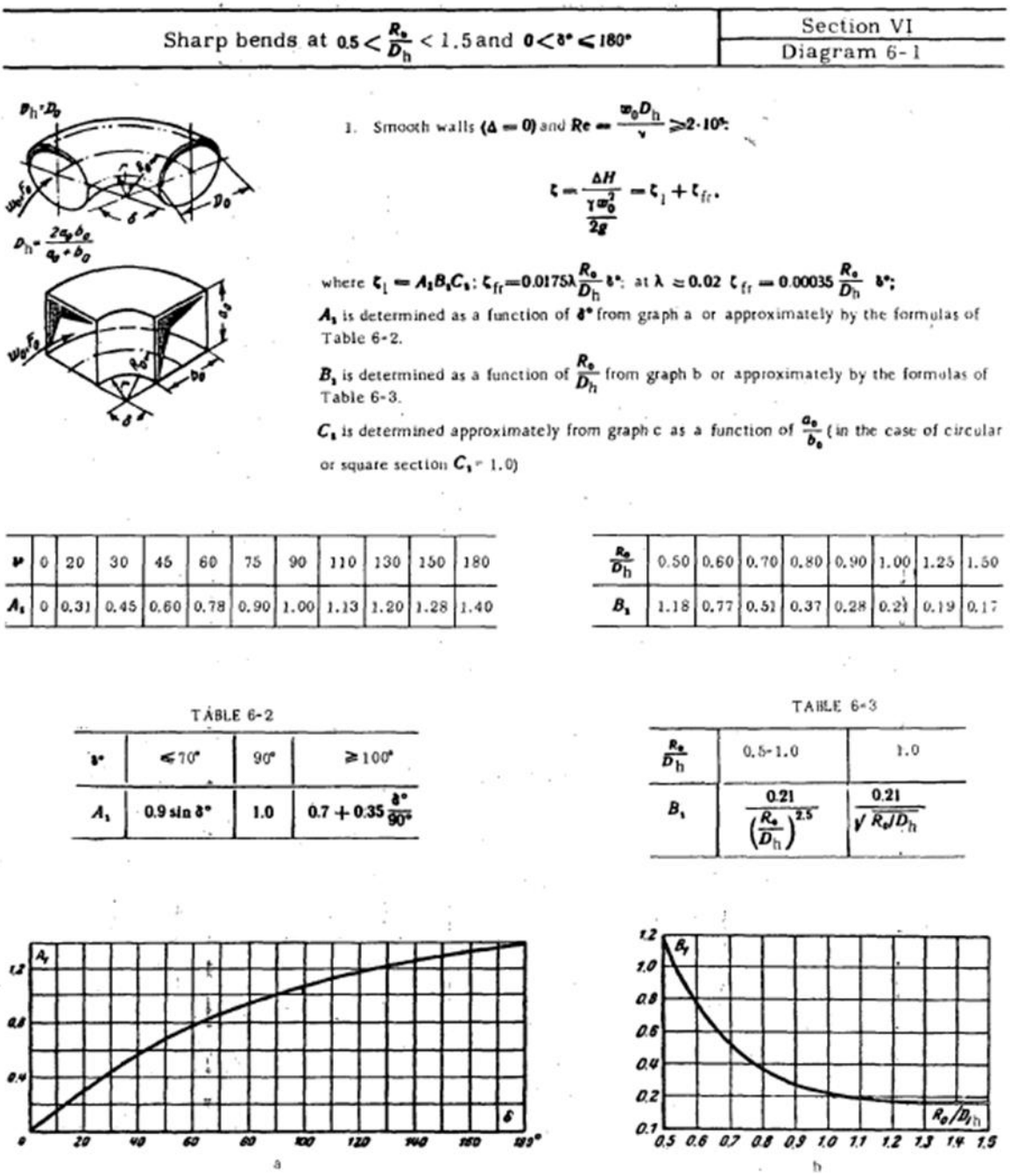

Sharp bends at $0.5 < \frac{R_0}{D_h} < 1.5$ and $0 < \delta^\circ < 180^\circ$ — Section VI, Diagram 6-1

1. Smooth walls ($\Delta = 0$) and $Re = \frac{w_0 D_h}{\nu} \geq 2 \cdot 10^5$:

$$\zeta = \frac{\Delta H}{\frac{\gamma w_0^2}{2g}} = \zeta_l + \zeta_{fr}.$$

where $\zeta_l = A_1 B_1 C_1$; $\zeta_{fr} = 0.0175 \lambda \frac{R_0}{D_h} \delta^\circ$; at $\lambda \simeq 0.02$ $\zeta_{fr} = 0.00035 \frac{R_0}{D_h} \delta^\circ$;

A_1 is determined as a function of δ° from graph a or approximately by the formulas of Table 6-2.

B_1 is determined as a function of $\frac{R_0}{D_h}$ from graph b or approximately by the formulas of Table 6-3.

C_1 is determined approximately from graph c as a function of $\frac{a_0}{b_0}$ (in the case of circular or square section $C_1 = 1.0$)

δ°	0	20	30	45	60	75	90	110	130	150	180
A_1	0	0.31	0.45	0.60	0.78	0.90	1.00	1.13	1.20	1.28	1.40

$\frac{R_0}{D_h}$	0.50	0.60	0.70	0.80	0.90	1.00	1.25	1.50
B_1	1.18	0.77	0.51	0.37	0.28	0.21	0.19	0.17

TABLE 6-2

δ°	$\leq 70^\circ$	90°	$\geq 100^\circ$
A_1	$0.9 \sin \delta^\circ$	1.0	$0.7 + 0.35 \frac{\delta^\circ}{90^\circ}$

TABLE 6-3

$\frac{R_0}{D_h}$	0.5–1.0	1.0
B_1	$\frac{0.21}{\left(\frac{R_0}{D_h}\right)^{2.5}}$	$\frac{0.21}{\sqrt{R_0/D_h}}$

Fig. A.6: Pressure loss diagram used to calculate hydraulic resistance of pipe and tube curvatures for bending radius 0.5< R/Dh < 1.5 (Idel'Chik 1960).

Sharp bends at $0.5 < \frac{R_0}{D_h} < 1.5$ and $0 < \theta^\circ \leq 180^\circ$ (cont'd) | Section VI, Diagram 6-1

$\frac{a_0}{b_0}$	0.25	0.50	0.75	1.0	1.5	2.0	3.0	4.0	5.0	6.0	7.0	8.0
C_1	1.30	1.17	1.09	1.00	0.90	0.85	0.85	0.90	0.95	0.98	1.00	1.00

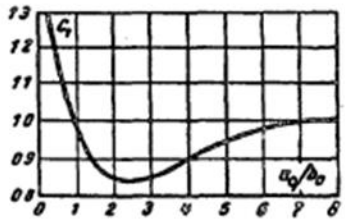

c

2. Rough walls ($\Delta > 0$) and $Re \leq 2 \cdot 10^6$:

$$\zeta = \frac{\Delta H}{\frac{\overline{w}_0^2}{2g}} = k_\Delta k_{Re} \zeta_1 + \zeta_{fr},$$

where k_Δ and k_{Re} are determined (tentatively) from Table 6-4 as a functions of Re and $\overline{\Delta} = \frac{\Delta}{D_h}$

TABLE 6-4

$\overline{\Delta}$	R_0/D_h									
	0.5-0.55				0.55-1.5					
	Re									
	$3 \cdot 10^3$-$4 \cdot 10^4$		$>4 \cdot 10^4$		$3 \cdot 10^3$-$4 \cdot 10^4$		$3 \cdot 10^4$-$2 \cdot 10^5$		$>2 \cdot 10^5$	
	k_{Re}	k_Δ	k_{Re}	k_Δ	k_{Re}	k_Δ	k_{Re}	k_Δ	k_{Re}	k_Δ
0	$45\lambda_{Re}$	1.0	1.0	1.0	$64\lambda_{Re}$	1.0	$64\lambda_{Re}$	1.0	1.0	1.0
0-0.001	$45\lambda_{Re}$	1.0	1.0	$1 + 0.5 \cdot 10^3\overline{\Delta}$	$64\lambda_{Re}$	1.0	$64\lambda_{Re}$	$\lambda_\Delta/\lambda_{sm}$	1.0	$1 + \overline{\Delta} \cdot 10^3$
>001	$45\lambda_{Re}$	1.0	1.0	≈ 1.5	$64\lambda_{Re}$	1.0	$64\lambda_{Re}$	≈ 2.0	1.0	≈ 2.0

λ_{Re} and λ_{sm} are determined as λ for commercially smooth pipes ($\Delta = 0$) at given Re from diagram 2-2

λ and λ_Δ are determined as λ for rough pipes ($\Delta > 0$) at given Re and $\overline{\Delta} = \frac{\Delta}{D_h}$ from diagrams 2-3 to 2-5;

ν is taken from § 1-3, b; Δ is taken from Table 2-1.

Fig. A.7: Pressure loss diagram used to calculate hydraulic resistance of pipe and tube curvatures for bending radius 0.5< R/Dh < 1.5 (cont.) (Idel'Chik 1960).

Smooth bends at $\frac{R_0}{D_h} > 1.5$ and $0 < \delta^\circ < 180^\circ$	Section VI Diagram 6-2

1. Smooth bends ($\Delta = 0$) and $Re = \frac{w_0 D_h}{\nu} \geq 2 \cdot 10^5$:

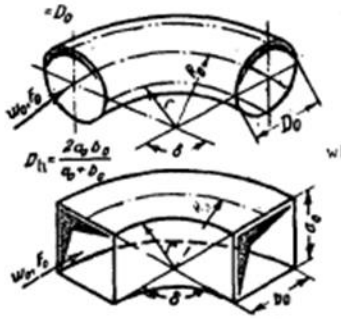

$$\zeta = \frac{\Delta H}{\frac{\gamma w_0^2}{2g}} = \zeta_1 + \zeta_{fr},$$

where $\zeta_1 = A_1 B_1 C_1$:

$$\zeta_{fr} = 0.0175 \lambda \frac{R_0}{D_h} \delta^\circ;$$

$$\lambda \approx 0.02 - \zeta_{fr} = 0.00035 \frac{R_0}{D_h} \delta^\circ;$$

A_1 is determined as a function of δ° from graph a or by the formulas of Table 6-5

TABLE 6-5

δ°	$\leq 70^\circ$	90°	$\geq 100^\circ$
A_1	$0.9 \sin \delta^\circ$	1.0	$0.7 + 0.35 \frac{\delta^\circ}{90^\circ}$

B_1 is determined as a function of $\frac{R_0}{D_h}$ from graph b, or by the formula

$$B_1 = \frac{0.21}{\sqrt{R_0 / D_h}};$$

C_1 is determined from graph c as a function of $\frac{a_0}{b_0}$ (for circular or square cross section $C_1 = 1.0$)

2. Rough walls ($\Delta > 0$) and $Re \geq 2 \cdot 10^5$:

$$\zeta = \frac{\Delta H}{\frac{\gamma w_0^2}{2g}} = k_\Delta k_{Re} \zeta_1 + \zeta_{fr},$$

where k_Δ, k_{Re} are determined (tentatively) from Table 6-6 as a function of Re and $\bar{\Delta} = \frac{\Delta}{D_h}$

TABLE 6-6

$\bar{\Delta}$	Re					
	$3 \cdot 10^3 - 4 \cdot 10^4$		$4 \cdot 10^4 - 2 \cdot 10^5$		$> 2 \cdot 10^5$	
	k_{Re}	k_Δ	k_{Re}	k_Δ	k_{Re}	k_Δ
0	$64/\lambda_{Re}$	1.0	$64/\lambda_{Re}$	1.0	1.0	1.0
0-0.001	$64/\lambda_{Re}$	1.0	$64/\lambda_{Re}$	$1 + \bar{\Delta}^{1/3} \cdot 10^2$	1.0	$1 + \bar{\Delta}^{1/3} \cdot 10^2$
>0.001	$64/\lambda_{Re}$	1.0	$64/\lambda_{Re}$	≈ 2.0	1.0	≈ 2.0

λ is determined as a function of the given Re and $\bar{\Delta}$ from diagrams 2-2 to 2-5;
λ_{Re} is determined as λ for commercially smooth pipes ($\Delta = 0$) at given Re from diagram 2-2;
ν is taken from § 1-3,b; Δ is taken from Table 2-1.

Fig. A.8: Pressure loss diagram used to calculate hydraulic resistance of pipe and tube curvatures for bending radius R/Dh > 1.5 (Idel'Chik 1960).

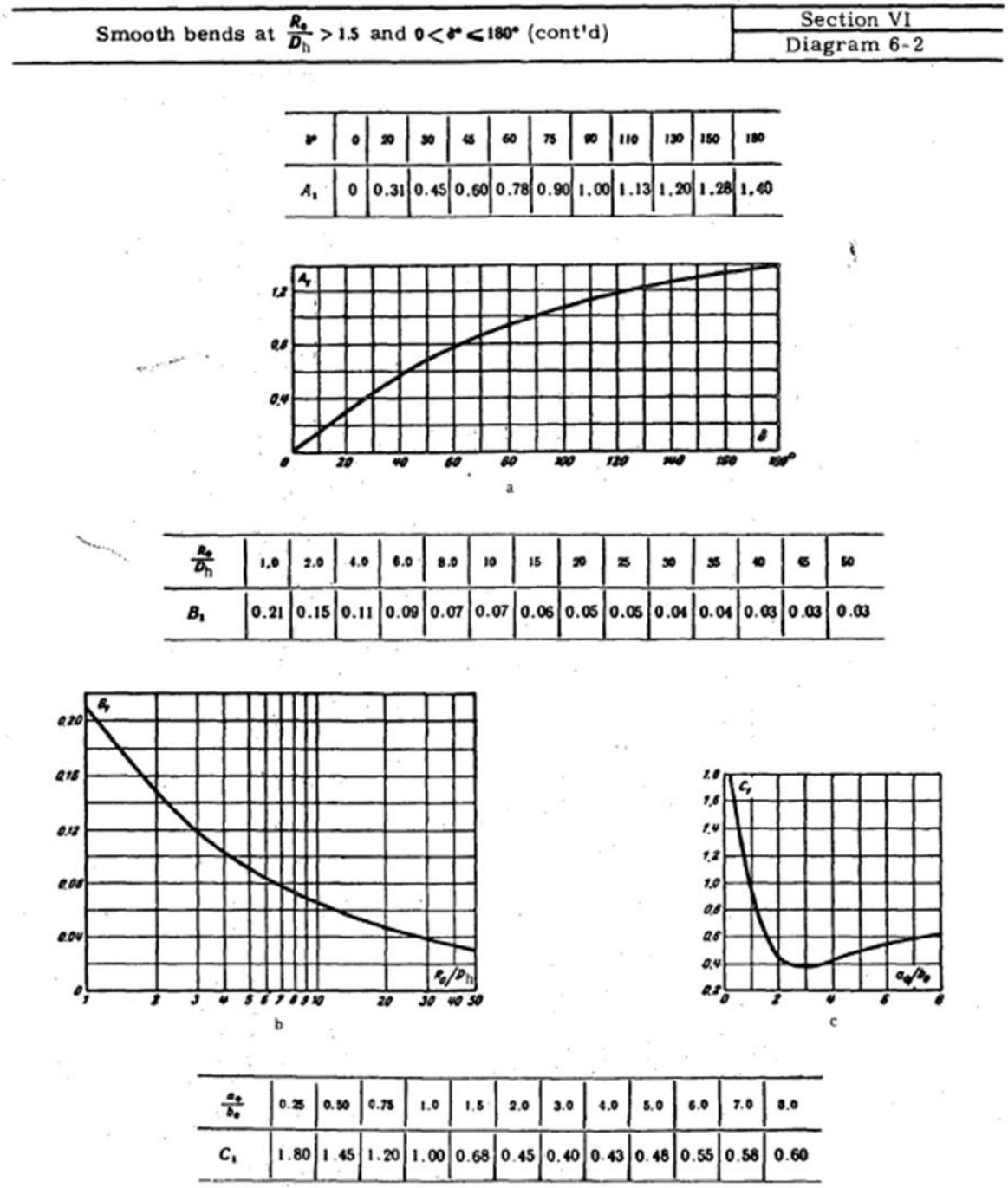

Smooth bends at $\frac{R_0}{D_h} > 1.5$ and $0 < \delta^\circ \leq 180^\circ$ (cont'd) — Section VI, Diagram 6-2

δ°	0	20	30	45	60	75	90	110	130	150	180
A_δ	0	0.31	0.45	0.60	0.78	0.90	1.00	1.13	1.20	1.28	1.40

a

$\frac{R_0}{D_h}$	1.0	2.0	4.0	6.0	8.0	10	15	20	25	30	35	40	45	50
B_δ	0.21	0.15	0.11	0.09	0.07	0.07	0.06	0.05	0.05	0.04	0.04	0.03	0.03	0.03

b

c

$\frac{a_0}{b_0}$	0.25	0.50	0.75	1.0	1.5	2.0	3.0	4.0	5.0	6.0	7.0	8.0
C_δ	1.80	1.45	1.20	1.00	0.68	0.45	0.40	0.43	0.48	0.55	0.58	0.60

Fig. A.9: Pressure loss diagram used to calculate hydraulic resistance of pipe and tube curvatures for bending radius R/Dh > 1.5 (cont.) (Idel'Chik 1960).